OSP 85462

MIT

AN ANALYSIS OF LONGSHORE CURRENTS AND ASSOCIATED SEDIMENT TRANSPORT IN THE SURF ZONE

by

D.W. Ostendorf

O.S. Madsen

DEPARTMENT
OF
CIVIL
ENGINEERING

RALPH M. PARSONS LABORATORY

FOR

WATER RESOURCES AND HYDRODYNAMICS

Department of Civil Engineering
Massachusetts Institute of Technology

SCHOOL OF ENGINEERING
MASSACHUSETTS INSTITUTE OF TECHNOLOGY
Cambridge, Massachusetts 02139

Report No. 241

April 1979

MIT report, no. 241.

Ostendorf, D.W., and O.S. Madsen.

An analysis of longshore currents and associated
sediment transport in the surf zone.

1979.

f3a (234) NAAM	Datum uitlening	Datum terugontvangst
vakgroep Kustwaterbouwkunde.		

NAAM	Datum uitlening	Datum terugontvangst

700714

NOTICE

Technical Report No. 242 entitled, "User's Manual for the MIT Simulation Model," is a manual for TR 225. It includes a deck of computer cards and sells for $75.00. It will not be distributed, but will be available by special order only.

AN ANALYSIS OF LONGSHORE CURRENTS

AND ASSOCIATED SEDIMENT TRANSPORT

IN THE SURF ZONE

by

D. W. Ostendorf

O. S. Madsen

RALPH M. PARSONS LABORATORY

FOR

WATER RESOURCES AND HYDRODYNAMICS

Department of Civil Engineering

Massachusetts Institute of Technology

Report No. 241

April 1979

ABSTRACT

Two momentum based longshore current models and a preliminary longshore sediment transport model are derived, calibrated and tested in the present investigation. The Linear Longshore Current Model predicts the relatively small longshore current induced by monochromatic, two dimensional, gravity waves of finite height and near normal incidence breaking on a plane, impermeable, gently sloping bottom in the presence of a shorenormal jetty when the offshore wave height, wave period, wave angle and water depth are known, along with the beach slope and roughness. The Nonlinear Longshore Current Model predicts a longshore current using the same input as its linear counterpart, but the nonlinear model removes the assumptions of a relatively small current and near normal wave incidence and is valid only for uniform longshore conditions. The Linear Longshore Sediment Transport Model predicts the integrated, time averaged longshore sediment transport for a relatively small current and near normal wave incidence under uniform longshore conditions and also describes the initial response of a plane bed downstream of a shorenormal jetty.

The longshore current models may be considered as a series of modifications of the original model of Longuet-Higgins (1970), while the Linear Longshore Sediment Transport Model is a surf zone application of the work of Madsen and Grant (1976a) on nonbreaking wave induced sediment transport.

Calibration yields physically plausible behavior for the three model parameters while fixed bed, laboratory movable bed and field

testing show a general longshore current model accuracy of about 20%, where the latter two data bases only test the Linear Longshore Current Model. The Linear Longshore Sediment Transport Model matches the laboratory data to an accuracy of about 20% but overpredicts the field data by a factor of 5; in view of the latter finding, the model should only be considered as an order of magnitude estimator of longshore sediment transport.

To aid in model use, examples of the three models are presented in an appendix in the back of this report.

ACKNOWLEDGMENTS

iv

TABLE OF CONTENTS

LIST OF FIGURES

LIST OF TABLES

NOTATION

English Alphabet

Symbol   Definition (units)

A Cnoidal dispersion parameter

$\langle A_b \rangle$ Surf zone averaged near bottom particle excursion
             amplitude (ℓ)

$\vec{A}_s$ Convective stress ($m/\ell\text{-}t^2$)

A_s^x Shorenormal convective stress ($m/\ell\text{-}t^2$)

A_s^y Longshore convective stress ($m/\ell\text{-}t^2$)

A^{ij} Convection stress tensor (m/t^2)

A^{xx} Convection induced transport of shorenormal momentum
             in shorenormal direction (m/t^2)

A^{xy} Convection induced transport of longshore momentum
             in shorenormal direction (m/t^2)

A^{yx} Convection induced transport of shorenormal momentum
             in longshore direction (m/t^2)

A^{yy} Convection induced transport of longshore momentum
             in longshore direction (m/t^2)

A_B^{xy} Convection induced transport of longshore momentum
             through the breaker line (m/t^2)

a_s Incident wave amplitude at time averaged shore line (ℓ)

B Cnoidal energy transport function parameter

BK Brebner and Kamphuis (1963) data base

$\vec{c}$ Phase velocity (ℓ/t)

Symbol	Definition (units)
$\vec{c}_B$	Breaking wave phase velocity (ℓ/t)
c^*	Dimensionless phase speed
c_B^*	Dimensionless breaking wave phase speed
c_T^*	Transitional dimensionless phase speed
$c_1 - c_3$	Modified Longuet-Higgins Model constants
c_4	Breaking wave iteration constant
c_5	Linear Longshore Current Model constant
c_6, c_7	Linear Longshore Sediment Transport Model constants
$c_8 - c_{13}$	Nonlinear Longshore Current Model constants
D	Wave energy dissipation rate (m/t^3)
D_{sz}	Wave energy dissipation rate inside the breaker line (m/t^3)
D_w	Wave energy dissipation rate beyond the breaker line (m/t^3)
DAS	Run index
d	Still water depth (ℓ)
d_s	Grain size (ℓ)
E	Wave energy (m/t^2)
$\vec{E}_F$	Wave energy flux ($m-\ell/t^3$)
$(\vec{E}_F)_G$	Wave energy flux at gage location ($m-\ell/t^3$)
E_G	Wave energy at gage location (m/t^2)
E_i	Wave energy in the ith wave train (m/t^2)
f_s	Current friction factor
$\bar{f}_s$	28 run average f_s
f_{sz}	Surf zone friction factor

Symbol	Definition (units)
f_w	Jonsson wave friction factor
$\overline{f}_w$	28 run average f_w
GE	Galvin and Eagleson (1965) data base
g	Gravitational acceleration (ℓ/t^2)
H	Wave height (ℓ)
H_B	Breaking wave height (ℓ)
H_G	Wave height at generator (ℓ)
H_o	Deep water wave height (ℓ)
h	Time averaged water depth (ℓ)
<h>	Surf zone averaged, time averaged water depth (ℓ)
h_B	Time averaged water depth at breaker line (ℓ)
h_G	Time averaged water depth at generator (ℓ)
I	Run index
$\vec{i}$	Unit shorenormal vector
J	Run index
$\vec{j}$	Unit longshore vector
K	Run index
KO	Komar (1969) data base
k	Wave number
k_s	Relative roughness (ℓ)
L	Wave length (ℓ)
L_o	Deep water wave length (ℓ)
ℓ	Length (ℓ)
ℓ_f	Fluctuating length scale (ℓ)

Symbol	Definition (units)
m	Mass (m)
M	Battjes' correlation constant
N	Longuet-Higgins' lateral mixing constant
n	Wave energy transport function
n_B	Breaking wave energy transport function
n_G	Wave energy transport function at gage location
n_i	Energy transport function of ith wave train
n_Q	Sample size
P_{sz}	Mixing parameter
$\vec{P}_w$	Wave setup stress $(m/\ell\text{-}t^2)$
P_w^x	Shorenormal wave setup stress $(m/\ell\text{-}t^2)$
P_w^y	Longshore wave setup stress $(m/\ell\text{-}t^2)$
PMT	Putnam, Munk and Traylor (1949) data base
p	Instantaneous pressure $(m/\ell\text{-}t^2)$
p_b	Pressure at bottom $(m/\ell\text{-}t^2)$
p_f	Randomly fluctuating pressure $(m/\ell\text{-}t^2)$
p_η	Pressure at free surface $(m/\ell\text{-}t^2)$
Q_{cal}	Calibrating velocity error
Q_q	Total time averaged longshore sediment transport error
$\overline{Q}_q$	Sample mean Q_q
Q_v	Velocity error
$\overline{Q}_v$	Sample mean Q_v
Q_α	Relative wave height error
$\overline{Q}_\alpha$	Sample mean Q_α

Symbol	Definition (units)
$\vec{q}$	Sediment transport (m/ℓ-t)
q_s^y	Time averaged longshore sediment transport (m/ℓ-t)
$\vec{q}^*$	Dimensionless sediment transport
$(q^*)_s^x$	Dimensionless time averaged shorenormal sediment transport
$(q^*)^y$	Dimensionless longshore sediment transport
$(q^*)_s^y$	Dimensionless time averaged longshore sediment transport
R	Ratio of reflected to incident wave height
R_s	Current Reynolds number
R_w	Wave Reynolds number
S_Q	Sample standard deviation
$\vec{S}_w$	Local driving stress (m/ℓ-t^2)
S_w^x	Shorenormal local driving stress (m/ℓ-t^2)
S_w^y	Longshore local driving stress (m/ℓ-t^2)
S^{ij}	Radiation stress tensor (m/t^2)
S^{xx}	Wave induced transport of shorenormal momentum in shorenormal direction (m/t^2)
S^{xy}	Wave induced transport of longshore momentum in shorenormal direction (m/t^2)
S^{yx}	Wave induced transport of shorenormal momentum in longshore direction (m/t^2)
S^{yy}	Wave induced transport of longshore momentum in longshore direction (m/t^2)
S_B^{xy}	Wave induced transport of longshore momentum through the breaker line (m/t^2)

Symbol	Definition (units)
S^*	Dimensionless parameter
SJ	Shay and Johnson (1951) data base
SV	Saville (1949, 1950) data base
s	Specific gravity
T	Wave period (t)
$\vec{T}_f$	Reynolds stress $(m/\ell\text{-}t^2)$
T_f^x	Shorenormal Reynolds stress $(m/\ell\text{-}t^2)$
T_f^y	Longshore Reynolds stress $(m/\ell\text{-}t^2)$
T_i	Period of ith wave train (t)
T^{ij}	Fluctuation stress tensor (m/t^2)
T^{xx}	Fluctuation induced transport of shorenormal momentum in shorenormal direction (m/t^2)
T^{xy}	Fluctuation induced transport of longshore momentum in shorenormal direction (m/t^2)
T^{yx}	Fluctuation induced transport of shorenormal momentum in longshore direction (m/t^2)
T^{yy}	Fluctuation induced transport of longshore momentum in longshore direction (m/t^2)
T_B^{xy}	Fluctuation induced transport of longshore momentum through the breaker line (m/t^2)
t	Time (t)
U	Ursell number
$\vec{u}$	Instantaneous velocity (ℓ/t)
u	Instantaneous shorenormal velocity (ℓ/t)

Symbol	Definition (units)

$\vec{u}_f$ Randomly fluctuating velocity (ℓ/t)

u_f Randomly fluctuating shorenormal velocity (ℓ/t)

$|\vec{u}_f|_s$ Time averaged norm of randomly fluctuating velocity (ℓ/t)

$\vec{u}_s$ Current (ℓ/t)

u_s Shorenormal current (ℓ/t)

$|u_s|_B$ Absolute value of shorenormal current at breaker line (ℓ/t)

$\vec{u}_w$ Wave orbital velocity (ℓ/t)

u_w Shorenormal wave orbital velocity (ℓ/t)

u_w' Maximum shorenormal wave orbital velocity (ℓ/t)

$(\vec{u}_w)_b$ Near bottom wave orbital velocity (ℓ/t)

$|\vec{u}_w|_b'$ Maximum value of norm of near bottom wave orbital velocity (ℓ/t)

v Instantaneous longshore velocity (ℓ/t)

v_c Characteristic longshore current (ℓ/t)

v_f Randomly fluctuating longshore velocity (ℓ/t)

v_s Longshore current (ℓ/t)

$\langle v_s \rangle$ Surf zone averaged (0 to x_B) longshore current (ℓ/t)

v_s' Maximum longshore current (ℓ/t)

v_w Longshore wave orbital velocity (ℓ/t)

v^* Dimensionless longshore current

v_B^* Dimensionless longshore current at breaker line

$(v^*)'$ Maximum dimensionless longshore current

$\langle v^* \rangle$ Dimensionless surf zone averaged current

w Instantaneous vertical velocity (ℓ/t)

Symbol	Definition (units)
w_F	Fall velocity (ℓ/t)
w^*	Dimensionless fall velocity
X	Run index
x	Shorenormal distance (ℓ)
x_B	Shorenormal distance between time averaged shore line and breaker line (ℓ)
x_m	Shorenormal distance to measurement location (ℓ)
x_r	Shorenormal distance between time averaged shore line and swash mark (ℓ)
x_s	Shorenormal distance between time averaged and still water shore lines (ℓ)
x^*	Dimensionless shorenormal distance
$(x^*)'$	Dimensionless shorenormal location of maximum longshore current
y	Longshore distance (ℓ)
y_c	Characteristic longshore distance (ℓ)
y^*	Dimensionless longshore distance
z	Vertical distance (ℓ)

Greek Alphabet

Symbol	Definition (units)
α	Relative wave height
α_B	Relative breaking wave height
β	Angle between bottom and horizontal plane (deg)
Γ	Lateral mixing coefficient

Symbol	Definition (units)
γ	Relative wave length
γ_B	Relative breaking wave length
γ_T	Transitional relative wave length
Δ	Modified angle between bottom and horizontal plane (deg)
δ	Local current strength
ϵ	$M\ell_f |\vec{u}_f|_s$ or kinematic eddy viscosity (ℓ^2/t)
ζ	Longshore sediment transport coefficient
η	Instantaneous free surface elevation (ℓ)
η_f	Randomly fluctuating free surface elevation (ℓ)
η_r	Vertical distance between swash mark and still water level (ℓ)
η_s	Time averaged free surface elevation (ℓ)
η_s'	Vertical distance between time averaged shore line and still water level (ℓ)
η_w	Wave free surface elevation partition (ℓ)
$(\eta_s)_B$	Time averaged free surface elevation at the breaker line (ℓ)
θ	Angle between wave crest and bottom contour (deg)
θ_B	Angle between breaking wave crest and bottom contour (deg)
θ_G	Angle between wave crest and bottom contour at wave generator (deg)
θ_i	Angle between crest of ith wave train and bottom contour (deg)
θ_o	Angle between deep water wave crest and bottom contour (deg)
κ	Linear current strength

Symbol	Definition (units)
λ_c	Characteristic nonlinear current reduction factor
λ_1	Convective current reduction factor
λ_2	Nonlinear current reduction factor
ν	Fluid kinematic viscosity (ℓ^2/t)
ξ_B	Modified Battjes breaker parameter
ρ	Fluid density (m/ℓ^3)
ρ_s	Sediment density (m/ℓ^3)
τ^x	Shorenormal shear stress ($m/\ell\text{-}t^2$)
τ^y	Longshore shear stress ($m/\ell\text{-}t^2$)
τ_{5o}	Quadrature estimate of $(\tau_b^y)_s^*$ at $\delta = .50$
$\vec{\tau}_b$	Instantaneous bottom shear stress ($m/\ell\text{-}t^2$)
τ_b^x	Shorenormal bottom shear stress ($m/\ell\text{-}t^2$)
τ_b^y	Longshore bottom shear stress ($m/\ell\text{-}t^2$)
τ_η^x	Shorenormal free surface shear stress ($m/\ell\text{-}t^2$)
τ_η^y	Longshore free surface shear stress ($m/\ell\text{-}t^2$)
$(\vec{\tau}_b)_s$	Time averaged bottom shear stress ($m/\ell\text{-}t^2$)
$(\tau_b^x)_s$	Time averaged shorenormal bottom shear stress ($m/\ell\text{-}t^2$)
$(\tau_b^y)_s$	Time averaged longshore bottom shear stress ($m/\ell\text{-}t^2$)
$<(\tau_b^y)_s>$	Surf zone averaged, time averaged longshore bottom shear stress ($m/\ell\text{-}t^2$)
$(\tau_b^y)^*$	Dimensionless longshore bottom shear stress
$(\tau_b^y)_m^*$	Interpolated estimate of $(\tau_b^y)_s^*$
$(\tau_b^y)_s^*$	Dimensionless time averaged longshore bottom shear stress
$(\tau_b^y)_{s5}^*$	Five point Gauss quadrature estimate of $(\tau_b^y)_s^*$

Symbol	Definition (units)
ϕ	Wave phase (rad)
$\vec{\psi}$	Shields parameter
ψ_c	Critical Shields parameter
ω	Wave frequency (rad/sec)

Subscripts

Symbol	Definition
B	Conditions at breaker line
b	Conditions at the bottom
c	Characteristic or critical quantity
f	Randomly fluctuating quantity
G	Conditions at wave gage or wave generator
i	Conditions of ith wave train
o	Conditions in deep water
s	Time averaged quantity
w	Wave quantity
η	Conditions at the free surface

Superscripts

Symbol	Definition
x	Shorenormal component of vector quantity
y	Longshore component of vector quantity
'	Maximum quantity
*	Dimensionless quantity
ij	Transport of j momentum in i direction

Other conventions

Symbol	Definition
< >	Surf zone averaged quantity, 0 to x_B
→	Vector quantity
–	Sample mean quantity
| |	Norm of a vector quantity

1 INTRODUCTION

1.1 Significance of Longshore Currents and Longshore Sediment Transport

The proper design and maintenance of structures and effective management of activities along coast lines require a quantitative understanding of the motion of water and sediment in the surf zone. The prediction of longshore currents and the resulting longshore sediment transport generated by obliquely incident breaking water waves is a logical starting point towards this understanding.

It is natural to begin with the water motion since the water, in the form of traveling waves, serves as a medium transporting momentum from offshore sources, such as the atmosphere, to the nearshore area. If the traveling waves attain a height comparable to the water depth they will break, forming a surf zone where forces needed to resist the incoming flux of momentum are established. In the absence of local wave generation, two such forces are possible: setup, which is defined as a change in the time average water surface elevation, and bottom shear, which is the resistive drag felt by a steady current flowing over the bottom. When the waves break at an angle to the shore line, they contain a component of momentum parallel to the shore line, so that a steady current parallel to the shore line, or longshore current, may be induced, thus giving rise to a balancing bottom shear force. This breaking wave-longshore current mechanism may be realistically schematized and measured, particularly when the bottom is a fixed bed, and is accordingly amenable to analytical

1

modeling and verification; the Linear Longshore Current Model and the Nonlinear Longshore Current Model, which are new models developed in this investigation, extend the previous modeling efforts.

When the bottom shear is sufficiently strong and the bottom is a movable bed, the water will erode sediment off the bottom and transport it to calmer areas for subsequent deposition, causing a change in shore line configuration with attendant impacts on coastal structures and land use. Since the sediment receives momentum from the water, it is physically appropriate that longshore current models, which describe the water motion, serve as input to models of longshore sediment transport. One such model is the Linear Longshore Sediment Transport Model developed in this report, based on the Linear Longshore Current Model.

1.2 Problem Statement

The instantaneous fluid velocity, pressure, and free surface elevation in the vicinity of the surf zone are complicated functions of space and time since the surf zone represents the breakdown of wave motion into random fluctuations and a current accompanied by varying amounts of air entrainment. The sediment load is in reality comprised of particles of different size, sphericity and specific gravity with spatial and temporal variations in velocity and concentration. The complexity of the actual flow field must be reduced if there is to be any hope for a quantitative description; accordingly, any analytical model of surf zone dynamics will deal with an idealized

environment in which certain stresses and accelerations are neg-
lected.

The idealized environment considered in the present investiga-
tion consists of the surf zone formed by a simple wave train breaking
on a simple beach, as summarized in Table 1-1.

The governing equations and boundary conditions specifying the
flow field are further simplified by neglecting the stresses and
accelerations shown in Table 1-2.

The Linear Longshore Current Model and the Linear Longshore
Sediment Transport Model are predictors of the longshore current v_s
and the time averaged longshore sediment transport q_s^y occurring when
waves of known period T, height H and angle θ at a given time averaged
water depth h break on a beach of given slope $\tan\beta$, grain size d_s and
specific gravity s. The linear v_s and q_s^y predictions, which are valid
when the longshore current is small compared to the wave orbital
velocity and the waves are of near normal incidence, vary in the
longshore y and shorenormal x directions. The longshore current is
assumed to be constant with depth.

The Nonlinear Longshore Current Model, which is also uniform in
the vertical z direction, predicts v_s from the same input as its
linear counterpart, but incorporates the effect of a finite current
and oblique wave incidence. The nonlinear prediction, which corre-
sponds to fully developed conditions and accordingly is a function
of x alone, approaches the fully developed Linear Longshore Current
Model expression when the current and angle of incidence are small,

3

Table 1-1

Idealized Environment

WAVE TRAIN

Two dimensional, horizontally propagating waves[o]

Monochromatic waves

Oblique angle of incidence[3]

Near normal angle of incidence[1,2]

Homogeneous, incompressible fluid

Gravity waves

BEACH

Impermeable beach

Plane beach

Gentle sloping beach

Semi-infinite beach[2]

Infinite beach[1,3]

Cohesionless sediment

Uniform, spherical sediment particles

CURRENT

Comparable magnitude relative to wave orbital motion[3]

Small magnitude relative to wave orbital motion[1,2]

---

o Assumptions apply to all models unless noted otherwise

1 Modified Longuet-Higgins Model

2 Linear Longshore Current Model and Linear Longshore Sediment Transport Model

3 Nonlinear Longshore Current Model

Table 1-2

Neglected Stresses and Accelerations

No wind stress

No atmospheric pressure gradient

No Coriolis acceleration

No tides

No local time average acceleration

---

so that the two models are consistent solutions to special cases of the breaking wave-longshore current interaction.

The surf zone coordinate system is sketched in Figure 1-1.

1.3 Fixed Bed Longshore Current Data

Galvin and Eagleson (1965), Putnam, Munk and Traylor (1949), Brebner and Kamphuis (1963) and Eagleson (1965) all measure longshore currents induced by essentially two dimensional, horizontally propagating, monochromatic water waves breaking on plane, stationary, impermeable, fixed bed laboratory beaches set into constant depth basins as suggested in Table 1-3, where the G, o and B subscripts refer to generator, deep water and breaker line conditions, respectively. The Galvin and Eagleson (1965), Putnam et al. (1949) and Brebner and Kamphuis (1963) data sets are represented by GE, PMT and BK, respectively. The Eagleson (1965) data is taken in the developing region of a relatively strong current in violation of the conditions in Table 1-1 and accordingly receives no further consideration in the present investigation. Table 1-4 lists the reported variables for the three fixed bed studies, with the norm of the breaking wave phase velocity $|\vec{c}_B|$ and time averaged free surface elevation η_s. As sketched in Figure 1-1, x_s, x_r and x_B refer to shorenormal distances between the still water and time averaged shore lines, the time averaged shore line and the swash mark denoting the extent of wave runup, and the time averaged shore line and the breaker line, respectively. The brackets < > and the single prime indicate surf zone averaged and maximum quantities, respectively.

5
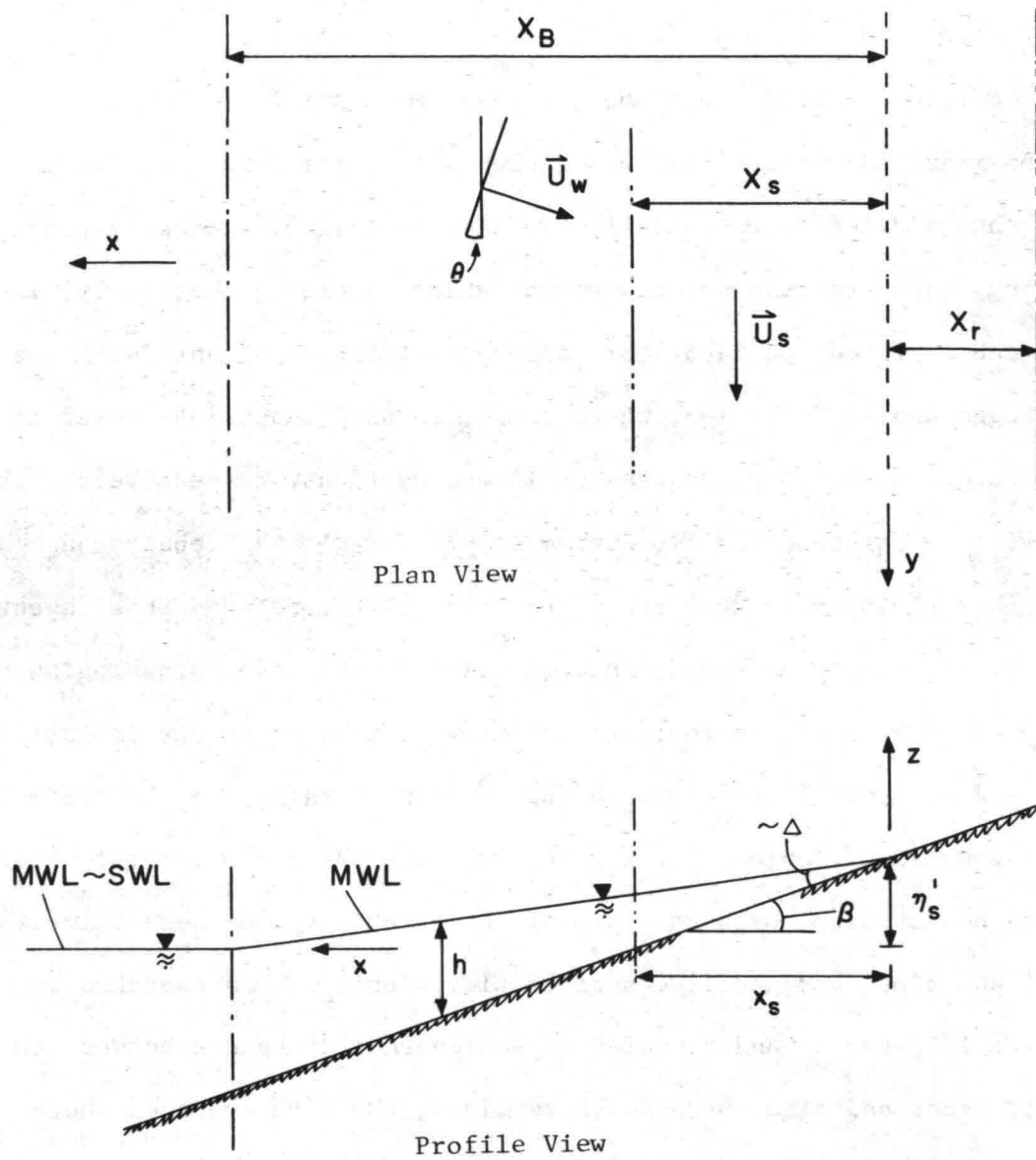
Figure 1-1: Surf Zone Coordinate System

6

Table 1-3

Longshore Currents over a Fixed Bed

Basin, Beach and Wave Generator Conditions

	GE	PMT	BK
BASIN			
Length (ft)	45	58	100
Width (ft)	22	39	50
h_g (ft)	1.15	<2	1.50
Training Wall Refraction	Most	None	All
BEACH			
Surface	Concrete	Variable	Indented Concrete
$\tan\beta$	0.109	0.066–0.260	0.050,0.100
WAVE GENERATOR			
Type	Plunger	Flap	Flap
T (sec)	0.90–1.50	0.72–2.32	0.78–1.13
θ (o)	10–51(θ_G)	10–60(θ_B)	20–60(θ_G)
H (ft)	0.05–0.21 (H_G)	0.12–0.47 (H_B)	0.075–0.258 (H_o)

Table 1-4

Longshore Currents over a Fixed Bed

Reported Variables

	GE	PMT	BK
WAVES			
H	H_G, H_B	H_B	H_o
θ	θ_G, θ_B	θ_B	θ_o
T	T	T	T
$|\vec{c}_B|$	Yes	No	No
SURF ZONE GEOMETRY			
x	$(x_r + x_s), (x_B - x_s)$	None	None
h	h_G	h_B	h_G
η_s	Yes	No	No
CURRENTS			
Location	$v_s(x,y)$	$\langle v_s \rangle$	$v_s'(y)$

1.3.1 Galvin and Eagleson (1965)

As suggested by Table 1-4, the Galvin and Eagleson (1965) data base is the most complete for a given set of basin, beach and wave generator conditions. A plunger-type wave generator at three alignments $\theta_G (I = 1-3)$ generates 12 different waves (J= 1-12) as shown in Table 1-5. H_G is measured with a resistance-type wave gage in the constant depth region in front of the wave generator, while T is

Table 1-5

Galvin and Eagleson (1965)

Run Classification

I		1		2		3
θ_G (degrees)		10		27		51
J	1	2	3	4	5	6
T (sec)	1.00	1.125	1.25	1.375	1.50	1.25
H_G (ft)	0.191	0.167	0.143	0.121	0.105	0.050
J	7	8	9	10	11	12
T (sec)	1.25	1.25	1.25	1.25	1.50	1.00
H_G (ft)	0.098	0.124	0.130	0.156	0.062	0.110

obtained from the plunger frequency. The waves propagate shoreward between two training walls normal to the wave generator and refract over the plane beach until breaking, where H_B, θ_B, $(x_B - x_s)$ and, in some cases, $|\vec{c}_B|$ are measured. The training walls for the I = 1, 3 runs are refracted for 1.25 sec and 1.50 sec waves, respectively, and kept straight for I = 2, with the upstream wall extending onto dry land and the downstream wall ending 2.2 ft from the still water shore line. The beach, which is constructed of smooth concrete, is assigned a relative roughness k_s of 0.001 ft for the purpose of testing the longshore current models. The breaker line is defined as the location of vertical free surface slope with θ_B and $(x_B - x_s)$ determined by overhead sighting while the experiment is in progress,

H_B measured with a resistance-type wave gage and $|\vec{c}_B|$ with a second gage positioned a fixed distance along a wave ray from the first. $\eta_s(x,y)$ is measured across 8 equispaced transects normal to the bottom contours, each consisting of 6 damped piezometers of which at least 4 are in or near the surf zone. h_G is checked with a point gage, and $(x_r + x_s)$ is obtained by visual observation. $v_s(x,y)$ is measured across 7 transects normal to the bottom contours and located 2 ft, 6 ft (7 ft for $J = 2$), 9 ft, 11 ft, 13 ft, 15 ft and 17 ft, respectively, downstream of the upstream training wall with as many as 7 stations in a given transect. These transects are numbered 1 through 7, respectively. Longshore current velocity is measured with a propeller-type miniature current meter 0.052 ft in diameter positioned, when possible, at mean depth and calibrated against the timed travel of wooden surface floats.

Only a portion of the GE data is used. The models of the present investigation contain a wave refraction component as well as an empirical breaking criterion, so that it is possible to use generator conditions, which are easier to measure and accordingly more accurate than breaker line conditions, as input. Since the GE data are used to determine the form of the longshore current profile, all transects with three or less stations are excluded from consideration. Transects 1 and 7, located within two wavelengths of a training wall, are omitted to reduce the diffractive effects of training wall misalignment on the measured flow field, while transects 2, 3 and 4 are excluded from strong current runs on the assumption that they are in a

region of developing current in violation of the idealized environment of Table 1-1.

Table 1-6 lists the GE data adopted for calibration and testing of the Linear Longshore Current Model and Nonlinear Longshore Current Model. The K index denotes the transect number and X the station number of a given velocity measurement, with X increasing in the positive x direction. The shorenormal station distance x_m is measured from the still water shore line.

1.3.2 Putnam, Munk and Traylor (1949)

The waves of the Putnam, Munk and Traylor (1949) data base are caused by a flap-type generator aligned at a constant, but unspecified, angle with respect to the basin walls; H_G and h_G are similarly unreported, while T is reported and measured by timing the generator frequency. The waves break on plane beaches of varying slopes set at different unspecified angles with respect to the basin walls and finished with three different fixed surfaces. The surfaces, which consist of sheet metal or smooth cement, glued natural sand of unreported size and one-quarter inch pea gravel bonded with a thin grout, are, for the purposes of the present investigation, assigned relative roughness values of 0.001 ft, 0.0033 ft and 0.0208 ft, respectively. H_B and h_B are measured with electric point gages, while θ_B is obtained from vertical photographs. Longshore currents are measured by timed travel of dye along the beach section 5 ft to 15 ft downstream of the upstream basin wall. Putnam et al. (1949) note that the length of

11

Table 1-6

Galvin and Eagleson (1965)

Data Used in Longshore Current Model Tests

I	J	K	X	1	2	3	4	5
			x_m(ft)	-0.17	0.33	0.83	1.33	1.83
1	1	5	v_s(fps)	0.37	0.49	0.47	0.42	0.23
1	1	6	v_s(fps)	0.34	0.52	0.49	0.45	0.35
			x_m(ft)	-0.17	0.33	0.83	1.33	1.83
1	2	5	v_s(fps)	0.38	0.57	0.51	0.43	0.29
1	2	6	v_s(fps)	0.38	0.64	0.60	0.51	0.29
			x_m(ft)	-0.17	0.33	0.83	1.33	1.83
1	3	5	v_s(fps)	0.37	0.48	0.51	0.28	0.16
1	3	6	v_s(fps)	0.42	0.53	0.50	0.31	0.16
			x_m(ft)	-0.17	0.33	0.83	1.33	1.83
1	4	2	v_s(fps)	0.21	0.24	0.26	0.18	0.15
1	4	3	v_s(fps)	0.51	0.52	0.31	0.16	0.19
1	4	4	v_s(fps)	0.47	0.50	0.43	0.28	0.16
1	4	5	v_s(fps)	0.41	0.62	0.49	0.27	0.17
1	4	6	v_s(fps)	0.34	0.50	0.45	0.33	0.15
			x_m(ft)	-0.17	0.33	0.83	1.33	
1	5	2	v_s(fps)	0.15	0.44	0.47	0.26	
1	5	3	v_s(fps)	0.24	0.41	0.37	0.27	
1	5	4	v_s(fps)	0.27	0.40	0.38	0.27	
1	5	5	v_s(fps)	0.19	0.42	0.41	0.28	
1	5	6	v_s(fps)	0.27	0.38	0.41	0.28	
			x_m(ft)	-0.17	0.33	0.83	1.33	
1	6	3	v_s(fps)	0.13	0.24	0.13	0.13	
1	6	4	v_s(fps)	0.13	0.23	0.16	0.14	
1	6	5	v_s(fps)	0.12	0.23	0.17	0.13	
1	6	6	v_s(fps)	0.16	0.23	0.16	0.12	

Table 1-6 (Continued)

I	J	K	X	1	2	3	4	5	6
			x_m(ft)	-0.17	0.33	0.83	1.33	1.83	
1	7	2	v_s(fps)		0.25	0.16	0.15	0.15	
1	7	3	v_s(fps)	0.13	0.25	0.20	0.13	0.15	
1	7	4	v_s(fps)	0.13	0.28	0.21	0.17	0.15	
1	7	5	v_s(fps)	0.14	0.37	0.23	0.14	0.15	
1	7	6	v_s(fps)	0.15	0.29	0.28	0.13	0.14	
			x_m(ft)	-0.17	0.33	0.83	1.33	1.83	
1	8	2	v_s(fps)	0.16	0.26	0.29	0.19	0.16	
1	8	3	v_s(fps)	0.25	0.30	0.31	0.15	0.16	
1	8	4	v_s(fps)	0.31	0.36	0.35	0.17	0.17	
1	8	5	v_s(fps)	0.30	0.41	0.39	0.25	0.14	
1	8	6	v_s(fps)	0.28	0.43	0.49	0.26	0.14	
			x_m(ft)	-0.17	0.33	0.83	1.33	1.83	
1	9	5	v_s(fps)	0.34	0.46	0.43	0.26	0.14	
1	9	6	v_s(fps)	0.30	0.51	0.50	0.27	0.14	
			x_m(ft)	-0.17	0.33	0.83	1.33	1.83	
1	10	5	v_s(fps)	0.35	0.54	0.57	0.39	0.20	
1	10	6	v_s(fps)	0.49	0.63	0.58	0.41	0.20	
			x_m(ft)	0.30	0.53	0.80	1.06	1.47	1.76
2	1	6	v_s(fps)	1.68	1.76	1.64	1.57	1.15	0.93
			x_m(ft)	-0.06	0.24	0.54	0.84	1.24	1.64
2	2	5	v_s(fps)	1.17	1.65	1.69	1.57	1.30	0.79
2	2	6	v_s(fps)	1.10	1.57	1.61	1.56	1.23	0.85
			x_m(ft)	0.26	0.46	0.76	1.06	1.46	1.73
2	3	5	v_s(fps)	1.53	1.49	1.45	1.11	0.81	0.43
2	3	6	v_s(fps)	1.71	1.75	1.61	1.32	0.87	0.52

Table 1-6 (Continued)

I	J	K	X	1	2	3	4	5	6
			x_m(ft)	−0.06	0.24	0.54	0.84	1.24	1.64
2	4	5	v_s(fps)	0.63	1.51	1.66	1.36	0.31	0.34
2	4	6	v_s(fps)	0.83	1.38	1.53	1.33	0.88	0.39
			x_m(ft)	−0.06	0.24	0.54	0.84	1.14	1.54
2	5	5	v_s(fps)	0.97	1.22	1.27	1.13	0.70	0.36
2	5	6	v_s(fps)	0.78	1.21	1.27	1.19	0.77	0.43
			x_m(ft)	−0.06	0.24	0.54	0.84	1.14	1.53
2	7	5	v_s(fps)	0.36	0.73	0.90	0.85	0.44	0.15
2	7	6	v_s(fps)	0.44	1.03	0.95	0.70	0.46	0.17
			x_m(ft)	−0.07	0.22	0.54	0.84	1.24	1.64
2	8	5	v_s(fps)	0.80	1.25	1.30	1.04	0.75	0.27
2	8	6	v_s(fps)	0.74	1.30	1.42	1.10	0.72	0.30
			x_m(ft)	−0.06	0.24	0.54	0.84	1.24	1.64
2	10	5	v_s(fps)	1.27	1.58	1.53	1.44	1.15	0.84
2	10	6	v_s(fps)	1.30	1.75	1.75	1.63	1.23	0.92
			x_m(ft)	0.28	0.78	1.28	1.78		
3	1	5	v_s(fps)	2.07	1.85	1.41	0.70		
3	1	6	v_s(fps)	2.18	2.04	1.46	0.80		
			x_m(ft)	0.28	0.78	1.28	1.78		
3	2	5	v_s(fps)	1.73	1.71	1.07	0.56		
3	2	6	v_s(fps)	1.88	1.61	1.00	0.65		
			x_m(ft)	0.31	0.81	1.31	1.81		
3	3	5	v_s(fps)	2.04	1.79	0.98	0.53		
3	3	6	v_s(fps)	1.96	1.80	1.08	0.60		
			x_m(ft)	0.31	0.81	1.31	1.81		
3	4	5	v_s(fps)	1.82	1.74	0.99	0.51		
3	4	6	v_s(fps)	1.74	1.56	1.05	0.60		

Table 1-6 (Continued)

			X	1	2	3	4
I	J	K	x_m(ft)	0.31	0.81	1.31	1.81
3	5	5	v_s(fps)	1.02	0.85	0.46	0.41
3	5	6	v_s(fps)	0.82	0.78	0.57	0.44
			x(ft)	0.28	0.78	1.28	1.78
3	7	5	v_s(fps)	1.24	0.97	0.43	0.40
3	7	6	v_s(fps)	1.11	0.97	0.51	0.41
			x(ft)	0.31	0.81	1.31	1.81
3	8	5	v_s(fps)	1.60	1.33	0.64	0.47
3	8	6	v_s(fps)	1.49	1.24	0.70	0.49
			x_m(ft)	0.31	0.81	1.31	1.81
3	9	5	v_s(fps)	1.90	1.59	0.86	0.48
3	9	6	v_s(fps)	1.87	1.59	0.92	0.51
			x_m(ft)	0.31	0.81	1.31	1.81
3	10	5	v_s(fps)	2.16	1.74	1.11	0.59
3	10	6	v_s(fps)	2.08	1.92	1.25	0.61
			x_m(ft)	0.31	0.81	1.31	1.81
3	12	5	v_s(fps)	1.50	0.99	0.53	0.43
3	12	6	v_s(fps)	1.57	1.09	0.57	0.42

the beach is 10 or more times x_B for all runs, and that all waves break well inside the toe of the beach slope.

Since the models of the present investigation contain an empirical breaking criterion only one of the reported variables h_B and H_B may be used as input for model testing; h_B is selected since it requires one less free surface determination. The currents are assumed to represent $<v_s>$ in the absence of information specifying the location of dye injection. As with the GE data, the strong current $\tan\beta = 0.26$ runs of the PMT data are excluded from consideration on the assumption that the longshore current is accelerating convectively in the measured flow region. Table 1-7 lists the adopted data.

1.3.3 Brebner and Kamphuis (1963)

The third fixed bed data set adopted for use is that of Brebner and Kamphuis (1963), who report deep water wave characteristics H_o and θ_o as well as T. H is measured using an electric point gage seaward of a point where $h/L = 0.3$ on the actual sloping beach or an imaginary extension of this beach where L is the wavelength, while θ_G is measured from the relative alignment of the wave generator and the beach, with small amplitude wave theory adopted to compute the corresponding deep water values; the method of measuring T is unspecified. The beach surface is smooth concrete artificially roughened by indentations created by pressing a board with nailheads at one inch spacing into the concrete beach; in the absence of further details concerning the roughness, however, the smooth concrete $k_s = 0.001$ ft value is assumed. Brebner and Kamphuis (1963) note

16

Table 1-7

Putnam, Munk and Traylor (1949)

Data Used in Longshore Current Model Tests

I	k_s(ft)	$\tan\beta$	T(sec)	h_B(ft)	θ_B(o)	$<v_s>$ (fps)
1	0.0033	0.066	1.00	0.75	18.3	0.78
2	0.0033	0.066	1.06	0.44	13.8	0.64
3	0.0033	0.066	1.14	0.56	14.6	0.82
4	0.0033	0.066	1.15	0.41	12.6	0.68
5	0.0033	0.066	1.25	0.39	11.7	0.76
6	0.0033	0.066	1.32	0.40	11.7	0.75
7	0.0033	0.066	1.40	0.37	10.9	0.64
8	0.0208	0.098	0.95	0.36	30.1	1.03
9	0.0208	0.098	1.33	0.27	21.4	0.46
10	0.0208	0.098	1.67	0.20	18.0	0.20
11	0.0208	0.098	1.99	0.19	16.4	0.15
12	0.001	0.100	0.99	0.32	28.0	1.68
13	0.001	0.100	1.32	0.27	22.8	1.45
14	0.001	0.100	1.63	0.23	18.8	0.96
15	0.001	0.100	1.98	0.22	18.4	0.76
16	0.001	0.139	0.83	0.43	56.6	2.46
17	0.001	0.139	0.91	0.33	45.3	2.31
18	0.001	0.139	1.00	0.29	38.8	2.22
19	0.001	0.139	1.12	0.24	33.2	1.93
20	0.001	0.139	1.35	0.25	31.1	1.52
21	0.0033	0.144	1.90	0.24	17.6	0.75
22	0.0033	0.144	2.13	0.23	17.2	0.66
23	0.0033	0.144	2.22	0.24	17.3	0.50
24	0.0208	0.143	1.08	0.47	30.4	1.32
25	0.0208	0.143	1.36	0.38	24.6	0.63
26	0.0208	0.143	1.58	0.27	19.3	0.36
27	0.0208	0.143	1.91	0.26	18.4	0.32
28	0.0208	0.143	2.32	0.30	19.1	0.18
29	0.0033	0.241	0.72	0.48	18.2	1.33
30	0.0033	0.241	0.92	0.52	16.5	1.27
31	0.0033	0.241	1.14	0.28	10.4	0.53
32	0.0033	0.241	1.22	0.27	10.6	0.69

that the maximum longshore current v_s' is measured, using the timed travel of dye injected at a point just inside the breaker line and 15 to 20 ft downstream of the upstream training wall. Table 1-8 lists the data adopted for testing of the longshore current models.

Table 1-8

Brebner and Kamphuis (1963)

Data Used in Longshore Current Model Tests

$\tan\beta = 0.05$

I	H_o(ft)	θ_o(o)	T(sec)	v_s'(fps)
1	0.075	21.9	1.13	0.49
2	0.089	20.9	1.00	0.56
3	0.112	20.3	0.87	0.62
4	0.124	20.1	0.78	0.68
5	0.106	21.9	1.13	0.66
6	0.129	20.9	1.00	0.61
7	0.157	20.3	0.87	0.67
8	0.172	20.1	0.78	0.69
9	0.151	21.9	1.13	0.71
10	0.167	20.9	1.00	0.73
11	0.207	20.3	0.87	0.80
12	0.212	20.1	0.78	0.81
13	0.174	21.9	1.13	0.84
14	0.211	20.9	1.00	0.80
15	0.242	20.3	0.87	0.82
16	0.257	20.1	0.78	0.84
17	0.076	33.1	1.13	0.63
18	0.089	31.4	1.00	0.61
19	0.113	30.5	0.87	0.65
20	0.125	30.1	0.78	0.64
21	0.107	33.1	1.13	0.76
22	0.130	31.4	1.00	0.68
23	0.158	30.5	0.87	0.76
24	0.172	30.1	0.78	0.78
25	0.153	33.1	1.13	0.86
26	0.168	31.4	1.00	0.78
27	0.208	30.5	0.87	0.90
28	0.212	30.1	0.78	0.90
29	0.176	33.1	1.13	0.96
30	0.212	31.4	1.00	0.92

Table 1-8 (Continued)

tanβ = 0.05

I	H_o(ft)	θ_o(o)	T(sec)	v_s'(fps)
31	0.244	30.5	0.87	0.98
32	0.258	30.1	0.78	1.03
33	0.077	44.5	1.13	0.66
34	0.090	42.1	1.00	0.80
35	0.113	40.7	0.87	0.68
36	0.125	40.2	0.78	0.83
37	0.109	44.5	1.13	0.79
38	0.131	42.1	1.00	0.89
39	0.158	40.7	0.87	1.00
40	0.172	40.2	0.78	1.07
41	0.156	44.5	1.13	0.87
42	0.170	42.1	1.00	1.07
43	0.209	40.7	0.87	1.04
44	0.213	40.2	0.78	1.12
45	0.179	44.5	1.13	1.06
46	0.214	42.1	1.00	1.07
47	0.243	40.7	0.87	1.15

tanβ = 0.10

I	H_o(ft)	θ_o(o)	T(sec)	v_s'(fps)
1	0.075	21.9	1.13	0.44
2	0.089	20.9	1.00	0.47
3	0.112	20.3	0.87	0.67
4	0.124	20.1	0.78	0.82
5	0.106	21.9	1.13	0.49
6	0.129	20.9	1.00	0.67
7	0.157	20.3	0.87	0.83
8	0.172	20.1	0.78	0.99
9	0.151	21.9	1.13	0.63
10	0.167	20.9	1.00	0.80
11	0.207	20.3	0.87	0.96
12	0.212	20.1	0.78	1.07
13	0.174	21.9	1.13	0.63
14	0.211	20.9	1.00	0.88
15	0.242	20.3	0.87	1.04
16	0.257	20.1	0.78	1.16
17	0.076	33.1	1.13	0.60
18	0.089	31.4	1.00	0.81
19	0.113	30.5	0.87	0.84
20	0.125	30.1	0.78	0.91

Table 1-8 (Continued)

$\tan\beta = 0.10$

I	H_o(ft)	θ_o(o)	T(sec)	v_s'(fps)
21	0.107	33.1	1.13	0.83
22	0.130	31.4	1.00	0.97
23	0.158	30.5	0.87	1.04
24	0.172	30.1	0.78	1.14
25	0.153	33.1	1.13	0.94
26	0.168	31.4	1.00	1.12
27	0.208	30.5	0.87	1.25
28	0.212	30.1	0.78	1.32
29	0.176	33.1	1.13	1.07
30	0.212	31.4	1.00	1.25
31	0.244	30.5	0.87	1.29
32	0.258	30.1	0.78	1.32
33	0.077	44.5	1.13	0.70
34	0.090	42.1	1.00	0.83
35	0.113	40.7	0.87	0.88
36	0.125	40.2	0.78	1.05
37	0.109	44.5	1.13	0.91
38	0.131	42.1	1.00	0.96
39	0.158	40.7	0.87	1.10
40	0.172	40.2	0.78	1.22
41	0.156	44.5	1.13	1.08
42	0.170	42.1	1.00	1.18
43	0.209	40.7	0.87	1.36
44	0.213	40.2	0.78	1.53
45	0.179	44.5	1.13	1.21
46	0.214	42.1	1.00	1.34
47	0.243	40.7	0.87	1.48
48	0.077	44.5	1.13	0.66
49	0.090	42.1	1.00	0.74
50	0.113	40.7	0.87	0.90
51	0.125	40.2	0.78	1.03
52	0.109	44.5	1.13	0.85
53	0.131	42.1	1.00	0.95
54	0.158	40.7	0.87	1.10
55	0.172	40.2	0.78	1.26
56	0.156	44.5	1.13	1.03
57	0.170	42.1	1.00	1.14
58	0.209	40.7	0.87	1.35
59	0.213	40.2	0.78	1.56
60	0.179	44.5	1.13	1.09
61	0.214	42.1	1.00	1.29
62	0.243	40.7	0.87	1.42
63	0.081	56.7	1.13	0.61

Table 1-8 (Continued)

tanβ = 0.10

I	H_o(ft)	θ_o(o)	T(sec)	v_s'(fps)
64	0.092	53.1	1.00	0.75
65	0.113	51.0	0.87	0.89
66	0.125	50.3	0.78	1.06
67	0.113	56.7	1.13	1.02
68	0.133	53.1	1.00	0.97
69	0.159	51.0	0.87	1.13
70	0.172	50.3	0.78	1.35
71	0.163	56.7	1.13	1.06
72	0.173	53.1	1.00	1.19
73	0.209	51.0	0.87	1.43
74	0.213	50.3	0.78	1.52
75	0.187	56.7	1.13	1.29
76	0.218	53.1	1.00	1.43
77	0.246	51.0	0.87	1.73
78	0.258	50.3	0.78	1.79
79	0.092	70.9	1.13	0.74
80	0.096	64.7	1.00	0.83
81	0.115	61.5	0.87	0.87
82	0.125	60.5	0.78	0.99
83	0.130	70.9	1.13	0.86
84	0.139	64.7	1.00	1.01
85	0.161	61.5	0.87	1.10
86	0.173	60.5	0.78	1.25
87	0.186	70.9	1.13	1.03
88	0.180	64.7	1.00	1.15
89	0.212	61.5	0.87	1.28
90	0.214	60.5	0.78	1.48
91	0.214	70.9	1.13	1.12
92	0.227	64.7	1.00	1.27
93	0.248	61.5	0.87	1.42
94	0.259	60.5	0.78	1.66

1.4 Laboratory Longshore Sediment Transport Data

The data of Krumbein (1944), Saville (1949, 1950), Shay and Johnson (1951), Sauvage de Saint Marc and Vincent (1954), Savage (1962), Price and Tomlinson (1968) and Fairchild (1970) are available for use in the present investigation. Only Krumbein (1944), Saville (1949, 1950) and Shay and Johnson (1951) report the equilibrium beach profile data necessary to use the Linear Longshore Sediment Transport Model, thus most of the available data is excluded from the present investigation. Krumbein (1944) reports a nonuniform beach slope accompanied by beach cusps implying a longshore periodicity on his beach; this data is consequently neglected so that the experiments of Saville (1949, 1950) and Shay and Johnson (1951) comprise the laboratory longshore sediment transport data base of the present investigation. The two data sets are preferred to as SV and SJ, respectively in the present investigation.

1.4.1 Saville (1949, 1950)

Saville (1949, 1950) measures longshore currents and longshore sediment transport induced by two dimensional monochromatic water waves generated by a flap type wave generator set in a basin 66 ft x 122 ft, with h_G = 1.48 ft. The waves propagate without training wall refraction onto a movable bed 6 ft wide, 60 ft long, aligned at a 10° angle to the wave generator, and consisting of a uniform sand of median diameter d_s = 0.30 mm and specific gravity s = 2.69. The initial beach slope is 0.10 and tests are continued until equilibrium beach slopes are established, after which time the bottom profile is

22

measured across three shorenormal transects with a moving point gage. Wave period is measured by timing the motion of the generator and the breaker angle is obtained from overhead photographs, while wave height is measured at an unspecified location using a point gage. Saville (1949, 1950) reports deep water wave height values, obtained with linear wave theory. Longshore currents are measured by the timed travel of a dye injected into the surf zone at an unspecified location.

Sediment transport is measured at two locations along the beach. At the mid-beach location, shorenormal hoppers set flush to the beach surface are intended to measure longshore bed load, while a large trap at the downstream end of the beach measures the total longshore load, which is carried into the trap by a pump induced steady current. Sediment is introduced manually at the upstream end and just down-stream of the mid beach hoppers at rates equal to those measured in the large trap and the mid beach hoppers, respectively.

Table 1-9 shows the data that tests the Linear Longshore Sediment Transport Model. The bottom slope is computed in accordance with

$$\tan\beta = 0.134 - 0.94 \frac{H_o}{L_o} \qquad (.02 < \frac{H_o}{L_o} < .06) \qquad (1\text{-}1)$$

where L_o is deep water wave length given by the linear wave expression, e.g., Madsen (1976)

$$L_o = gT^2/2\pi \qquad (1\text{-}2)$$

with gravitational acceleration g. Eq. (1-1) is a least squares regression, e.g., Benjamin and Cornell (1970), on eight equilibrium pro-

23

Table 1-9

Saville (1949, 1950)

Data Used in Longshore Sediment Transport Model Tests

$h_G = 1.48$ ft $\qquad \theta_G = 10^\circ$

$d_s = 0.30$ mm $\qquad s = 2.69$

I	T(sec)	H_o(ft)	H_G(ft)	$<v_s>$(fps)	$\int_o^\infty q_s^y dx \ (\frac{\text{lbs dry}}{\text{hr}})$
1	0.74	0.15	0.15	0.32	23.3
2	0.85	0.13	0.13	0.27	40.2
3	0.94	0.12	0.12	0.25	62.6
4	1.00	0.11	0.10	0.21	56.8
5	0.74	0.17	0.17	0.40	29.9
6	0.85	0.15	0.15	0.32	48.7
7	0.99	0.13	0.12	0.24	88.2

files reported by Saville (1949) and by Shay and Johnson (1951); the measured slopes fall within 20% of the predicted values. Two of Saville's (1949, 1950) runs with exceptionally low deep water wave steepness ($\frac{H_o}{L_o} = 0.015, 0.007$) are discarded since the equilibrium profile exposes the lip of a concrete retaining wall under the breaker line, giving rise to a discontinuous bottom in the surf zone. The wave generator angle θ_G is used instead of θ_B since it is easier to measure, while H_G is computed from the reported H_o values using linear wave refraction, e.g., Madsen (1976) and the remaining data of Table 1-9. The reported longshore current data are taken to represent fully developed $<v_s>$ in the absence of knowledge about the de-

24

tails of dye injection, while the relative roughness is taken as the median grain size since Saville (1949, 1950) does not report the presence of bed forms in the surf zone. The sediment transport data are the total load figures measured in the large trap, selected because of the potential for the mid beach traps to collect sediment which would otherwise oscillate in the longshore direction due to a longshore component of the wave motion. It should be noted that the adopted transport data has inaccuracies of its own since the flow field is affected by wave diffraction near the basin wall and the current near the end of the beach is induced by a pump, not by waves. In defense of the data, the establishment of an equilibrium profile does require that the wave induced longshore current in the mid beach area transport sand at a rate equal to the supply and removal rate at either end of the test section and Saville (1949, 1950) runs his tests for 8 to 20 hours after equilibrium is established, presumably without further changes in bottom slope.

1.4.2 Shay and Johnson (1951)

Shay and Johnson (1951) measure longshore sediment transport in the same basin as Saville (1949, 1950) and, for the $\theta_G = 10^o$ runs which are the only data used in the present investigation, on the same beach as well. The test procedures are the same with the exception of the $\tan\beta$ determination, which is done by tracing the bottom profile onto a piece of sheet metal inserted normal to the shoreline. Shay and Johnson (1951) cite H_G values but do not report data for bed load transport or longshore current velocity for this generator angle.

25

Table 1-10 lists the data used in the present investigation. Shay and Johnson (1951) report equilibrium beach profiles for the $\theta_G = 10^{\circ}$ runs and for one 30° run; the profiles establish Eq. (1-1) which is used to compute the $\tan\beta$ values of Table 1-10. As with the Saville (1949, 1950) data, low wave steepness runs are ignored; this

Table 1-10

Shay and Johnson (1951)

Data Used in Longshore Sediment Transport Model Tests

$\theta_G = 10^{\circ}$		$d_s = 0.30$ mm		$S = 2.69$	
I	h_G(ft)	T(sec)	H_G(ft)	$\tan\beta$	$\int_0^{\infty} q_s^y dx$ ($\frac{\text{lbs dry}}{\text{hr}}$)
1	1.44	1.08	0.11	0.116	65.4
2	1.48	1.00	0.11	0.112	73.8
3	1.48	0.86	0.15	0.096	38.1

eliminates the 30° run and some 10° runs from the data base. The figures listed in Table 1-10 are averages of the Shay and Johnson (1951) data since the authors test a given set of experimental conditions several times and report each repeated run.

1.5 Field Longshore Sediment Transport Data

The data of Komar (1969), which are judged as the best available by Greer and Madsen (1978) in a review of field longshore sediment transport data, are the only data considered in the present investigation. The data are referred to as KO in the present investigation.

Komar (1969) measured longshore currents and longshore sediment transport at Silver Strand Beach near Coronado, California, from November 1967 to September 1968, and at El Moreno Beach on the northwest shore of the Gulf of California in Baja California, Mexico, from May 1966 to May 1968. The El Moreno data receives no further consideration since the longshore currents are large compared to the wave orbital velocity in violation of the linearizing assumptions of Table 1-1; the Silver Strand currents are small, however, so that the Silver Strand data constitutes the field data base of the present investigation.

E_i, θ_i and T_i, as listed in Table 1-11, are estimated by Komar (1969) from energy density spectra measured at an array of digital wave staffs and pressure transducers aligned parallel to the bottom contours in an unspecified depth of water; DAS is Komar's (1969) run index, E_i is the sum of the energy density of the ith wave train in the spectrum, T_i corresponds to the frequency containing peak energy density and θ_i is obtained from the phase lag between the wave sensors where there is good coherence between the periods of record at each sensor. When two or more energy density peaks are present two or more sets of parameters are presented, with the minimum energy density between adjacent peaks distinguishing one wave train from another. Small θ_i values preclude runs 132 and 133 from consideration since the data is more sensitive to errors in θ determination as θ approaches zero.

Komar (1969) measures longshore currents for three sets of the DAS runs by the timed travel of a dye patch or slightly buoyant floats placed in the surf zone.

Table 1-11

Komar (1969) - Silver Strand Beach

Reported Wave Data

DAS	T_i(sec)	$E_i(\frac{erg}{cm^2} \times 10^{-3})$	θ_i(o)	$[|\vec{E}_F|\cos\theta]_i\ (\frac{erg}{cm\ sec} \times 10^{-6})$
138	17.5	274	1.0	164
	7.58	537	9.6	300
139	18.2	338	0	203
	7.56	564	10.0	297
140	16.1	216	1.8	132
	7.56	619	8.1	332
198	14.2	53.9	6.4	30.9
	8.53	81.7	11.8	43.1
199	14.2	76.3	7.0	43.6
	8.53	89.2	12.4	46.9
200	12.8	92.0	6.7	51.9
	9.14	92.6	11.9	48.9
201	12.8	98.6	5.6	55.8
	8.53	71.9	13.3	37.6
	12.8	68.6	4.5	41.1
202	9.14	63.4	10.0	36.0
	5.78	46.5	−16.5	22.0
	12.8	82.7	6.8	49.4
203	9.14	69.6	9.3	39.4
	4.93	74.0	−8.3	32.8
	12.8	63.1	4.6	36.8
204	9.14	58.9	9.3	32.0
	5.13	49.3	−5.2	22.0
	12.8	50.6	8.1	29.3
205	9.14	88.9	8.8	48.4
	4.93	67.3	−2.0	36.3

Komar (1969) assumes that longshore sediment transport occurs as a sediment layer of constant thickness moving at a uniform velocity so that the transport rate determination consists of estimating the thickness and the longshore velocity of the layer. The thickness and velocity estimates for three sets of DAS runs are obtained at Silver Strand Beach by using core samples to measure the horizontal and vertical distribution of a fluorescent sand tracer three or four hours after its injection into the surf zone. Tracer injection and core sampling occur under submerged conditions at Silver Strand Beach since the tidal range is insufficient to expose an appreciable amount of the surf zone. The sediment comprising the beach is a uniform sand of median diameter 0.175 mm and specific gravity 2.65, with an average bottom slope of about 0.034.

Table 1-12 lists the data adopted for use in testing the Linear Longshore Sediment Transport Model. The longshore current data are the values reported by Komar (1969), while the total time averaged longshore sediment transport rates are mass flow rates computed from reported volumetric rates using Komar's (1969) suggested porosity of 0.4. It should be noted that the assumption of a spatially uniform moving layer underlying the transport data may be questioned on physical grounds since the longshore bottom shear stress imparting momentum to the layer varies with shorenormal distance, as discussed in Section 4.4.1. The assumption may be questioned on observational grounds as well since Komar's (1969) contours of tracer concentration show appreciable shorenormal variation which may be partially attributed to a varying moving layer velocity.

Table 1-12

Komar (1969) - Silver Strand Beach

Data Used in Longshore Sediment Transport Model Tests

$\tan\beta = 0.034$ $d_s = 0.175$ mm $s = 2.65$

DAS	h_G (cm)	H_G (cm)	T (sec)	θ_G (o)	$<v_s>$ (cm/sec)	$\int_o^\infty (q)_s^y dx$ (g m/sec x 10^{-3})
138-140	410	82	11.0	6.1	55.9	47.9
198-201	370	36	10.6	9.2	14.6	7.4
202-205	410	39	8.9	3.4	12.6	6.0

The wave parameters of Table 1-12 are equivalent monochromatic nonlinear wave parameters derived in the present investigation from Komar's (1969) reported data using wave energy considerations. The first task is to establish the time averaged water depth at the sensors where conditions are represented by the G subscript. In the course of his wave refraction calculations, Komar (1969) computes the shorenormal component of wave energy flux $\vec{E}_F$ for the ith wave train and reports the values in Table 1-11. As discussed in Section 3.1.3, the wave energy flux is a function of the time averaged water depth so that, using the linear theory originally employed by Komar (1969) the energy flux values of Table 1-11 yield estimates of h_G. The estimates for a given set of DAS runs are averaged to obtain h_G for the appropriate current and sediment transport measurements, as cited in Table 1-12.

With h_G established, representative values of H_G, T and θ_G are

derived to formulate a reasonable equivalent wave. First, the mono-
chromatic wave energy E defined by

$$E = \frac{\rho g H^2}{8} \tag{1-3}$$

is equated to the total spectral energy

$$E_G = \sum_{\text{wave trains}} E_i \tag{1-4}$$

thus providing an equivalent H_G. The wave energy flux given by

$$\vec{E}_F = E n \vec{c} \tag{1-5}$$

where n is the energy transport function, is used to generate the
equivalent period T in accordance with

$$|\vec{E}_F|_G T = \sum_{\text{wave trains}} (|\vec{E}_F| T)_i \tag{1-6}$$

with $(n|\vec{c}|)_G$, which is an implicit function of T, h_G and H_G, computed
using the nonlinear wave theory of Section 4.1.1 and $(n|\vec{c}|)_i$ computed
using linear theory and the data of Table 1-11. Finally, θ_G assures
equivalence of the longshore radiation stress tensor element, i.e.,
anticipating Eqs. (3-37)

$$(E\, n\, \cos\theta\, \sin\theta)_G = \sum_{\text{wave trains}} (E\, n\, \cos\theta\, \sin\theta)_i \tag{1-7}$$

where again n_G is computed with nonlinear wave theory and $(E\, n\, \cos\theta\sin\theta)_i$
is computed using linear theory and the data of Table 1-11. Table 1-12
presents appropriate DAS averages for the equivalent wave parameters.

31

The intent of all this reanalysis is to replace the spectral wave data with a plausible equivalent monochromatic wave whose properties are described by a wave theory consistent with that of the Linear Longshore Sediment Transport Model.

1.6 Outline of Present Investigation

The idealized environment and data base discussed in the preceding sections describe a relatively simple surf zone which may be analytically modeled and tested. The present investigation develops the Linear Longshore Current Model as an extension of an existing model by allowing for longshore nonuniformity and a finite wave height. The Linear Longshore Current Model in turn leads to the Linear Longshore Sediment Transport Model, which also allows for longshore nonuniformity and a finite wave height, and the Nonlinear Longshore Current Model. The Nonlinear Longshore Current Model approximates the effect of a finite longshore current as well as oblique wave incidence and a finite wave height, but is only valid for uniform longshore conditions.

The development proceeds in Section 2 with a statement of the conservation of mass and horizontal momentum in the surf zone, where the flow field is assumed to be comprised of highly simplified time averaged, wave and randomly fluctuating partitions. The conservation equations are depth integrated and time averaged using the approach of Phillips (1977) and they accordingly describe the transport of mass and horizontal momentum through a vertical column of fluid under a

32

unit free surface area; the forces and gradients of horizontal momen-
tum flux in the momentum equation appear as a balance of convective,
local driving, Reynolds, bottom shear and wave setup stresses in the
surf zone. The section concludes by presenting a modification of
Battjes' (1974) breaker parameter ξ_B, which characterizes useful em-
pirical knowledge of surf zone hydrodynamics observed by other in-
vestigators.

The analysis of Longuet-Higgins (1970) is restated, with minor
modifications, in Section 3 to describe the stresses under the assump-
tions of longshore uniformity, linear long waves of near normal incid-
ence and a relatively small current. The resulting differential
balance of stresses is linearized and cast into a governing differ-
ential equation closely resembling that of Longuet-Higgins (1970)
with the local driving stress balanced by shorenormal wave setup and
longshore Reynolds and linearized bottom shear stress components. The
resulting solution, which is termed the Modified Longuet-Higgins Model,
is comprised of the modified bottom slope $\tan\Delta$ and the longshore cur-
rent profile $v_c v^*$ where v^* is the dimensionless form of the profile
and v_c is the dimensional scale. With the Modified Longuet-Higgins
Model as bakcground, a brief survey of other existing momentum based
uniform longshore current profile models is presented.

The Linear Longshore Current Model, Linear Longshore Sediment
Transport Model and Nonlinear Longshore Current Model are derived in
Section 4. All three models assume that the modified bottom slope
satisfies the shorenormal momentum equation and the form of the long-

33

shore current profile $v*$ is similar to that of the Modified Longuet-Higgins Model with scaling reduced to account for the effects of a finite wave height. A modification of Madsen's (1976a) empirical breaking criterion is also included in the models to facilitate longshore current and longshore sediment transport prediction when offshore wave parameters are known.

The Linear Longshore Current Model integrates the depth integrated conservation of mass and longshore momentum equations from the mean shore line to the breaker line in the presence of longshore nonuniformity introduced by a shorenormal jetty. The resulting integrated linear longshore stress balance which neglects wave diffraction, is similar to the balance analyzed by Eagleson (1966) with the added inclusion of a longshore Reynolds stress component. The nonuniformity acts to further reduce the scale of the longshore current since part of the driving stress is spent on current acceleration, which appears as the convective stress term in the balance. The convective current reduction factor λ_1 is the analytical solution to the integrated linear longshore stress balance governing the motion.

The Linear Longshore Sediment Transport Model is derived by assuming a steady flow sediment transport formula to be valid on an instantaneous basis in the surf zone, following the approach of Reyman (1976). The formula, which is proposed by Madsen and Grant (1976a) for nonbreaking wave motion, relates longshore sediment transport and the longshore bottom shear stress component of the Linear Longshore Current Model and is considered on a time averaged, shorenormal integrated basis.

The Nonlinear Longshore Current Model presents the nonlinear current reduction factor λ_2 which models nonlinear bottom shear stress due to a finite current under uniform longshore conditions. λ_2 is the solution to the integrated longshore stress balance for uniform longshore conditions with the nonlinear bottom shear term evaluated on a numerical basis. The nonlinear current reduction factor is expressed as a curve fitted function of wave and beach parameters.

The bottom and Reynolds stresses of the Linear Longshore Current Model and the Nonlinear Longshore Current Model are characterized by the surf zone friction factor f_{sz} and the lateral mixing coefficient Γ respectively, and it is the business of Section 5 to establish and test physically plausible predictors of these parameters using the fixed bed data of Section 1. The resulting predictors are assumed valid for movable beds and the longshore sediment transport coefficient ζ relating longshore bottom shear stress and sediment transport components is subsequently calibrated using the laboratory movable bed and field data of Section 1.

The three models are critically evaluated in Section 6 with emphasis on model inconsistencies and systematic errors in model testing in order to identify areas for future model improvement. The investigation closes with Appendices I and II which present numerical examples of the three models and a listing of computer subroutines, respectively.

2 STRESS BALANCE AND SURF ZONE EMPIRICISM

2.1 Flow Field Partitions

The instantaneous velocity and free surface elevation in the surf zone are assumed to be comprised of uncorrelated partitions

$$\vec{u} = \vec{u}_s + \vec{u}_w + \vec{u}_f \tag{2-1}$$

$$\eta = \eta_s + \eta_w \tag{2-2}$$

where the s, w and f subscripts denote time averaged, wave and randomly fluctuating partitions, respectively. The shorenormal and longshore velocity components are further assumed to be constant with depth, i.e.,

$$\frac{\partial u}{\partial z} = \frac{\partial v}{\partial z} = 0 \tag{2-3}$$

The assumed specification of surf zone hydrodynamics is extended by the adoption of hydrostatic pressure,

$$p = \rho g (\eta - z) \tag{2-4}$$

where p is instantaneous pressure and ρ is fluid density.

The justification of these highly simplified partitions rests on the analytical simplicity of the resulting models along with the models' ability to match longshore current and longshore sediment transport predictions with the data of Section 1.

In keeping with model simplicity, the wave partition is treated as a monochromatic long wave, while the contribution of the randomly fluctuating partition to the surf zone hydrodynamics is taken to be

36

the result of nonzero correlations of fluctuating velocity components, so that η_f and P_f are ignored in the present investigation.

The assumed vertical homogeneity of Eq.(2-3) is consistent with the longshore current and sediment transport data base, which is comprised of single values of flow parameters at given (x,y) locations; the homogeneity also anticipates the treatment of the conservation equations on a depth integrated basis. The field data of Meadows (1976) suggest that v_s does not vary appreciably with depth in the surf zone.

2.2 Conservation of Mass Equation

Consider the instantaneous conservation of mass equation for a homogeneous, incompressible fluid

$$\frac{\partial u}{\partial x} + \frac{\partial v}{\partial y} + \frac{\partial w}{\partial z} = 0 \tag{2-5}$$

with vertical velocity component w. Following Phillips (1977), Eq. (2-5) is integrated over the instantaneous water depth using kinematic boundary conditions and Leibnitz's Rule with the result

$$\frac{\partial}{\partial x} [u(\eta + d)] + \frac{\partial}{\partial y} [v(\eta + d)] + \frac{\partial}{\partial t} (\eta + d) = 0 \tag{2-6}$$

where the vertical homogeneity of Eq. (2-3) is invoked and d is the still water depth.

Expanding and time averaging Eq. (2-6) in view of the assumed partitions of Eqs. (2-1) and (2-2), the depth integrated, time averaged conservation of mass equation is obtained for steady flow

$$\frac{\partial}{\partial x} [u_s h + (u_w \eta_w)_s] + \frac{\partial}{\partial y} [v_s h + (v_w \eta_w)_s] = 0 \tag{2-7}$$

37

with the shorenormal wave and current components u_w and u_s, and longshore wave orbital velocity component v_w. Eq. (2-7) describes the time averaged transport of fluid mass through a column of fluid under a unit area of the free surface, making use of the relation

$$h = d + \eta_s \qquad\qquad\qquad (2\text{-}8)$$

which follows from the definitions of h, d and η.

2.3 Conservation of Horizontal Momentum Equation

The surf zone stress balance is the depth integrated, time averaged conservation of horizontal momentum equation describing the hydrodynamics of the surf zone in the absence of the stresses and accelerations of Table 1-2.

2.3.1 Depth integration

Consider the instantaneous conservation of horizontal momentum for a homogeneous incompressible fluid in the absence of Coriolis acceleration, e.g., White (1974)

$$\rho\left\{\frac{\partial u}{\partial t} + \frac{\partial(u^2)}{\partial x} + \frac{\partial(uv)}{\partial y} + \frac{d(uw)}{\partial z}\right\} = -\frac{\partial p}{\partial x} + \frac{\partial \tau^x}{\partial z}$$

$$\qquad\qquad\qquad (2\text{-}9)$$

$$\rho\left\{\frac{\partial v}{\partial t} + \frac{\partial(vu)}{\partial x} + \frac{\partial(v^2)}{\partial y} + \frac{\partial(vw)}{\partial z}\right\} = -\frac{\partial p}{\partial y} + \frac{\partial \tau^y}{\partial z}$$

The shear stresses τ^x, τ^y are assumed to be confined to thin layers at the fluid boundaries; these boundaries are presumed to be essentially horizontal so that vertical gradients dominate horizontal gradients. The superscripts denote vector component direction and t is time.

38

Following Phillips (1977), Eq.(2-9) is integrated over the
instantaneous water depth using Leibnitz' Rule and appropriate kine-
matic boundary conditions with the result

$$\rho\{\frac{\partial}{\partial t} (\int_{-d}^{\eta} u dz) + \frac{\partial}{\partial x} (\int_{-d}^{\eta} u^2 dz) + \frac{\partial}{\partial y} (\int_{-d}^{\eta} uv dz)\}$$

$$= -\frac{\partial}{\partial x} (\int_{-d}^{\eta} p dz) + p_\eta \frac{\partial \eta}{\partial x} + p_b \frac{\partial d}{\partial x} + \tau_\eta^x - \tau_b^x$$

$$\text{(2-10)}$$

$$\rho\{\frac{\partial}{\partial t} (\int_{-d}^{\eta} v dz) + \frac{\partial}{\partial x} (\int_{-d}^{\eta} vu dz) + \frac{\partial}{\partial y} (\int_{-d}^{\eta} v^2 dz)\}$$

$$= -\frac{\partial}{\partial y} (\int_{-d}^{\eta} p dz) + p_\eta \frac{\partial \eta}{\partial y} + p_b \frac{\partial d}{\partial x} + \tau_\eta^y - \tau_b^y$$

where the η and b subscripts denote conditions at the free surface
and bottom, respectively.

The RHS of Eq. (2-10) may be simplified using the hydrostatic
pressure distribution of Eq. (2-4) to integrate out the pressure term

$$-\frac{\partial}{\partial x} (\int_{-d}^{\eta} p dz) = -p_b (\frac{\partial d}{\partial x} + \frac{\partial \eta}{\partial x})$$

$$\text{(2-11)}$$

$$-\frac{\partial}{\partial y} (\int_{-d}^{\eta} p dz) = -p_b (\frac{\partial d}{\partial y} + \frac{\partial \eta}{\partial y})$$

where

$$p_b = \rho g (\eta + d)$$

and p_η is arbitrarily set equal to 0 in the absence of an atmospheric

39

pressure gradient. The viscous shear stress at the free surface must be negligible in the absence of wind so that τ^x_η and τ^y_η vanish as well. Incorporating these simplifications into Eq. (2-10)

$$\rho\{\frac{\partial}{\partial t}[u(\eta + d)] + \frac{\partial}{\partial x}[u^2(\eta + d)] + \frac{\partial}{\partial y}[uv(\eta + d)]\}$$

$$= -\rho g(\eta + d)\frac{\partial \eta}{\partial x} - \tau^x_b$$

$$\rho\{\frac{\partial}{\partial t}[v(\eta + d)] + \frac{\partial}{\partial x}[vu(\eta + d)] + \frac{\partial}{\partial y}[v^2(\eta + d)]\}$$

$$= -\rho g(\eta + d)\frac{\partial \eta}{\partial y} - \tau^y_b$$

(2-12)

where vertical homogeneity is invoked.

2.3.2 Time averaging

The surf zone stress balance is obtained by substituting the flow partitions of Eqs. (2-1) and (2-2) into Eq. (2-12) and time averaging. The local acceleration terms vanish identically for steady time average flow while a typical expanded convection term is given by

$$\frac{\partial}{\partial x}[uv(\eta + d)]_s$$

(2-13)

$$= \frac{\partial}{\partial x}\{[u_s v_s + (u_w v_w)_s + (u_f v_f)_s]h + u_s(v_w \eta_w)_s + v_s(u_w \eta_w)_s\}$$

and a typical pressure term is

$$-\rho g[(\eta + d)\frac{\partial \eta}{\partial x}]_s = -\rho g[h\frac{\partial \eta_s}{\partial x} + \frac{\partial(\eta_w^2)_s}{2\partial x}]$$

(2-14)

where u_f and v_f are shorenormal and longshore velocity fluctuations. Time averaging Eq. (2-12) and then regrouping terms

$$\vec{A}_s + \vec{S}_w + \vec{T}_f + (\vec{\tau}_b)_s = \vec{P}_w \qquad (2\text{-}15)$$

Eq. (2-15) is a stress balance because the depth integration focuses attention on a column of fluid under a unit area of the free surface so that the forces and gradients of momentum flux appear as a balance of stresses. Following White (1974), a positive stress is a net efflux of positive momentum from this column.

The wave setup term $\vec{P}_w$ is the stress exerted by a tilting water surface, i.e.,

$$\vec{P}_w = -\rho g h \left[\frac{\partial \eta_s}{\partial x} \vec{i} + \frac{\partial \eta_s}{\partial y} \vec{j} \right] \qquad (2\text{-}16)$$

It is treated as an external stress since it contains no momentum flux terms; the pressure gradient is positive in the direction of decreasing free surface elevation.

The convective $\vec{A}_s$, local driving $\vec{S}_w$ and Reynolds $\vec{T}_f$ stresses are the horizontal gradients of the convection A^{ij}, radiation S^{ij} and fluctuation T^{ij} stress tensors which describe the depth integrated flux of horizontal momentum due to steady, wave and randomly fluctuating partitions, respectively. Thus

$$\vec{A}_s = \left[\frac{\partial A^{xx}}{\partial x} + \frac{\partial A^{yx}}{\partial y} \right] \vec{i} + \left[\frac{\partial A^{xy}}{\partial x} + \frac{\partial A^{yy}}{\partial y} \right] \vec{j} \qquad (2\text{-}17)$$

$$\vec{S}_w = \left[\frac{\partial S^{xx}}{\partial x} + \frac{\partial S^{yx}}{\partial y} \right] \vec{i} + \left[\frac{\partial S^{xy}}{\partial x} + \frac{\partial S^{yy}}{\partial y} \right] \vec{j} \qquad (2\text{-}18)$$

41

$$\vec{T}_f = [\frac{\partial T^{xx}}{\partial x} + \frac{\partial T^{yx}}{\partial y}]\ \vec{i} + [\frac{\partial T^{xy}}{\partial x} + \frac{\partial T^{yy}}{\partial y}]\ \vec{j} \tag{2-19}$$

where

$$A^{ij} = \rho \begin{vmatrix} [u_s^2 h + 2u_s(u_w \eta_w)_s] & [u_s v_s h + u_s(v_w \eta_w)_s + v_s(u_w \eta_w)_s] \\ [u_s v_s h + u_s(v_w \eta_w)_s + v_s(u_w \eta_w)_s] & [v_s^2 h + 2v_s(v_w \eta_w)_s] \end{vmatrix} \tag{2-20}$$

$$S^{ij} = \rho \begin{vmatrix} [(u_w^2)_s h + \frac{g(\eta_w^2)_s}{2}] & [(u_w v_w)_s h] \\ [(u_w v_w)_s h] & [(v_w^2)_s h + \frac{g(\eta_w^2)_s}{2}] \end{vmatrix} \tag{2-21}$$

$$T^{ij} = \rho \begin{vmatrix} [(u_f^2)_s h] & [(u_f v_f)_s h] \\ [(u_f v_f)_s h] & [(v_f^2)_s h] \end{vmatrix} \tag{2-22}$$

with column j indicating a transport of j momentum in the row i direction. $\vec{i}$ and $\vec{j}$ are unit shorenormal and longshore vectors, respectively. The concept of a radiation stress is due to Longuet-Higgins and Stewart (1960), who derive the tensor as a second order phenomenon associated with small amplitude wave propagation in water of intermediate depth. The use of the term "Reynolds stress" in the present investigation should not be confused with the classical definition, e.g., White (1974), which associates the term with the fluctuating velocity correlation at a given location in the flow field.

42

The present investigation defines the Reynolds stress as the horizontal gradient of the depth integrated fluctuating velocity correlation, as suggested by Eq. (2-19).

The time averaged bottom shear stress $(\vec{\tau}_b)_s$ is modeled with a time averaged drag law expression based on near bottom wave orbital and current partitions

$$(\vec{\tau}_b)_s = \frac{1}{2} \rho f_{sz} [(\vec{u}_s + \vec{u}_w)_b |\vec{u}_s + \vec{u}_w|_b]_s \tag{2-23}$$

where the surf zone friction factor f_{sz} is assumed to be independent of time and space. The justification of Eq. (2-23) and indeed of the present modeling approach rests on the physically plausible behavior of the surf zone friction factor when it is calibrated with the data base of Section 1.

2.4 Surf Zone Empiricism

The solutions of the stress balance developed in the present investigation ignore the observed surf zone phenomena of wave runup, wave reflection, longshore periodicity and air entrainment while assuming a linear wave height variation within the breaker line. The surf zone empiricism of this section demonstrates that these assumptions are reasonable when

$$0.3 < \xi_B < 0.7 \tag{2-24}$$

where ξ_B is the modified Battjes breaker parameter.

43

2.4.1 Modified Battjes breaker parameter

The complexity of the actual fluid motion in the surf zone leaves ample room for useful empirical models of various aspects of surf zone hydrodynamics. A good deal of information is conveyed by Battjes' (1974) breaker parameter ξ_B for waves of normal incidence breaking on plane beaches, where

$$\xi_B = \frac{\tan\beta}{(H_B/L_o)^{1/2}} \qquad (\theta = 0) \qquad (2\text{-}25)$$

Battjes (1974) notes that ξ_B may be considered as the ratio of bottom slope to breaking wave steepness. This interpretation suggests a modified Battjes breaker parameter defined for waves of oblique incidence

$$\xi_B = \frac{\gamma_B \tan\beta \cos\theta_B}{(2\pi\alpha_B)^{1/2}} \qquad (2\text{-}26)$$

where the $\cos\theta_B$ factor reflects the decreased bottom slope in the oblique direction of wave propagation. $(H_B/L_o)^{1/2}$ is expressed for later convenience in terms of relative wave length and height parameters γ and α, respectively, evaluated at breaking, where

$$\gamma = T(g/h)^{1/2} \qquad (2\text{-}27)$$

$$\alpha = H/h \qquad (2\text{-}28)$$

The relative wave length and height parameters govern wave propagation, as discussed in Section 4.1.1.

44

Battjes' breaker parameter, which is based on the work of earlier
investigators, characterizes such surf zone features as wave runup,
wave reflection, longshore periodicity, linear wave decay and air
entrainment. The empirical expressions describing these phenomena,
although based on normal wave incidence, are assumed to be valid for
waves of oblique incidence in light of their qualitative use in the
present investigation.

Using Galvin's (1968) breaker classification system and data,
which are also for waves of normal incidence, Battjes (1974) estab-
lishes the transitional ξ_B values of Table 2-1; in view of Eq. (2-24),
the present investigation studies transitional spilling-plunging
breakers.

Table 2-1

Battjes (1974) and Galvin (1968)

Transitional ξ_B Values - Breaker Classification

ξ_B Values	Breaker Classification
$\xi_B > 2.0$	Surging or Collapsing
$2.0 > \xi_B > 0.4$	Plunging
$0.4 > \xi_B$	Spilling

2.4.2 Wave runup and the swash zone

Hunt's (1959) empirical equation describing wave runup for break-
ing waves normally incident on plane slopes may be approximated using
ξ_B in accordance with

45

$$\eta_r/H_B \cong \xi_B \qquad (\xi_B < 2.3) \qquad\qquad\qquad (2\text{-}29)$$

where wave runup η_r is the vertical distance between the swash mark and the still water level.

The importance of the swash zone, which is the region between maximum and minimum shore lines, is reflected in the ratio η_s'/η_r, where η_s' (see Figure 1.1) is the vertical distance between the time averaged shore line and the still water level. As η_s'/η_r approaches unity, the instantaneous shore line approaches its time averaged position and the swash zone decreases in importance; a condition which is physically appropriate for an analytical model that assumes the continuous presence of water over the majority of the surf zone. When η_s'/η_r decreases, the swash zone dominates the surf zone as is the case for strongly plunging breakers with their higher ξ_B values, and a different approach than that of the present analysis may be warranted.

The wave setup model of Section 3.1.3 yields an expression for the maximum wave setup. Substituting x=0 into Eq. (3-32),

$$\eta_s' = \frac{3\alpha_B^2 h_B}{8} \qquad\qquad\qquad (2\text{-}30)$$

so that the desired ratio is simply

$$\eta_s'/\eta_r = \frac{3\alpha_B}{8\xi_B} \qquad (\eta_s'/\eta_r < 1) \qquad\qquad (2\text{-}31)$$

The upper limit of Eq. (2-24) yields a minimum η_s'/η_r ratio of about

46

0.5; the data of Bowen, Inman and Simmons (1968) suggest that this may be conservatively low.

2.4.3 Wave reflection and longshore periodicity

Battjes (1974) demonstrates that ξ_B may also be used to assess the importance of wave reflection of normally incident waves on impermeable slopes with

$$R \overset{\sim}{=} 0.1 \ \xi_B^2 \qquad (R < 1) \tag{2-32}$$

where R is the ratio of reflected to incident wave height. It should be noted that Battjes (1974) expresses Eq. (2-32) in terms of H_G where, in the context of a breakwater, H_G is based on the wave height at the intersection of the slope $\tan\beta$ with a much flatter bottom. Anticipating the use of Eq. (2-32) as an indicator of the order of magnitude of reflection, and noting that wave height appears to the one-half power in the definition of ξ_B, the use of ξ_B in Eq. (2-32) is judged to be appropriate, particularly since Battjes (1974) assumes $H_G = h_G$ to interpret ξ_B as the ratio of bottom slope to breaking wave steepness.

The upper ξ_B limit of Eq. (2-24) thus insures that R < 0.1 so that, with wave energy proportional to H^2, reflected wave energy will be less than 1% of the incident wave energy.

Battjes' breaker parameter may also be related to the occurrence of edge waves, which are periodic in the longshore direction and accordingly give rise to such longshore periodic phenomena as rip currents and beach cusps. Minzoni and Whitham (1977), drawing upon prior stud-

47

ies, suggest that a normally incident wave of frequency ω can generate an edge wave of one half the incident wave frequency when the parameter $\dfrac{\omega^2 a_s}{g \tan^2 \beta}$ falls within the range

$$0.8 < \frac{\omega^2 a_s}{g \tan^2 \beta} < 2 \qquad (2\text{-}33)$$

where a_s is the incident wave amplitude at the time averaged shore line and the limits are imposed by dissipation induced by viscosity and wave breaking. If a_s is taken as the breaking wave amplitude, then Eq. (2-33) may be expressed as a ξ_B based criterion for half-harmonic edge wave generation

$$2 > \xi_B > 1 \qquad (2\text{-}34)$$

In view of Eqs.(2-24) and (2-34) half-harmonic edge waves are excluded from consideration in the present investigation. It should be noted that analytical and experimental studies find edge waves at much lower frequencies for spilling breakers; these are also ignored because the low frequencies imply longshore length scales much greater than the characteristic horizontal length scale x_B.

2.4.4 Other surf zone characteristics

Analytical modeling of surf zone hydrodynamics is greatly facili-tated by assuming a linear wave height variation inside the breaker line, i.e.,

$$H = \alpha_B h \qquad (x \le x_B) \qquad (2\text{-}35)$$

48

Laboratory data for breaking waves normally incident on plane slopes, e.g., Bowen et al. (1968) and Horikawa and Kuo (1966) show that the linear variation is reasonably valid for surf zones satisfying the ξ_B range of Eq. (2-24) and, in contrast to popular belief, these data suggest that Eq. (2-35) is inappropriate for waves with ξ_B values well within the spilling breaker range.

As noted by Galvin (1968), plunging breakers entrain more air than spilling breakers in violation of the Table 1-1 assumption of homogeneous, incompressible fluid so that the neglect of air entrainment provides another reason for an upper ξ_B limit.

49

3 MODIFIED LONGUET-HIGGINS MODEL

As suggested by Table 1-1, the Modified Longuet-Higgins Model pre-
dicts longshore currents induced by waves of near normal incidence
breaking over an infinite beach. The model invokes the implied long-
shore homogeneity and assumes linear long wave theory and a relatively
small current to reduce the stress balance of Eq. (2-15) to

$$S_w^x = P_w^x$$

$$S_w^y + T_f^y + (\tau_b^y)_s = 0$$

(3-1)

where $\vec{S}_w$ and T_f^y are comprised of shorenormal gradients only. The modi-
fied bottom slope of Eq. (3-30) is the solution the shorenormal compon-
ent of Eq. (3-1) while the longshore current of Eqs. (3-61), (3-62) and
(3-76) is the solution to the longshore component of Eq. (3-1).

3.1 Modified Bottom Slope

3.1.1 Shorenormal current

The Modified Longuet-Higgins Model uses linear long wave theory to
describe the wave partition of the assumed flow field so that, recalling
Eq. (2-28),

$$u_w \vec{i} + v_w \vec{j} = \frac{\alpha}{2} (gh)^{1/2} \cos\phi [-\cos\theta \vec{i} + \sin\theta \vec{j}]$$

(3-2)

$$\phi = -kx \cos\theta + ky \sin\theta - \omega t$$

(3-3)

$$\eta_w = \frac{H}{2} \cos\phi$$

(3-4)

where wave reflection is neglected in accordance with the discussion

50

of Section 2.4.3 and the wave propagates with a component in the negative x direction, ϕ is the phase angle and k is the wavenumber. The linear long wave theory and the conservation of mass equation combine to provide an estimate of the shorenormal current strength.

Noting that the infinite beach assumption and neglect of longshore periodicity adopted in the Modified Longuet-Higgins Model preclude longshore gradients, the depth integrated, time averaged conservation of mass equation of Section 2.2 becomes

$$u_s = - \frac{(u_w \eta_w)_s}{h} \tag{3-5}$$

after shorenormal integration from 0 to x. Recalling linear long wave theory, and Eq. (2-28)

$$u_s = \frac{\alpha^2}{8} (gh)^{1/2} \cos\theta \tag{3-6}$$

so that u_s flows seaward to balance the wave induced shoreward mass transport. Comparing the shorenormal current and wave components,

$$u_s/u_w' = \alpha/4 \tag{3-7}$$

where u_w' is the maximum shorenormal orbital velocity. Since α is of order unity in the surf zone, the shorenormal wave velocity dominates the shorenormal current in the Modified Longuet-Higgins Model.

3.1.2 Shorenormal convective and bottom shear stresses inside the breaker line

Recalling Eqs. (2-15)-(2-19), the absence of longshore gradients simplifies the shorenormal component of the stress balance to

51

$$A_s^x + S_w^x + T_f^x + (\tau_b^x)_s = P_w^x \qquad (3\text{-}8)$$

where

$$A_s^x = \frac{dA^{xx}}{dx} \quad , \quad S_w^x = \frac{dS^{xx}}{dx} \quad , \quad T_f^x = \frac{dT^{xx}}{dx}$$

In view of Eqs. (2-20) and (2-21), the smallness of the shorenormal current suggests that the shorenormal wave induced momentum flux dominates the current induced flux so that A_s^x is neglected.

Evaluating the shorenormal radiation stress tensor component for linear long waves

$$S^{xx} = \frac{\rho g H^2}{8} \left(\cos^2\theta + \frac{1}{2}\right) \qquad (3\text{-}9)$$

so that for near normal incidence, the local driving stress inside the breaker line becomes

$$S_w^x = \frac{3\rho \alpha_B^2}{8} \, gh \, \frac{dh}{dx} \qquad (x \leq x_B) \qquad (3\text{-}10)$$

where the positive sign suggests a net influx of negative shorenormal momentum and the linear wave height decay of Eq. (2-35) is used.

Recalling Eq. (2-23) the bottom shear stress is a function of the norm of the near bottom wave and current velocity, which may be expressed as

$$|\vec{u}_s + \vec{u}_w|_b = \left(|\vec{u}_s|^2 + |\vec{u}_w|_b^2 + 2\{u_s u_w + v_s v_w\}\right)^{1/2} \qquad (3\text{-}11)$$

The Modified Longuet-Higgins Model linearizes the time averaged bottom shear stress by assuming a relatively small current

$$|\vec{u}_s| \ll |\vec{u}_w|_b' \qquad (3\text{-}12)$$

52

and waves of near normal incidence

$$v_w \ll u_w \qquad\qquad (3\text{-}13)$$

Eliminating the lowest order terms from consideration, the near bottom wave and current velocity norm may be approximated as

$$|\vec{u}_s + \vec{u}_w|_b \simeq |\vec{u}_w|'_b \left(\cos^2\phi - 2\,\frac{u_s}{|\vec{u}_w|'_b}\,\cos\theta\cos\phi\right)^{1/2} \qquad (3\text{-}14)$$

where $|\vec{u}_w|'_b$ is used to normalize the expression and the wave component is expressed in the form of Eq. (3-2). The small current assumption permits Taylor expansion of Eq. (3-14),

$$\left[|\vec{u}_s + \vec{u}_w|_b\right] \simeq |\vec{u}_w|'_b \left(|\cos\phi| - \frac{u_s}{|\vec{u}_w|'_b}\,\cos\theta\,\frac{\cos\phi}{|\cos\phi|}\right) \qquad (3\text{-}15)$$

Using Eq. (3-15) in the time averaging process, with $\cos^2\theta \sim 1$,

$$\left[(\vec{u}_s + \vec{u}_w)_b |\vec{u}_s + \vec{u}_w|_b\right]_s \sim |\vec{u}_w|'_b |\cos\phi|_s (2u_s\vec{i} + v_s\vec{j}) \qquad (3\text{-}16)$$

Accordingly, recalling Eq. (2-23), the linearized time averaged bottom shear stress is given by

$$(\vec{\tau}_b)_s = \frac{\rho f_{sz}}{\pi} |\vec{u}_w|'_b (2u_s\vec{i} + v_s\vec{j}) \qquad (3\text{-}17)$$

Comparing the shorenormal local driving and time averaged bottom shear stresses inside the breaker line,

$$(\tau_b^x)_s / S_w^x \simeq \frac{\alpha_B f_{sz}}{3\pi \left(\frac{dh}{dx}\right)} \qquad (x \le x_B) \qquad (3\text{-}18)$$

53

Taking the flat, rough beach data of Table 3-1 as a worst case, the estimate of Eq. (3-18) suggests that $(\tau_b^x)_s / S_w^x < 0.2$ so that bottom shear may be neglected in the shorenormal momentum equation inside the breaker line.

Table 3-1

Typical Wave and Beach Parameters

$\alpha_B = 1.0$		
$\dfrac{dh}{dx} = \tan\Delta = 0.01$	flat beach	
$\dfrac{dh}{dx} = \tan\Delta = 0.10$	steep beach	
$f_{sz} = 0.02$	rough beach	
$f_{sz} = 0.005$	smooth beach	

3.1.3 Shorenormal Reynolds stress inside the breaker line

Recalling Eqs. (2-19), (2-22) and (3-8), the shorenormal Reynolds stress component is given by

$$T_f^x = \rho \frac{d}{dx}[(u_f^2)_s h] \qquad (3-19)$$

This stress may be approximated by

$$T_f^x \stackrel{\sim}{=} \rho \frac{d}{dx}[|\vec{u}_f|_s^2 h] \qquad (3-20)$$

since u_f is perfectly correlated with itself and may reasonably be assumed to be of the order $|\vec{u}_f|_s$, where $|\vec{u}_f|_s$ characterizes the largest eddies of the turbulence, which carry most of the momentum.

54

The characteristic randomly fluctuating velocity inside the breaker line is estimated as

$$|\vec{u}_f|_s = (D_{sz}/\rho)^{1/3} \qquad (x \le x_B) \qquad (3\text{-}21)$$

Battjes (1975) equates an inviscid estimate of turbulent energy dissipation to the wave energy dissipation rate inside the breaker line D_{sz} to obtain Eq. (3-21). This estimate is physically appropriate in that the randomly fluctuating velocity partition is explicitly related to the wave breaking process producing the turbulence; equating the turbulent energy production and dissipation is reasonable in view of the neglect of air entrainment which, by virtue of compressibility, would provide an alternative sink of energy.

The divergence theorem, e.g., Hildebrand (1962) for wave energy in the absence of longshore gradients is given by

$$-\frac{d}{dx} [|\vec{E}_f|\cos\theta] = -D \qquad (3\text{-}22)$$

where $D = \frac{\partial E}{\partial t}$ is the wave energy dissipation rate per unit free surface area and there is a net influx of wave energy into the column of fluid under consideration. Recalling Eqs. (1-3) and (1-5) and noting that $n=1$ and $|\vec{c}| = (gh)^{1/2}$ for linear long waves, Eq. (3-22) yields

$$D_{sz} = \frac{5\rho\alpha_B^2}{16} (gh)^{3/2} \frac{dh}{dx} \qquad (3\text{-}23)$$

where linear wave height decay inside the surf zone and near normal wave incidence are invoked.

In view of Eqs. (3-2), (3-21) and (3-23), the velocity fluctuation

inside the breaker line may be compared to the wave partition which is characterized by its maximum near bottom value,

$$|\vec{u}_f|_s / |\vec{u}_w|_b' \cong [2.5 \, (\frac{dh}{dx})/\alpha_B]^{1/3} \qquad\qquad (3\text{-}24)$$

Accordingly, steeper slopes imply relatively stronger random fluctuations of velocity. Recalling the typical wave and beach parameters of Table 3-1, the fluctuating velocity partition is roughly between 30% and 60% of the wave partition. The relative importance of the shore-normal Reynolds stress component may be assessed by combining Eqs. (3-10), (3-20), (3-21) and (3-23) with the result

$$T_f^x / S_w^x \cong 2 (\frac{dh}{dx})^{2/3} \qquad (x \leq x_B) \qquad\qquad (3\text{-}25)$$

Taking the steep beach as a worst case, $T_f^x / S_w^x < .4$, so that the Reynolds stress component may be reasonably neglected from the shore-normal stress balance. Consequently, the shorenormal component of the stress balance inside the breaker line of the Modified Longuet-Higgins Model is a simple balance of local driving stress and wave setup components, i.e., in view of Eqs. (2-16) and (3-10)

$$\frac{3\rho\alpha_B^2}{8} gh \frac{dh}{dx} = - \rho gh \frac{d\eta_s}{dx} \qquad (x \leq x_B) \qquad\qquad (3\text{-}26)$$

3.1.4 Wave setup in the surf zone

Recalling that Eq. (2-8) may be differentiated to yield

$$\frac{dh}{dx} = \tan\beta + \frac{d\eta_s}{dx} \qquad\qquad (3\text{-}27)$$

56

Eq. (3-26) may be solved for $\frac{dh}{dx}$, yielding

$$\frac{dh}{dx} = \tan\Delta \qquad (x \leq x_B) \qquad\qquad (3-28)$$

The modified bottom slope $\tan\Delta$, which is suggested in an appendix to Longuet-Higgins (1970), is defined by

$$\tan\Delta = \tan\beta / (1 + \frac{3\alpha_B^2}{8}) \qquad\qquad (3-29)$$

and, for small $\tan\beta$, is approximated by the angle sketched in Figure 1-1.

Longuet-Higgins and Stewart (1962) deduce theoretically that the wave setup is relatively small at and beyond the breaker line, a conclusion supported by the measurements of Bowen et al. (1968) as well as Galvin and Eagleson (1965). Accordingly, the actual time averaged free surface elevation is essentially at the still water level seaward of the breaker line and rises at a constant slope shoreward of the breaker line, as sketched in Figure 1-1.

This configuration, while physically realistic, is difficult to deal with analytically, although series type solutions, e.g., Bowen (1969), obtained using the Method of Frobenius, e.g., Hildebrand (1962) are possible. The simple assumption

$$h = x\tan\Delta \qquad (x > 0) \qquad\qquad (3-30)$$

is adopted in the Modified Longuet-Higgins Model. With negligible setup at the breaker line, Eq. (3-30) is equivalent to Eq. (3-28) inside the surf zone, which is the primary area of interest.

The wave setup in the surf zone η_s may be obtained by noting that the modified bottom slope of Eq. (3-30) implies

$$\frac{d\eta_s}{dx} = -\frac{3\alpha_B^2}{8}\tan\Delta \qquad (3\text{-}31)$$

in view of Eq. (3-27). Integrating Eq. (3-31) and recalling that $(\eta_s)_B = 0$ by definition of the co-ordinate axes, the wave setup is given by

$$\eta_s = \frac{3\alpha_B^2}{8}(x_B - x)\tan\Delta \qquad (3\text{-}32)$$

Eq. (3-32) is used to find the maximum wave setup η_s' used in the swash zone discussion of Section 2.4.2, along with the distance between still water and mean shore lines. Referring to Figure 1-1, this latter quantity is simply

$$x_s = \eta_s'/\tan\beta \qquad (3\text{-}33)$$

so that, in view of Eq. (2-30),

$$x_s = \frac{3\alpha_B^2 h_B}{8\tan\beta} \qquad (3\text{-}34)$$

3.2 Longshore Stress Balance

The longshore component of the stress balance of Eq. (2-15) in the absence of longshore gradients is given by

$$A_s^y + S_w^y + T_f^y + (\tau_b^y)_s = 0$$

where

$$\qquad (3\text{-}35)$$

$$A_s^y = \frac{dA^{xy}}{dx}, \quad S_w^y = \frac{dS^{xy}}{dx}, \quad T_f^y = \frac{dT^{xy}}{dx}$$

58

For near normal incidence and a weak current, the wave transport clearly cominates the current transport of momentum in view of Eqs. (2-20) and (2-21) so that A_s^y is not considered in the Modified Longuet-Higgins Model; thus the adopted longshore conservation equation is a balance of local driving, Reynolds and bottom shear stresses.

3.2.1 Local driving stress

Consider the radiation stress component S^{xy} for waves in water of intermediate depth

$$S^{xy} = \int_{-d}^{\eta_s} (u_w v_w)_s \, dz \tag{3-36}$$

This more general definition, which is consistent with the linear long wave expression of Eq. (2-21) in shallow water, follows from the original radiation stress expression put forth by Longuet-Higgins and Stewart (1960). Introducing linear theory into Eq. (3-36), it can be shown that

$$S^{xy} = -E \, n \, \cos\theta \sin\theta \tag{3-37}$$

where, for linear waves

$$n = \frac{1}{2} + kh/\sinh 2kh \quad \text{(Stokes energy transport)} \tag{3-38}$$

The appearance of n and E in Eq. (3-37) suggests that S^{xy} can be expressed in terms of the shorenormal component of wave energy flux. Recalling Eq. (1-5),

$$S^{xy} = -|\vec{E}_F| \cos\theta \, \frac{\sin\theta}{|\vec{c}|} \tag{3-39}$$

59

The wave energy flux approach can be extended by noting that Snell's Law is valid for beaches with parallel bottom contours and small currents, e.g., Madsen (1976),

$$\frac{\sin\theta}{|\vec{c}|} = \text{constant} \tag{3-40}$$

so that S^{xy} is proportional to the shorenormal wave energy flux component. Combining Eqs. (3-22) and (3-39) in view of Eq. (3-35), the local longshore driving stress may be expressed as a function of the wave energy dissipation rate,

$$S_w^y = -D_{sz} \left(\frac{\sin\theta_B}{|\vec{c}_B|}\right) \qquad (x \leq x_B)$$

$$\tag{3-41}$$

$$S_w^y = -D_w \left(\frac{\sin\theta_B}{|\vec{c}_B|}\right) \qquad (x > x_B)$$

where D_w represents the wave energy dissipation rate beyond the breaker line, and knowledge of breaking wave conditions is anticipated.

The relative smallness of the longshore current implies that D_w may be approximated by the model of Madsen (1976), who estimates energy dissipation in the wave bottom boundary layer as

$$D_w = \frac{2\rho f_w}{3\pi} \left(|\vec{u}_w|'_b\right)^3 \tag{3-42}$$

where f_w is a Jonsson (1976a) wave friction factor.

The relative importance of dissipation within and beyond the breaker line may be assessed by using Eqs. (3-23), (3-42) and the modified bottom slope of Eq. (3-30) to compute (D_w/D_{sz}) at the breaker line with the result

60

$$(D_w/D_{sz})_B \cong \frac{4}{15\pi} \frac{\alpha_B f_w}{\tan\Delta} \qquad\qquad (3\text{-}43)$$

The flat beach of Table 3-1 is a reasonable worst case and a reasonable f_w value is 0.02; thus Eq. (3-43) yields $(D_w/D_{sz})_B < 0.2$, so that surf zone dissipation dominates dissipation beyond the breaker line for small currents.

Recalling Eqs. (3-23), (3-30) and (3-41), the local longshore driving stress component in the Modified Longuet-Higgins Model is given by

$$s_w^y = - \frac{5\rho\alpha_B^2}{16} (gh_B) \tan\Delta \sin\theta_B \left(\frac{h}{h_B}\right)^{3/2} \qquad (x \le x_B)$$

$$s_w^y = 0 \qquad\qquad\qquad\qquad (x > x_B)$$

$$(3\text{-}44)$$

where $|\vec{c}_B| = (gh_B)^{1/2}$, linear wave height decay is adopted and D_w is neglected. As suggested by the sign of Eq. (3-44), s_w^y represents a net influx of positive y momentum into a column of fluid in the surf zone.

3.2.2 Reynolds stress

The Modified Longuet-Higgins Model assumes the following formal expression for the depth integrated correlation of u_f and v_f

$$(u_f v_f)_s h = -\varepsilon \frac{dv_s}{dx} h \qquad (x > 0) \qquad\qquad (3\text{-}45)$$

where the sign suggests that the momentum flux is against the velocity gradient. Explicit expressions and physical interpretations for ε inside and beyond the breaker line are those put forth by Battjes (1975) and Longuet-Higgins (1970), respectively.

61

Battjes' (1975) estimate

$$\varepsilon = M\ell_f |\vec{u}_f|_s \qquad\qquad (x \leq x_B) \qquad\qquad (3\text{-}46)$$

is used inside the breaker line where ℓ_f is the length scale of the largest eddies and M is termed Battjes' correlation constant, which should be of order unity if the fluctuating scales are evaluated properly. Eqs. (3-45) and (3-46) are derived by noting that the mean shear $\dfrac{dv_s}{dx}$ maintains a correlation between u_f and v_f which would otherwise return to an uncorrelated state in the eddy turnover time $\ell_f/|\vec{u}_f|_s$, or $\varepsilon/|\vec{u}_f|_s^2$.

The fluctuating length scale is estimated as

$$\ell_f = h \qquad\qquad (x \leq x_B) \qquad\qquad (3\text{-}47)$$

since the largest eddies contributing to the depth integrated u_f, v_f correlation have a horizontal axis in the mean shear plane and are consequently constrained vertically.

Combining Eqs. (3-46) and (3-47), and recalling the fluctuating velocity scale estimate of Eqs. (3-21) and (3-23)

$$\varepsilon = M(\frac{5\alpha_B^2}{16}\tan^4\!\Delta)^{1/3} x\ (gh)^{1/2} \qquad (x \leq x_B) \qquad\qquad (3\text{-}48)$$

using the modified bottom slope of Eq. (3-30).

The mean shear $\dfrac{dv_s}{dx}$ generates the turbulence beyond the breaker line and ε is taken as a horizontal eddy viscosity in this region, determined by

$$\varepsilon = \Gamma x |\vec{u}_w|_b' \qquad\qquad (x > x_B) \qquad\qquad (3\text{-}49)$$

subject to

$$\varepsilon \quad \text{continuous} \qquad (x = x_B) \qquad\qquad (3\text{-}50)$$

where Γ is a lateral mixing coefficient. Eq. (3-49) is similar to the expression adopted by Longuet-Higgins (1970)

$$\varepsilon = N \; x \; (gh)^{1/2} \qquad (x > 0) \qquad\qquad (3\text{-}51)$$

who adopts $(gh)^{1/2}$ as his characteristic velocity instead of $|\vec{u}_w|'_b$; the correspondence becomes exact upon Longuet-Higgins' (1970) assumption

$$\alpha = \alpha_B \qquad (x > 0) \qquad\qquad (3\text{-}52)$$

with the factor $\alpha_B/2$ absorbed into the proportionality constant N.

The Modified-Longuet-Higgins Model, drawing upon the assumed linear long wave theory for waves of near normal incidence with negligible wave energy dissipation seaward of the breaker line, assumes Green's Law, i.e., Madsen (1976) to describe wave height variation seaward of the breaker line. Green's Law may be expressed as

$$\alpha = \alpha_B (h_B/h)^{5/4} \qquad (x > x_B) \qquad\qquad (3\text{-}53)$$

Since $|\vec{u}_w|'_b$ is given by Eq. (3-2) for linear long waves, ε becomes

$$\varepsilon = \frac{\Gamma\alpha_B}{2} \left(\frac{h_B}{h}\right)^{5/4} x \; (gh)^{1/2} \qquad (x > x_B) \qquad\qquad (3\text{-}54)$$

upon the combination of Eqs. (3-49) and (3-53), while the matching condition Eq. (3-50) yields a relation between Γ and M

$$\Gamma = M(2.5 \; \tan^4\Delta/\alpha_B)^{1/3} \qquad\qquad (3\text{-}55)$$

63

Combining Eqs. (3-35), (3-45), (3-48) and (3-54), the following
Modified Longuet-Higgins Model expression for the longshore component
of the Reynolds stress is obtained, in view of Eqs. (2-22) and (3-55)

$$T_f^y = - \frac{\rho \Gamma \alpha_B \tan\Delta}{2} \frac{d}{dx} [x^2 (gh)^{1/2} \frac{dv_s}{dx}] \qquad (x \leq x_B)$$

$$(3-56)$$

$$T_f^y = - \frac{\rho \Gamma \alpha_B \tan\Delta}{2} \frac{d}{dx} [x^2 (h_B/h)^{5/4} (gh)^{1/2} \frac{dv_s}{dx}] \qquad (x > x_B)$$

3.3 Solution to the Longshore Stress Balance

3.3.1 Characteristic shorenormal length and velocity scales

Following Longuet-Higgins (1970), the characteristic shorenormal
length scale of the Modified Longuet-Higgins Model is the shorenormal
distance between the time average shore line and the breaker line, so
that

$$x^* = x/x_B \qquad\qquad (3-57)$$

where the star superscript refers to a dimensionless variable.

The characteristic longshore current v_c is defined as the long-
shore current at the breaker line predicted by the Modified Longuet-
Higgins Model in the absence of Reynolds stresses, and accordingly
involves the balance of longshore local driving and bottom shear
stresses in Eq. (3-1), i.e.,

$$S_w^y + (\tau_b^y)_s = 0 \qquad\qquad (3-58)$$

Recalling Eqs. (3-17) and (3-2), the longshore bottom shear stress is given by

$$
(\tau_b^y)_s = \frac{\rho f_{sz} \alpha_B}{2\pi} (gh)^{1/2} v_s \qquad (x \le x_B)
$$

$$(3-59)$$

$$
(\tau_b^y)_s = \frac{\rho f_{sz} \alpha_B}{2\pi} (gh)^{1/2} (h_B/h)^{5/4} v_s \qquad (x > x_B)
$$

where linear wave height decay and Green's Law are used to describe wave height variation within and beyond the breaker line, respectively. $(\tau_b^y)_s$ is a net efflux of positive y momentum from the fluid column and consequently is positive. In view of Eq. (3-44), the balance of longshore local driving and bottom shear stress components may be solved for v_s

$$
v_s = \frac{5\pi\alpha_B}{8f_{sz}} \tan\Delta \sin\theta_B (gh_B)^{1/2} (h/h_B) \qquad (x \le x_B)
$$

$$(3-60)$$

$$
v_s = 0 \qquad (x > x_B)
$$

The characteristic velocity is obtained by evaluating Eq. (3-60) at the breaker line

$$
v_c = \frac{5\pi\alpha_B}{8f_{sz}} \tan\Delta \sin\theta_B (gh_B)^{1/2}
$$

$$(3-61)$$

so that, recalling the modified bottom slope assumption and noting that

$$
v^* = v_s/v_c
$$

$$(3-62)$$

the dimensionless longshore current profile in the absence of Reynolds stresses, as sketched in Figure 3-1, is given by

$$v^* = x^* \qquad (x^* \leq 1)$$

$$v^* = 0 \qquad (x^* > 1) \tag{3-63}$$

The linear current strength κ is defined as the ratio of the characteristic velocity to the maximum near bottom wave velocity at the breaker line, i.e.,

$$\kappa = v_c / (|\vec{u}_w|'_b)_B \tag{3-64}$$

Recalling Eqs. (3-2) and (3-61),

$$\kappa = \frac{5\pi \ \tan\Delta\sin\theta_B}{4f_{sz}} \tag{3-65}$$

It is convenient to express v_c in terms of κ,

$$v_c = \frac{\kappa\alpha_B}{2} (gh_B)^{1/2} \tag{3-66}$$

3.3.2 Dimensionless longshore current profile

With the inclusion of the Reynolds stress, the longshore component of the stress balance is obtained by substituting Eqs. (3-44), (3-56) and (3-59) into Eq. (3-1) with the result

$$-\frac{5\rho\alpha_B^2}{16} gh_B\tan\Delta \ \sin\theta_B \ (h/h_B)^{3/2} + \frac{\rho f_{sz}\alpha_B}{2\pi} (gh)^{1/2} \ v_s$$

$$-\frac{\rho\Gamma\alpha_B\tan\Delta}{2} \frac{d}{dx} [x^2 (gh)^{1/2} \frac{dv_s}{dx}] = 0 \qquad (x \leq x_B)$$

$$0 + \frac{\rho f_{sz}\alpha_B}{2\pi} (gh)^{1/2} (h_B/h)^{5/4} \ v_s$$

$$- \frac{\rho \Gamma \alpha_B \tan\Delta}{2} \frac{d}{dx} \left[x^2 (gh)^{1/2} (h_B/h)^{5/4} \frac{dv_s}{dx} \right] = 0 \qquad (x > x_B) \qquad (3\text{-}67)$$

The modified bottom slope implies that

$$h/h_B = x^* \qquad (x > 0) \tag{3-68}$$

so that Eq. (3-67) may be expressed in dimensionless form

$$- \frac{f_{sz}}{2\pi} x^{*3/2} + \frac{f_{sz}}{2\pi} x^{*1/2} v^* - \frac{\Gamma \tan\Delta}{2} \frac{d}{dx^*} \left[x^{*5/2} \frac{dv^*}{dx^*} \right] = 0 \qquad (x^* \leq 1)$$

$$\tag{3-69}$$

$$0 + \frac{f_{sz}}{2\pi} x^{*-3/4} v^* - \frac{\Gamma \tan\Delta}{2} \frac{d}{dx^*} \left[x^{*5/4} \frac{dv^*}{dx^*} \right] = 0 \qquad (x^* > 1)$$

after division by the factor $\rho \alpha_B v_c (gh_B)^{1/2}$. Noting that the dimensionless variables are of the order unity, the coefficients of Eq. (3-69) represent the order of magnitude of S_w^y, $(\tau_b^y)_s$ and T_f^y, respectively, so that the mixing parameter P_{sz}, defined by

$$P_{sz} = \frac{\pi \Gamma \tan\Delta}{f_{sz}} \tag{3-70}$$

is an estimate of the relative importance of the Reynolds stress compared to the local driving and bottom shear stress which are the same order of magnitude. Eq. (3-70) suggests that the Reynolds stress is more important on steeper beaches with smoother bottoms.

Introducing P_{sz} into Eq. (3-69), expanding the derivative and re-arranging terms, the governing equation of the Modified Longuet-Higgins Model is obtained

67

$$x^{*2} \frac{d^2 v^*}{dx^{*2}} + \frac{5}{2} x^* \frac{dv^*}{dx^*} - \frac{v^*}{P_{sz}} = - \frac{x^*}{P_{sz}} \qquad (x^* \leq 1)$$

(3-71)

$$x^{*2} \frac{d^2 v^*}{dx^{*2}} + \frac{5}{4} x^* \frac{dv^*}{dx^*} - \frac{v^*}{P_{sz}} = 0 \qquad (x^* > 1)$$

Eq. (3-71) is subject to the boundary and matching conditions

$$v^* \to 0 \qquad\qquad (x^* \to \infty) \tag{3-72}$$

$$v^* \to 0 \qquad\qquad (x^* \to 0) \tag{3-73}$$

$$v^* \text{ continuous} \qquad (x^* = 1) \tag{3-74}$$

$$\frac{dv^*}{dx^*} \text{ continuous} \qquad (x^* = 1) \tag{3-75}$$

It should be noted that Eqs. (3-45), (3-50) and (3-75) insure a continuous Reynolds stress across the breaker line.

The governing equation closely approximates that of Longuet-Higgins (1970); identical inside the surf zone, and slightly modified beyond to accommodate Eq. (3-53) in place of Eq. (3-52). The solution to Eq. (3-71), which is a second order, linear, equidimensional ordinary differential equation, homogeneous beyond the breaker line and nonhomogeneous within, subject to Eqs. (3-72) through (3-75), is obtained by an exponential change of variables, e.g., Hildebrand (1962), and is given by

$$v^* = c_1 \left(\frac{1-c_2}{c_2-c_3} \right) x^{*^{c_3}} + c_1 x^* \qquad (P_{sz} \neq 0.4, \ x^* \leq 1)$$

$$v^* = c_1 \left(\frac{1-c_3}{c_2-c_3} \right) x^{*^{c_2}} \qquad (P_{sz} \neq 0.4, \ x^* > 1)$$

68

$$v^* = 0.26x^* - 0.71x^* \ln x^* \qquad (P_{sz} = 0.4, \; x^* \leq 1)$$

$$v^* = 0.26x^{*-1.71} \qquad\qquad (P_{sz} = 0.4, \; x^* > 1) \qquad (3\text{-}76)$$

where

$$c_1 = (1 - 2.5P_{sz})^{-1}$$

$$c_2 = -\frac{1}{8} - (\frac{1}{64} + \frac{1}{P_{sz}})^{1/2}$$

$$c_3 = -\frac{3}{4} + (\frac{9}{16} + \frac{1}{P_{sz}})^{1/2}$$

The dimensionless profiles of Eq. (3-76) are sketched in Figure 3-1 along with the profile expected in the absence of Reynolds stresses, which is denoted by $P_{sz} = 0$. As suggested by the figure, the Reynolds stress, whose importance increases with increasing P_{sz}, diffuses the longshore current beyond the breaker line.

Maximum and surf zone averaged dimensionless longshore currents may be computed from Eq. (3-76); the resulting expressions are

$$(v^*)' = c_1(x^*)' \; (1 - 1/c_3) \qquad (P_{sz} \neq 0.4)$$

$$(3\text{-}77)$$

$$(v^*)' = 0.38 \qquad\qquad (P_{sz} = 0.4)$$

with $(x^*)'$ denoting the location of maximum current,

$$(x^*)' = \frac{c_3 - c_2}{c_3(1 - c_2)}^{\frac{1}{c_3 - 1}} \qquad (P_{sz} \neq 0.4)$$

$$(x^*)' = 0.53 \qquad\qquad (P_{sz} = 0.4)$$
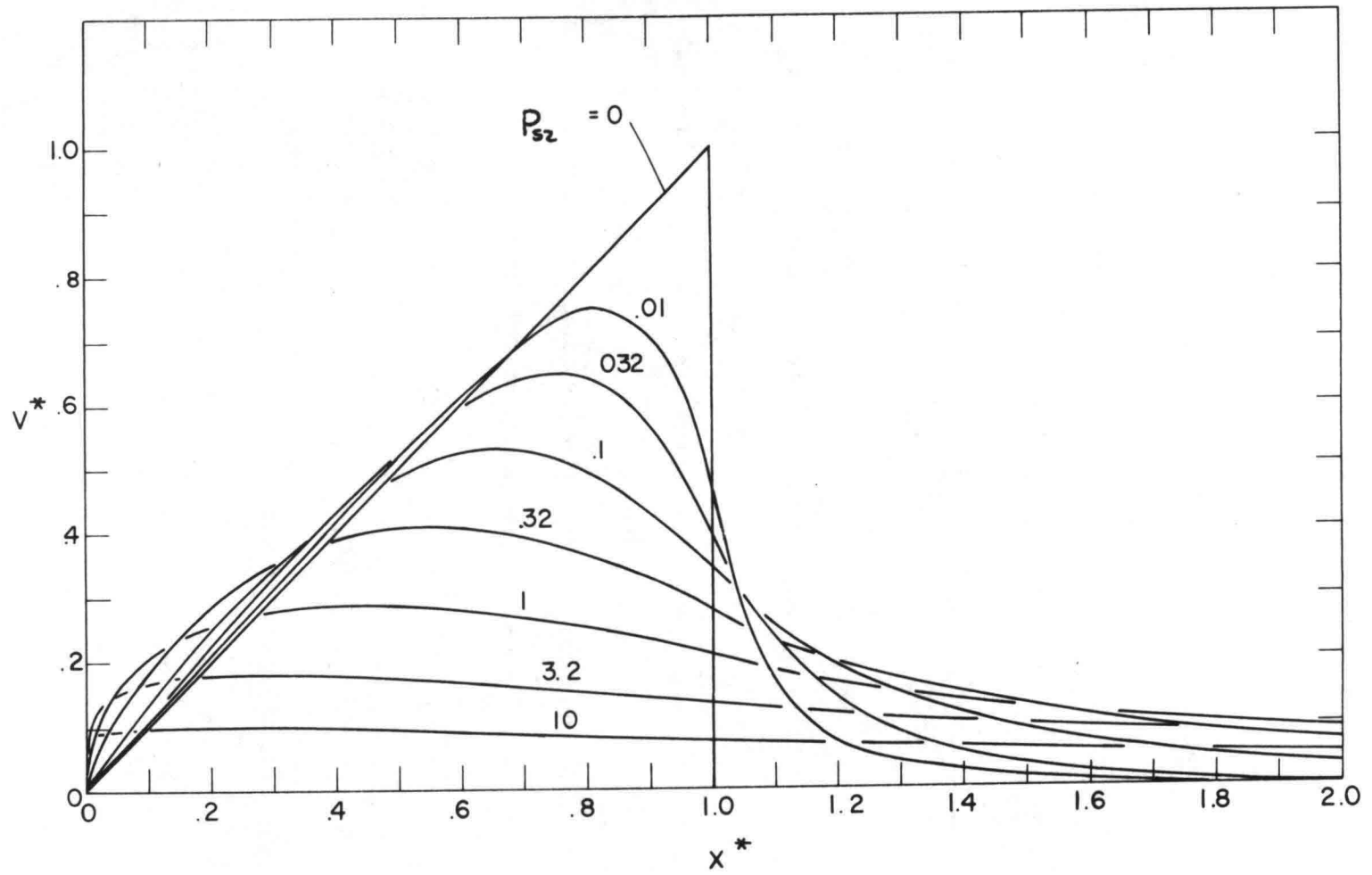
Figure 3-1: Dimensionless Longshore Current Profile

and

$$<v^*> = c_1 \left[\frac{1-c_2}{(c_2-c_3)(1+c_3)} + \frac{1}{2}\right] \qquad (P_{sz} \neq 0.4)$$

$$(3-78)$$

$$<v^*> = 0.31 \qquad (P_{sz} = 0.4)$$

where $<v^*>$ is based on the average longshore current between the time averaged shore line and the breaker line. These parameters are sketched as functions of P_{sz} in Figure 3-2.

3.4 Other Momentum Based Uniform Longshore Current Models

Bowen (1969), Thornton (1970), Jonsson, Skovgaard and Jacobsen (1974), James (1974a, 1974b) and Reyman (1976) use the   stress balance to derive models predicting a longshore current profile that is uniform in depth and longshore distance. The brief model summaries presented here are intended to identify physically plausible alternative formulations of the   stress balance with simple and accurate solutions and as such only discuss the differences between the Modified Longuet-Higgins Model and the other models. Elements of these models are used in the Linear Longshore Current Model and Nonlinear Longshore Current Model.

It should be noted that the model of Battjes (1974), which deals with random incident waves in the absence of Reynolds stress as originally proposed by Collins (1970), is excluded from present consideration which, as suggested in Table 1-1, deals with the laboratory condition of monochromatic waves over fixed bed beaches.

71
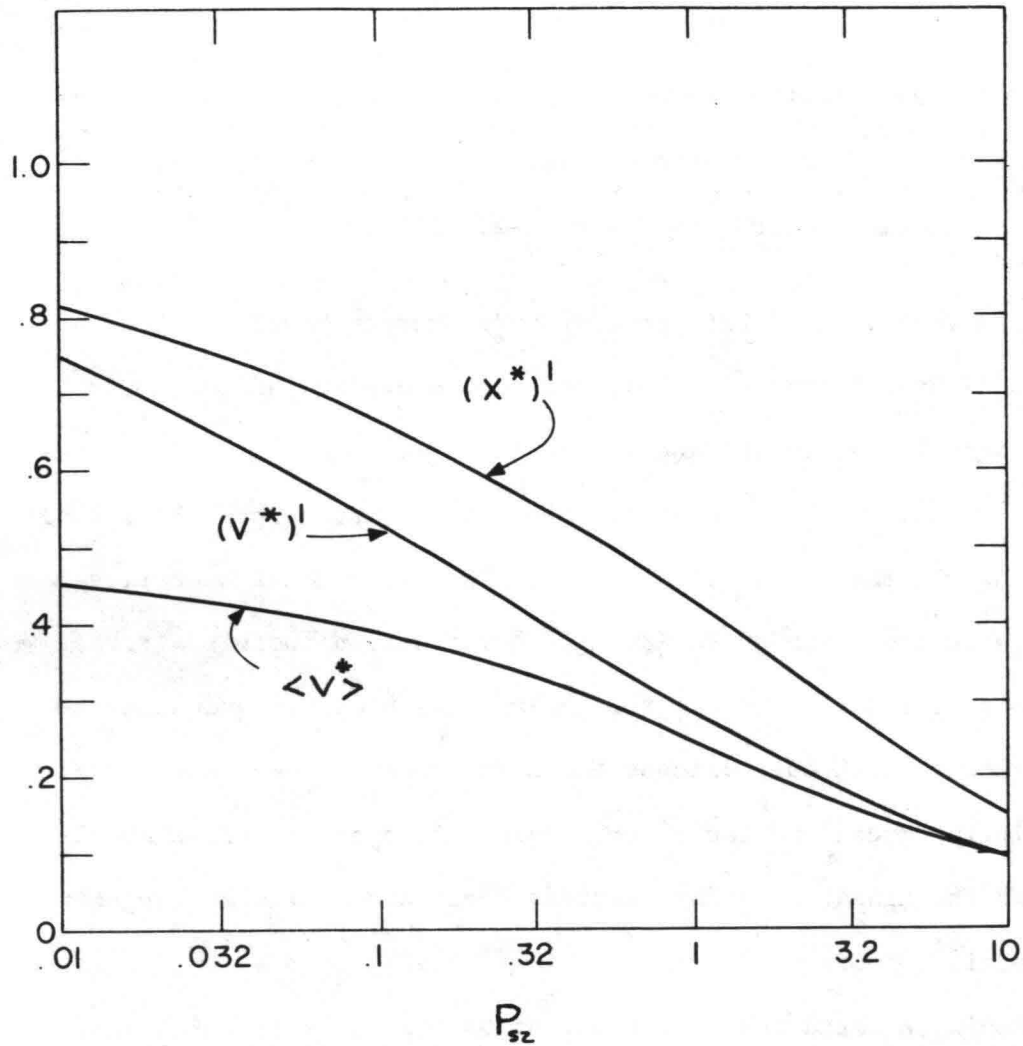
Figure 3-2:   Maximum and Surf Zone Averaged Dimensionless Longshore
Currents

72

3.4.1 Bowen (1969)

The idealized environment and neglected stresses and accelerations of Bowen's (1969) model conform to the assumptions of Tables 1-1 and 1-2.

Bowen (1969) derives expressions for his local driving stress by assuming a constant crest alignment throughout the surf zone while retaining the discontinuous water surface discussed in Section 3.1.4 and sketched in Figure 1-1. The longshore bottom shear stress component is assumed to be linear in the longshore current with a constant friction factor which has the dimensions of a velocity, while the Reynolds stress is assumed to be proportional to $d^2 v_s/dx^2$.

Bowen (1969) formulates his governing equation on a per unit mass basis and presents a solution in terms of four modified Bessel functions.

Physically speaking, it is unfortunate that Bowen (1969) formulates the   stress balance on a per unit mass basis in that the local driving and Reynolds stresses are depth integrated quantities whose horizontal gradients should include a variation in depth. This depth effect is accounted for in the driving stress term, but is omitted in Bowen's (1969) expression for the longshore Reynolds stress component, so that it is difficult to assign a physical meaning to the proportionality constant in the Reynolds stress term, which Bowen (1969) construes as a constant horizontal eddy viscosity. The longshore bottom shear stress component ignores the contribution of the wave motion which is assumed by Bowen (1969) to dominate the current; in this regard, the

linearized longshore bottom shear stress component of the Modified

Longuet-Higgins Model suggests that Bowen's (1969) dimensional fric-

tion factor is proportional to $|\vec{u}_w|_b'$ and as such varies appreciably

throughout the surf zone. On the positive side, Bowen (1969) includes

a realistic setup modification in his model and is the first investi-

gator to incorporate the three stresses of the   stress balance

into a longshore current model predicting a shorenormal profile.

The solution of Bowen (1969) is difficult to use because four

Bessel functions must be computed to evaluate a longshore current pro-

file and offers little hope of a predictive extension in that it

carries two unspecified constants which have a doubtful physical basis.

Bowen (1969) does not present much experimental verification for his

model; a single Galvin and Eagleson (1965) run (I = 1, J = 8) is

analyzed on a good fit basis to obtain values for the horizontal eddy

viscosity and dimensional friction factor which are accompanied by a

graph of measured and theoretical points. Bowen (1969) does state

qualitatively that the good agreement exhibited by the small current

run (I = 1, J = 8) breaks down for larger current runs, which may be

due to the fact that he makes no explicit allowance for a finite

current.

3.4.2 Thornton (1970)

Thornton (1970) relaxes some of the restrictions of the Modified

Longuet-Higgins Model by considering waves of oblique incidence on a

beach with parallel contours.

The variation of θ is evaluated using Snell's Law with phase speed given by solitary wave theory inside the breaker line and linear wave theory beyond. Thornton (1970) also allows for wave setup within and beyond the breaker line for waves of normal incidence. The Jonsson (1966a) friction factor for rough turbulent flow is used to describe the longshore bottom shear stress component, while the longshore Reynolds stress component contains a horizontal eddy viscosity that is the absolute value of the product of the horizontal wave excursion amplitude and horizontal wave orbital velocity. Both parameters vary across the surf zone.

Thornton's (1970) solution is a numerical model, and he presents typical profiles of time average depth and longshore current.

As noted by Jonsson et al. (1974), Thornton (1970) also fails to take depth variation into account when the longshore component of the Reynolds stress is evaluated, so that the governing equation and typical solutions presented by Thornton (1970) do not reflect the physical reasoning underlying his formulation of the stress balance. As suggested by Battjes (1975), the momentum transport due to waves is already present in the stress balance as the local driving stress, so that the use of wave parameters to obtain ε, which describes turbulent momentum transport, is open to question on physical grounds, particularly if the wave and fluctuating components are assumed to be uncorrelated. Thornton's longshore bottom shear stress component is on much firmer ground though, since he is the first to introduce the Jonsson (1966a) friction factor as a rational predictor of the bottom shear when waves dominate currents.

The removal of the plane beach and constant friction factor assumptions, while physically realistic, results in a numerical model so that Thornton's (1970) model of longshore currents is an unsolved differential equation and as such is difficult to use.

3.4.3 Jonsson, Skovgaard and Jacobsen (1974)

Jonsson, Skovgaard and Jacobsen (1974) allow for straight bottom contours with monotonically increasing depth in their idealized environment.

The local longshore driving stress incorporates oblique wave incidence within and beyond the breaker line. Jonsson et al. (1974) introduce an interpolation of a wave and a current friction factor into their nonlinear expression for the longshore bottom shear stress component based on the alignment of $(\vec{u}_s + \vec{u}_w)_b$; the authors invoke the near normal incidence assumption to express the resulting stress component in terms of an elliptic integral. Jonsson et al. (1974), like Thornton (1970), use the wave motion to describe ε in the longshore Reynolds stress component expression with no proportionality constant; however, the depth variation in the horizontal gradient of $h(u_f v_f)_s$ is properly accounted for in the Jonsson et al. (1974) model.

As is the case with Thornton (1970), the model of Jonsson et al. (1974) is a differential equation which is solved on a numerical basis, and is accordingly difficult to use.

Physically speaking, the longshore bottom shear stress component appearing in the stress balance of Jonsson et al. (1974) allows for a contribution from the longshore current. As indicated in Section 4.4.1,

the near normal incidence assumption excludes some of the finite cur-
rent contribution from the bottom shear stress estimate, however, so
that the friction factor of Jonsson et al. (1974), which must compen-
sate for this underestimation, may be too large for waves of oblique
incidence. The notable improvement of the Jonsson et al. (1974) model
is the suggestion of a plausible predictor for the friction factor as
a function of f_w, the current friction factor f_s and the relative
strength of the longshore current. The longshore Reynolds stress com-
ponent of Jonsson et al. (1974) is essentially identical to Thornton's
(1970) estimate, which is discussed in the preceding section.

Jonsson et al. (1974) show computed longshore current profiles for
wave and beach conditions of a Galvin and Eagleson (1965) run (I = 2,
J = 2), a run for the roughest beach of Putnam et al. (1949) as well as
a field experiment of Ingle (1966). The $<v_s>$ and v_s' measurements of
Putnam et al. (1949) and Ingle (1966) are in reasonable agreement with
the predicted profiles, while Jonsson et al. (1974) overestimate $v_s(x)$
measurements of Galvin and Eagleson (1965) seaward of the breaker line.
The authors note that their estimate of the horizontal eddy viscosity
is unreasonably large beyond the breaker line which may account for the
discrepancy between the prediction and the GE data. Jonsson et al.
(1974) observe that the beach roughness, which essentially determines
the friction factor, and the horizontal eddy viscosity control the
scale and the form of the profile, respectively.

3.4.4 James (1974a, 1974b)

James (1974a, 1974b) relaxes the plane beach assumption of the Modified Longuet-Higgins Model in his model for longshore currents.

The local driving stress is computed using Stokes and hyperbolic wave theories with a transitional function for waves of near normal incidence within and beyond the surf zone. James (1974a, 1974b) allows for wave setup inside and beyond the breaker line as well as a return current opposing the direction of wave propagation to account for mass transport. The longshore bottom shear stress component reflects the presence of a finite current and is evaluated by numerical integration over a wave period. James (1974a, 1974b), following the arguments of Longuet-Higgins (1970), assumes a horizontal eddy viscosity inside the breaker line that is proportional to the product of the maximum horizontal wave orbital velocity and the distance from shore. Beyond the breaker line, the author uses the measured decay of $(|\vec{u}_f|^2)_s$ with distance downstream of an oscillating grid to deduce that ε decreases inversely with water depth; with the proportionality obtained by matching eddy viscosities at the breaker line.

James' (1974a, 1974b) model for longshore currents is a set of differential equations which may only be solved on a numerical basis and as such is difficult to use.

James (1974a, 1974b) emphasizes that the use of finite height wave theory inside the breaker line is valid only for spilling breakers and a gently sloping bottom, a conclusion which is substantiated by other investigators of surf zone hydrodynamics, e.g., Divoky, Le Mehaute and

78

Lin (1970) and Iwagaki, Sakai, Tsukioka and Sawai (1974). Accordingly, the assumed constancy of α inside the surf zone adopted by James (1974a, 1974b) may be questioned in view of the discussion in Section 2.4.4; the applicability of this model to the common case of transitional spilling-plunging breakers of oblique incidence may be questioned as well. The longshore Reynolds stress component has a proportionality factor which identifies the relative importance of the random velocity fluctuations and as such is a step forward; however, the author's use of a $(|\vec{u}_f|^2)_s$ estimate to describe $(u_f v_f)_s$ behavior seaward of the breaker line ignores the fact that u_f and v_f may be weakly correlated. James (1974a, 1974b) is the first investigator to use quadrature to estimate the longshore bottom shear stress component so that the entire contribution of the longshore current is accounted for. It should be noted that the retention of the spilling breaker assumption is critical in shear stress evaluation since the α power series expansion for near bottom horizontal wave orbital velocity used in finite height wave theories diverges under a wave crest for transitional spilling-plunging breakers, a result which tends to invalidate the quadrature. In this regard, Iwagaki et al. (1974) note that second order Cnoidal theory, while providing a satisfactory estimate of horizontal near bottom wave orbital velocity under a wave trough, may actually predict a horizontal near bottom wave orbital velocity under a crest that opposes the direction of wave propagation for ε_B values as low as 0.16.

Spilling breaker requirement notwithstanding, James (1974a, 1974b)

79

compares his model with GE runs (I = 1, J = 6),(I = 1, J = 3) and
(I = 3, J = 5), one PMT laboratory run and one PMT field run, with good
agreement in all cases. As noted by the author, the GE run with high
longshore current speed is better fit with a lower friction factor than
the slower GE runs, a result which is in accord with the calibration of
the Longshore Current Model in Section 5.1.

3.4.5 Reyman (1976)

Reyman (1976) considers longshore currents induced by waves of near
normal incidence.

Reyman (1976) adopts the stress balance of the Modified Longuet-
Higgins Model inside the surf zone with the exclusion of the wave setup
allowance and assumes that horizontal eddy viscosity and near bottom
horizontal wave orbital velocity amplitude decay as $x^{-1/3}$ and $x^{-4/3}$,
respectively, seaward of the breaker line. Reyman (1976) notes that
the decay ocefficients yield an equidimensional governing differential
equation with an analytical solution and are reasonably representative
of the physical behavior of the Reynolds and bottom shear stress compon-
ents. The resulting dimensionless longshore current profiles are simi-
lar to those of the Modified Longuet-Higgins Model.

Reyman (1976) goes on to account for the presence of a finite cur-
rent in the longshore bottom shear stress component by assuming that
these dimensionless profiles describe the form of the longshore current
when the wave and current are of comparable magnitude. The character-
istic velocity is reduced by a factor determined from the integrated

80

nonlinear longshore stress balance. This balance is obtained by integrating the longshore component of the stress balance from the time averaged shore line to the breaker line, allowing for a nonlinear time averaged longshore bottom shear stress component. Reyman's (1976) bottom shear term is expressed in terms of an elliptic integral and as such is valid for waves of near normal incidence; the reduction factor is the iterative solution to the integrated nonlinear longshore stress balance and is presented in graphical form so that Reyman's (1976) model is simple to use.

Reyman (1976) compares predicted values of longshore currents with Komar's (1969) observations with reasonably accurate results.

4   NEW MODELS

The Linear Longshore Current Model, Linear Longshore Sediment Transport Model and Nonlinear Longshore Current Model adopt elements of the existing models described in the prior section. The three new models follow James (1974a, 1974b) in that they include the effects of finite wave height on the integrated driving stress S_B^{xy}, and they interpolate between f_s and f_w to predict the surf zone friction factor f_{sz}, as suggested by Jonsson et al. (1974).   Reyman's (1976) use of an integrated nonlinear stress balance and a reduced characteristic velocity to account for a finite current is repeated in the Nonlinear Longshore Current Model with the nonlinear longshore bottom shear stress component for oblique wave incidence obtained by numerical integration, following the suggestion of James (1974a, 1974b). Last and not the least important by any means is the use of a similarity assumption which equates the dimensionless longshore current profile of the new models to that of the Modified Longuet-Higgins Model, following Reyman's (1976) concept.

The first contribution of the present investigation to the state of the art is to include a breaking wave predictor so that offshore wave conditions may be used as model input. Greater model accuracy should follow since the offshore wave conditions are easier to measure and more likely to be accurate than breaking wave conditions which are presently required for use in the Modified Longuet-Higgins Model. The breaking wave predictor consists of an empirical breaking criterion combined with nonlinear wave theory. The integrated driving stress due

82

to nonlinear waves is smaller than that obtained using linear wave theory; the reduction is accounted for in the present investigation by scaling down the Modified Longuet-Higgins Model longshore current prediction by a factor n_B, which appears as part of the output of the breaking wave predictor.

Next, the effect of nonuniformity is investigated in the context of a developing longshore current downstream of a jetty. With the similarity assumption the effect of nonuniformity is expressed by a reduction factor λ_1, which is applied to the Modified Longuet-Higgins Model longshore current prediction and essentially accounts for the amount of driving stress absorbed by the longshore acceleration of the fluid inside the surf zone. The resulting Linear Longshore Current Model retains the linearizing small current assumption and the near normal wave incidence assumption of the Modified Longuet-Higgins Model and is accordingly analytical.

The third improvement of the present investigation consists of a simple model describing the transport of sediment in the longshore direction. The Linear Longshore Sediment Transport Model applies a steady flow relationship between bottom shear stress and sediment transport to the longshore motion of the surf zone on a time averaged, shorenormal integrated basis. The new model adopts the longshore bottom shear stress estimate of the Linear Longshore Current Model so that the resulting analytical prediction is valid only for small currents and near normal wave incidence.

Finally, the restrictive assumptions of a relatively small current

83

and near normal wave incidence are relaxed in the Nonlinear Longshore
Current Model which, however, requires uniform longshore conditions.
The relaxation of the two assumptions yields a nonlinear time averaged
longshore bottom shear stress which in turn reduces the scale of the
Modified Longuet-Higgins Model longshore current prediction by a factor
λ_2. Unlike its linear counterpart λ_2 must be determined numerically
and is subsequently represented by a curve fitted function.

4.1 Prediction of Breaker Conditions

The wave refraction theory used in the present investigation rests
upon a dispersion relationship, Snell's Law and an energy transport
function which describe phase speed, crest alignment and wave height
respectively, in terms of water depth, period, and, for finite height
waves, wave height. The presence of a finite wave height increases
the phase speed and decreases the efficiency with which a wave trans-
mits energy and, practically speaking, implies an iteration in compu-
tations since the unknown wave height appears implicitly in the dis-
persion and energy transport relationships. In the context of long-
shore currents, accounting for a finite wave height decreases the
integrated driving stress and the resulting longshore current relative
to the predictions obtained using linear wave theory.

Other investigators, e.g., Iwagaki (1968) and Svendsen and
Buhr Hansen (1977) demonstrate that Cnoidal wave theory describes
shoaling wave heights over a gently sloping bottom reasonably well,
even when the wave is close to breaking, particularly for waves of
small deep water steepness. The Cnoidal theory describes the observed

84

tendency of the wave height to increase rapidly as breaking is approached; the description is more accurate than linear or Stokes second order predictions, which underestimate the wave height near breaking. This evidence justifies the use of Cnoidal wave theory, as presented by Svendsen (1974), in conjunction with linear Stokes wave theory, e.g., Madsen (1976), and a transitional function to predict wave refraction in the present investigation. It should be added that the small wave steepness effect noted by Svendsen and Buhr Hansen (1977) argues for transitional spilling-plunging breakers, in view of the ξ_B definition of Eq. (2-25).

The assumption of an empirical breaking criterion fixes the location of the breaker line once a wave theory is specified. Madsen's (1976) empirical breaking criterion is adopted, with minor modifications, in the present investigation. The criterion limits the relative breaking wave height α_B; it should be noted that the nonlinear wave theory, which predicts higher waves in a given depth, moves the breaker line seaward of a prediction made using linear wave theory and the same α_B criterion.

4.1.1 Stokes-transitional-Cnoidal dispersion and energy transport

The incident gravity wave is assumed to be described by the known quantities (θ, H, h, T, g) which may be recombined into three dimensionless parameters using the Buckingham Π theorem. Following Svendsen (1974), the chosen parameters are θ, α, and γ, where γ and α are defined by Eqs. (2-27) and (2-28).

85

The relative wave length γ, so called because it is equal to L/h for linear long waves, may be expressed in terms of kh for Stokes waves by making use of Stokes' dispersion relationship, valid to second order

$$\omega^2 = kg \tanh kh \qquad \text{(Stokes waves)} \qquad (4\text{-}1)$$

Recalling Eq. (2-27) and noting that $\omega = 2\pi/T$, Eq. (4-1) may be expressed as

$$\gamma = 2\pi/(kh \tanh kh)^{1/2} \quad \text{(Stokes dispersion)} \qquad (4\text{-}2)$$

The Stokes dispersion relationship may also be expressed in terms of a dimensionless phase speed c^* in accordance with

$$c^* = \frac{2\pi}{\gamma^2 kh} \qquad \text{(Stokes waves)} \qquad (4\text{-}3)$$

where, per definition,

$$c^* = \frac{|\vec{c}|}{gT} \qquad (4\text{-}4)$$

and kh appears in parametric form. Eqs. (4-2) and (4-3) combine to yield the Stokes dispersion curve $c^*(\gamma)$ sketched in Figure 4-1. The Stokes energy transport function may also be evaluated indirectly in terms of γ in view of Eq. (3-38) which combines with Eq. (4-2) to yield the Stokes energy transport function shown in Figure 4-2.

Cnoidal wave dispersion reflects the finite wave height influence in the form of the relative wave height factor α in the relation

$$c^* = (1 + \alpha A)^{1/2}/\gamma \qquad \text{(Cnoidal dispersion)} \qquad (4\text{-}5)$$
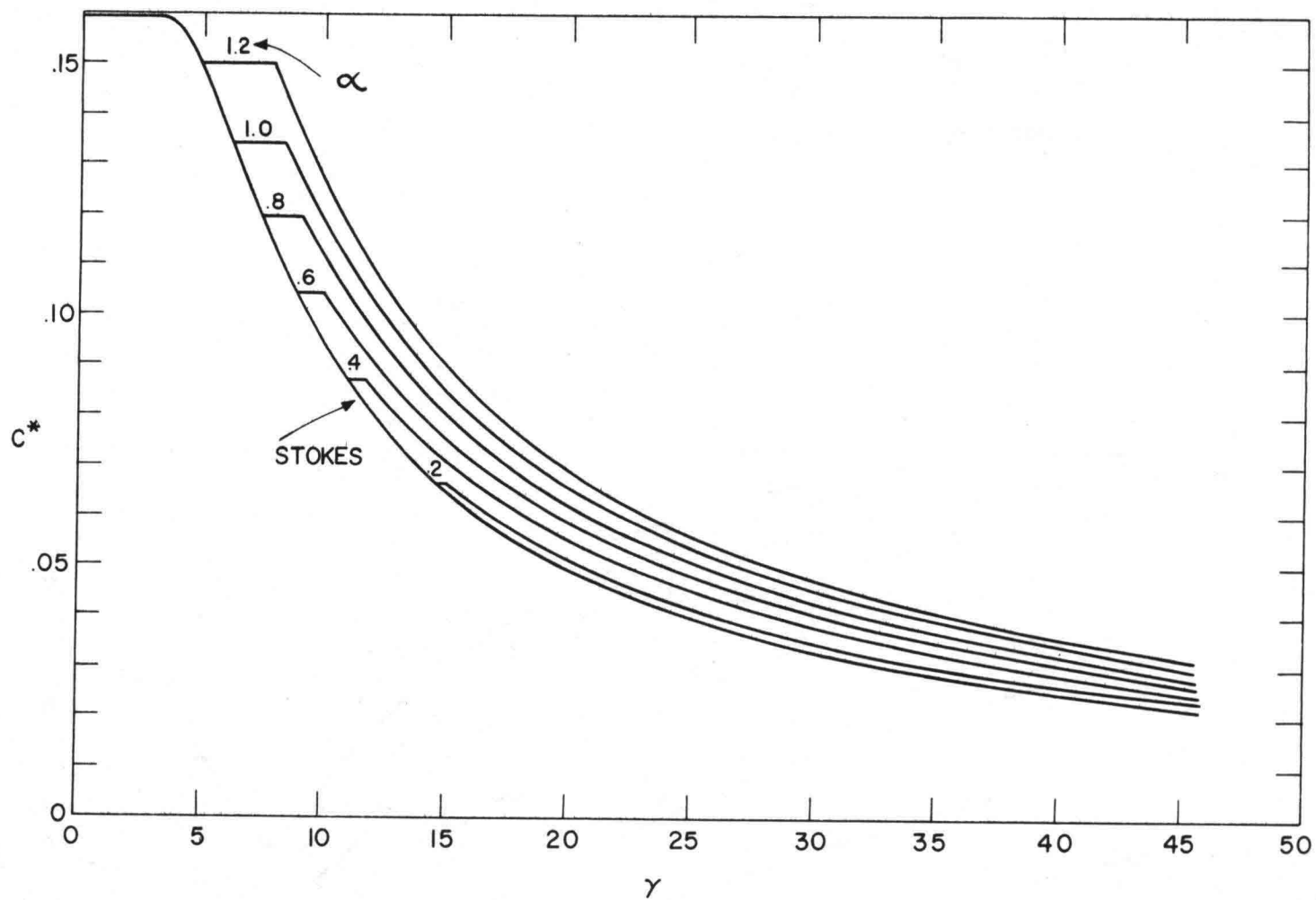
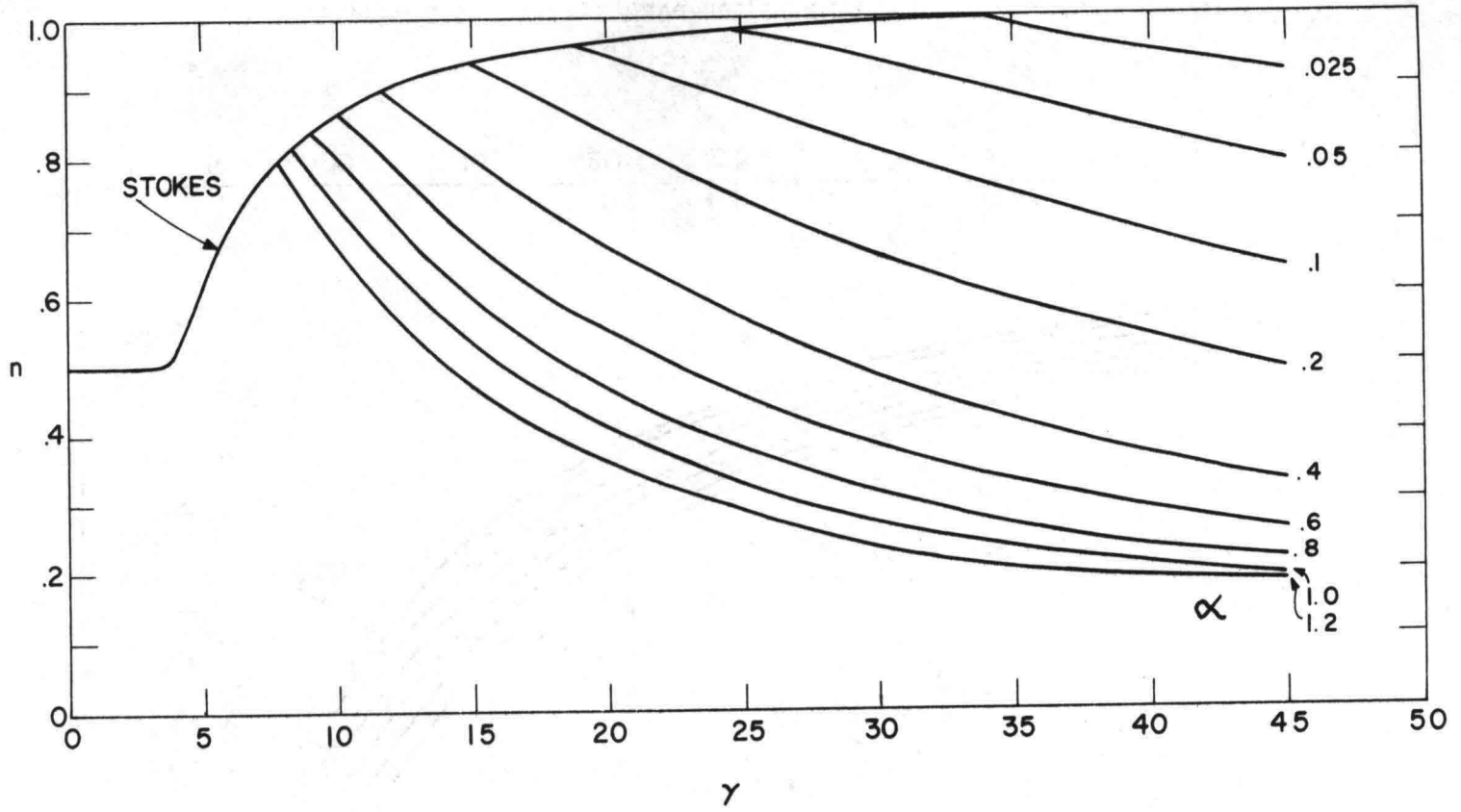Figure 4-1: Finite Wave Height Dispersion Relationship

Figure 4-2:   Finite Wave Height Energy Transport Function

where A is a function of the Ursell parameter U, which in turn is given by

$$U = \gamma^2 \alpha (1 + \alpha A) \tag{4-6}$$

so that, with A(U) provided by Svendsen (1974), Eq. (4-5) may be evaluated on an iterative basis, yielding the Cnoidal dispersion curves sketched in Figure 4-1. In similar fashion, Svendsen (1974) presents B(U) where

$$B = n/8 \qquad \text{(Cnoidal energy transport)} \tag{4-7}$$

so that, in view of Eq. (4-6), the Cnoidal energy transport function may be solved on an iterative basis, with the results sketched in Figure 4-2.

A transitional function is needed to insure a continuous prediction of wave dispersion and energy transport. An inspection of the B(U) tabulation by Svendsen (1974) shows that B approaches its linear long wave value of 0.125 as wave height approaches zero so that the energy transport function may serve as a reasonable basis for the arbitrary transition, which, as sketched in Figure 4-2, is simply

$$n = \begin{cases} n(\text{Cnoidal}) & [n(\text{Cnoidal}) < n(\text{Stokes})] \\ n(\text{Stokes}) & [n(\text{Stokes}) < n(\text{Cnoidal})] \end{cases} \tag{4-8}$$

so that the n transition occurs at the intersection $\gamma_T(\alpha)$ of the Stokes curve and the appropriate Cnoidal branch in Figure 4-2. As pointed out by Svendsen and Buhr Hansen (1977), an abrupt change of wave theories at a given $\gamma_T(\alpha)$ value results in a discontinuity in

89

either wave height or energy flux; in the present context, the discontinuity would appear in the c^* curves in Figure 4-1 as a drop along a given γ_T value from the appropriate α Cnoidal branch where $c^* = c_T^*$ (Cnoidal) down to the Stokes curve. To avoid this discontinuity, the following dispersive transition is adopted in the present investigation

$$c^* = c^*(\text{Cnoidal}) \qquad (\gamma > \gamma_T)$$

$$c^* = \begin{cases} c_T^*\ (\text{Cnoidal}) & [c_T^*\ (\text{Cnoidal}) > c^*\ (\text{Stokes})] \\ c^*\ (\text{Stokes}) & [c^*\ (\text{Stokes}) > c^*\ (\text{Cnoidal})] \end{cases} \qquad \begin{matrix} (4\text{-}9) \\ (\gamma_T > \gamma) \end{matrix}$$

so that, as sketched in Figure 4-1, a horizontal and not a vertical line connects the Cnoidal branches to the Stokes curve, thus forming a continuous transition between the two theories.

Cnoidal theory, which rests in part on the long wave assumption $h/L \ll 1$, cannot be applied for large depths, or small γ values, while Stokes theory cannot be applied for long waves of finite height, or large α values. In this regard, Svendsen and Buhr Hansen (1977) recommend an upper h/L_o limit of 0.10 for use of Cnoidal wave theory, which corresponds to a lower γ limit of 8. Madsen (1971), in a discussion of long waves, suggests that $U < 25$ for the use of Stokes long waves which corresponds to $n < .98$. These two criteria may be sketched onto Figure 4-2 to demonstrate that the Stokes-transitional-Cnoidal wave theory adopted in the present investigation is consistent with the recommendations of these investigators since n and c^* are at or near

90

their Stokes values for $\gamma < 8$, while for $n < .98$ and $\gamma > 15$, Cnoidal theory is in use, where the γ limit insures Stokes long waves.

4.1.2 Modified Madsen empirical breaking criterion

Madsen (1976) combines the empirical breaking criteria of earlier investigators for long waves of normal incidence breaking on plane impermeable beaches into the following equation:

$$\alpha_B = 0.72 \quad (1.0 + 6.4 \tan\beta) \quad (\tan\beta < 0.10)$$
$$\alpha_B = 1.18 \quad\quad\quad\quad\quad\quad\quad (\tan\beta > 0.10) \quad\quad\quad\quad (4-10)$$

The upper limit corresponds to the highest observed value of α_B appearing on the summary of investigations presented by Longuet-Higgins (1970).

Eq. (4-10) may be combined with the general breaking criterion of Miche (1944)

$$H_B/L_B = 0.14 \tanh (2\pi\, h_B/L_B) \quad\quad\quad\quad (4-11)$$

to yield the modified Madsen empirical breaking criterion, which is sensitive to bottom slope and depth varying wave parameters

$$(H/L)_B = 0.14\tanh\{(0.8 + 5\tan\beta)2\pi h_B/L_B\} \quad (\tan\beta < 0.10)$$
$$\quad\quad\quad\quad\quad\quad\quad\quad\quad\quad\quad\quad\quad\quad\quad\quad\quad\quad (4-12)$$
$$(H/L)_B = 0.14\tanh\{(.13)2\pi h_B/L_B\} \quad (\tan\beta > 0.10)$$

The modified Madsen empirical breaking criterion can be combined with the Stokes-transitional-Cnoidal wave theory of Section 4.1.1 to yield $\alpha_B(\gamma_B, \tan\beta)$ as sketched on Figure 4-3.
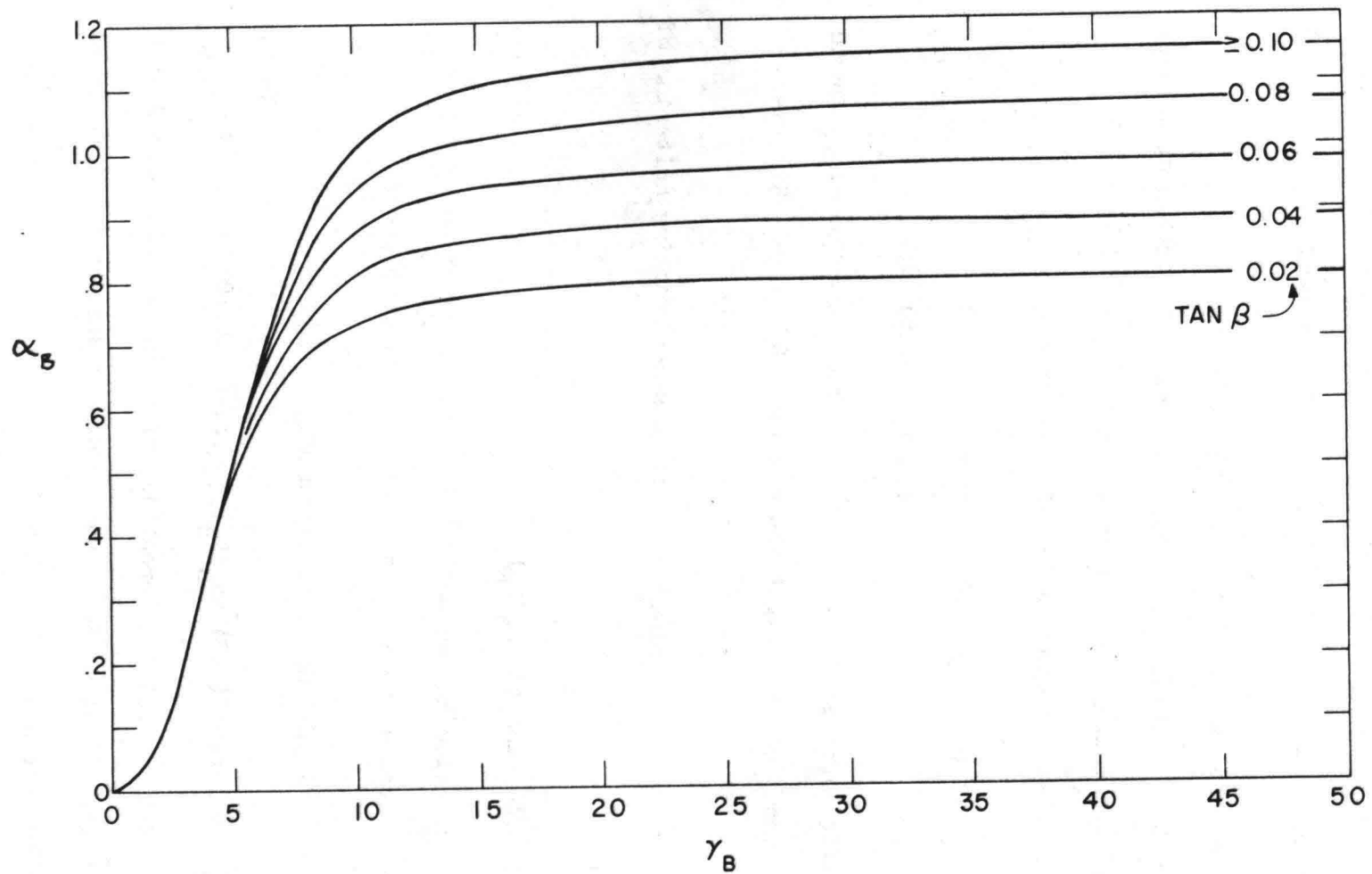
Figure 4-3: Modified Madsen Empirical Breaking Criterion

Noting that tanh $x \cong x$ in shallow water, Eq. (4-12) approaches the Madsen (1976) criterion for long waves, while with tanh $x \cong 1$ in deep water, Eq. (4-12) is seen to approach the Miche (1944) criterion for short waves. It should be noted that Figure 4-3 falls within 10% of the empirical curves presented by Goda (1970) for normally incident breaking waves on plane impermeable slopes.

The modified Madsen empirical breaking criterion is used in the present investigation which deals with obliquely incident waves; since the development of this criterion is predicated on normal wave incidence, some justification of the oblique application is appropriate. Accordingly, Table 4-1 presents a comparison of the α_B values measured by Galvin and Eagleson (1965) and by Putnam et al. (1949) with α_B values predicted using the theory of the present investigation.

Table 4-1

Modified Madsen Empirical Breaking Criterion

Systematic Errors in θ_B

	$0 < \theta_B \leq 10^o$		$10 < \theta_B \leq 20^o$		$20 < \theta_B \leq 30^o$		$30^o \leq \theta_B$	
	n_Q	$\overline{Q}_\alpha$	n_Q	$\overline{Q}_\alpha$	n_Q	$\overline{Q}_\alpha$	n_Q	$\overline{Q}_\alpha$
GE-6[*]	8	+0.25	8	+0.13	7	+0.15	2	+0.27
PMT	–	–	21	-0.27	4	-0.27	12	-0.24

[*]GE-6 = Galvin and Eagleson (1965) – transect 6

The table presents sample means of the random variable Q_α defined by

$$Q_\alpha = \frac{\alpha_B(\text{measured}) - \alpha_B(\text{predicted})}{\alpha_B(\text{predicted})} \qquad (4\text{-}13)$$

In order to identify systematic errors with θ_B, the GE and PMT data sets are subdivided into samples of size n_Q of comparable breaking angle, and sample means are computed in accordance with, e.g., Benjamin and Cornell (1970),

$$\overline{Q}_\alpha = \frac{1}{n_Q} \sum_{i=1}^{n_Q} (Q_\alpha)_i \qquad (4\text{-}14)$$

A fuller account of this type of data comparison is presented in Section 5.2.

Table 4-1 suggests that there is no systematic error in θ_B for prediction of α_B so that breaker angle does not appear to be an important factor in the determination of the breaker height to breaker depth ratio, and the oblique application of the modified Madsen empirical breaking criterion in the present investigation is judged to be reasonable. The underprediction and overprediction of α_B for the GE and PMT data bases, respectively, is not surprising in view of the difficulties inherent in the measurement of breaker conditions and the subjectivity in the definition of the breaker line itself. Indeed, a prime consideration in the design of the models of the present investigation is to establish conditions seaward of the breaker line as input parameters since these parameters may be measured with more accuracy and consistency.

94

4.1.3 Breaking wave iteration

The wave dispersion and energy transport functions, along with Snell's Law, S^{xy} constancy and the modified Madsen breaking criterion provide enough information to predict breaking wave conditions (α_B, γ_B, θ_B) when offshore conditions and the bottom slope (α, γ, θ, $\tan\beta$) are specified, where the dimensionless variables of the preceding section are adopted. As suggested by Table 4-2, the breaking wave prediction is an iteration on γ_B, and requires two known offshore parameters ($\sin\theta/c^*$, c_4) as input, where

$$c_4 = \gamma/(\alpha^2 n\ \sin 2\theta)^{1/4} \qquad\qquad (4\text{-}15)$$

and c^* and n may be obtained from Figures 4-1 and 4-2.

Following the iteration, assume a trial value γ_B; experience suggests 15.0 as a reasonable starting point. The γ_B estimate generates an α_B estimate with $\tan\beta$ known by virtue of the modified Madsen empir-

Table 4-2

Breaking Wave Iteration

---

1. Assume γ_B

2. Read $\alpha_B(\gamma_B, \tan\beta)$ from Figure 4-3

3. Read $c_B^*(\gamma_B, \alpha_B)$ from Figure 4-1

4. Read $\theta_B(c_B^*,\ \sin\theta/c^*)$ from Figure 4-4

5. Read $n_B(\gamma_B, \alpha_B)$ from Figure 4-2

6. Compute γ_B from Eq. (4-17)

7. Compare steps 1 and 6 and iterate

---

ical breaking criterion. With γ_B and α_B guessed, c_B^* may be obtained from the wave dispersion relationship and used with Snell's Law, Eq. (3-40), to obtain θ_B from known $\sin\theta/c^*$ as indicated on Figure 4-4.

The γ_B and α_B estimates also yield n_B, which may be used with the constancy of S^{xy} beyond the breaker line assumed in Section 3.2.1 to derive a second estimate of γ_B. Noting that Eq. (3-37) is valid for nonlinear waves, as shown by Longuet-Higgins (1972), the constancy of S^{xy} beyond the breaker line implies

$$H^2 n \sin 2\theta = H_B^2 n_B \sin 2\theta_B \qquad (x > x_B) \qquad (4-16)$$

which may be expressed as a second estimate of γ_B

$$\gamma_B = (\alpha_B)^{1/2} (n_B \sin 2\theta_B)^{1/4} c_4 \qquad (4-17)$$

This second estimate, if significantly different from the first estimate, may be iterated into step 2 until an acceptable closure is obtained.

Appendix I illustrates the breaking wave iteration.

4.1.4 Reduced integrated driving stress

As suggested by Eq. (3-37) and Figure 4-2, a finite wave height reduces the radiation stress component S^{xy} from its linear value due to a decrease in the wave energy transport function n; it follows that the local longshore driving stress and longshore current will be less than their Modified Longuet-Higgins Model counterparts as well since the model is based on linear wave theory. The present investigation
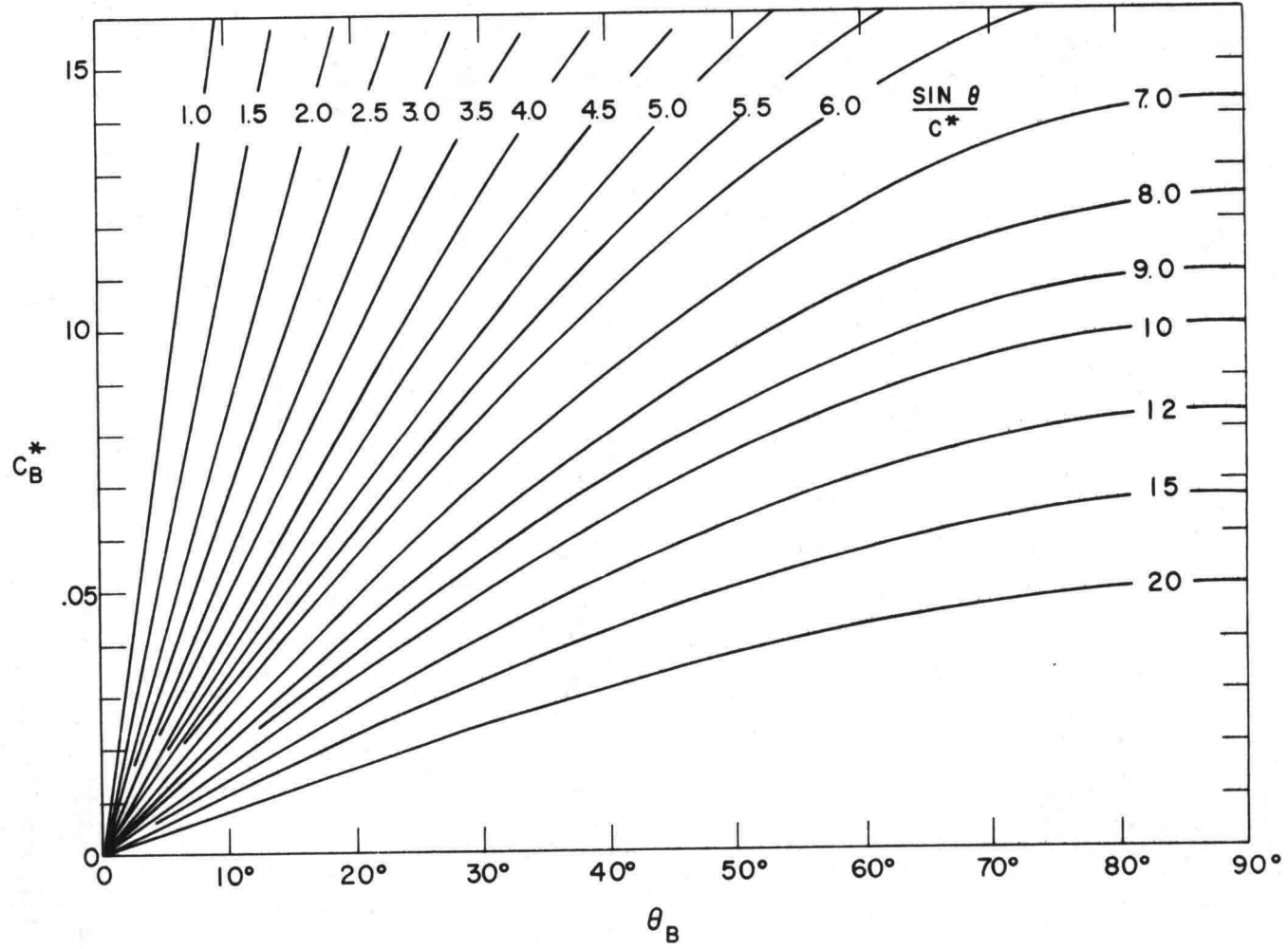
96

Figure 4-4: Snell's Law

follows Reyman (1976) and models the effect with the similarity assumption

$$v_s = (v^* v_c) \text{ constant} \qquad (4\text{-}18)$$

where the constant is determined by considering the depth integrated, time averaged conservation of longshore momentum on a shorenormal integrated basis.

Accordingly the longshore stress balance of Eq. (3-35) is integrated from the time averaged shore line to the breaker line in the absence of convective stresses, with the result

$$S_B^{xy} + T_B^{xy} + x_B <(\tau_b^y)_s> = 0 \qquad (4\text{-}19)$$

Eq. (4-19) describes the time averaged flux of longshore momentum under uniform longshore conditions through a fluid slice bounded by the bottom, time averaged free surface, breaker line and two shore-normal planes a unit longshore distance apart. With the assumption of near normal wave incidence and a relatively small current, the second and third terms of Eq. (4-19) are linear in v_s and may, in view of Eq. (4-18), be expressed as

$$T_B^{xy} + x_B <(\tau_b^y)_s> = \text{constant } [T_B^{xy} + x_B <(\tau_b^y)_s>]_{MLH} \qquad (4\text{-}20)$$

where the subscript represents terms computed under the additional Modified Longuet-Higgins Model assumption of linear wave motion. Eq. (4-19) must also hold for the integrated Modified Longuet-Higgins Model stresses, so that

$$[T_B^{xy} + x_B <(\tau_b^y)_s>]_{MLH} = -[S_B^{xy}]_{MLH} \qquad (4\text{-}21)$$

Combining Eqs. (4-19)-(4-21) then,

$$S_B^{xy} = \text{constant } [S_B^{xy}]_{MLH} \qquad (4\text{-}22)$$

and, recalling Eq. (3-37) with $n_B = 1.0$ in the Modified Longuet-Higgins Model, the simple result follows

$$\text{constant} = n_B \qquad (4\text{-}23)$$

4.2 Linear Longshore Current Model

The Linear Longshore Current Model predicts longshore currents generated by water waves of near normal incidence breaking over an infinite plane beach in the presence of a shorenormal jetty. The model follows the approach of Eagleson (1966) by neglecting wave diffraction, by assuming that η_s stays constant in the longshore direction, and by integrating the conservation equations from the time averaged shore line to the breaker line with the resulting balance

$$A_B^{xy} + x_B <\frac{\partial A^{yy}}{\partial y}> + S_B^{xy} + T_B^{xy} + x_B<(\tau_b^y)_s> = 0 \qquad (4\text{-}24)$$

As with the integrated balance of Section 4.1.4 the small current and near normal wave incidence assumptions of the Modified Longuet-Higgins Model are retained while the waves are of finite height; the difference here is the inclusion of integrated convective stresses in Eq. (4-24) due to longshore nonuniformity. The analysis is similar to

99

that of the preceding section. However, Reyman's (1976) similarity assumption expresses the nonuniform effects in terms of the convective current reduction factor whose solution is given by Eq. (4-49).

The modified bottom slope of Eq. (3-30) is adopted as the solution of the shorenormal momentum equation in the Linear Longshore Current Model.

4.2.1 Conservation of mass equation

Consider the depth integrated, time averaged conservation of mass equation which, with the retention of longshore gradients, is given by Eq. (2-7). Recalling linear wave theory of Eqs. (3-2)-(3-4) the correlation of v_w and η_w is given by

$$(v_w \eta_w)_s = \frac{\alpha H}{8} (gh)^{1/2} \sin\theta \qquad (4-25)$$

Noting that v_s is of order v_c, the relative importance of $(v_w \eta_w)_s$ in the conservation of mass equation is given by the ratio

$$\frac{[(v_w \eta_w)_s]_B}{v_c h_B} = \frac{f_{sz} \alpha_B}{5\pi \tan\Delta} \qquad (4-26)$$

in view of Eqs. (3-61) and (4-25). With the flat, rough beach of Table 3-1 as a worst case, $[(v_w \eta_w)_s]_B / v_c h_B < 0.2$ so that the depth integrated, time averaged conservation of mass equation may be safely approximated as

$$\frac{\partial}{\partial x} [u_s h + (u_w \eta_w)_s] + \frac{\partial (v_s h)}{\partial y} = 0 \qquad (4-27)$$

Integrating Eq. (4-27) from 0 to x_B and transposing terms,

$$[u_s h + (u_w \eta_w)_s]_B = -x_B <\frac{\partial}{\partial y} (v_s h)> \qquad (4-28)$$

Eq. (4-28) suggests that there is a net flux of mass flowing shoreward through the breaker line to accommodate the increased longshore flux of mass through the fluid slice bounded by the bottom, the breaker line, the free surface and two vertical shorenormal planes a unit longshore distance apart.

4.2.2 Integrated linear longshore stress balance

The Linear Longshore Current Model continues the Modified Longuet-Higgins Model's neglect of longshore gradients of time average free surface

$$\eta_s = \eta_s(x) \qquad (4-29)$$

Eq. (4-29) implicitly neglects wave diffraction due to the jetty along with the longshore periodicity discussed in Section 2.4.3. The neglect of diffraction suggests that the shore normal jetty has a length of the order x_B so that the incident waves approach the surf zone over an infinite plane beach; the use of an involved wave diffraction theory inside the breaker line is judged to be unwarranted due to the complexity of the actual motion in the surf zone. It should be noted that Liu and Mei (1976) analyze the diffraction caused by a shorenormal jetty extending far seaward of the breaker line; the analysis is numerical and ignores convection and Reynolds stresses. The continued neglect of longshore periodicity implied by Eq. (4-29) may be ques-

101

tioned since the Linear Longshore Current Model deals with longshore length scales comparable to those of the low frequency edge waves described earlier. The justification of Eq. (4-29) thus rests upon model simplicity and the Linear Longshore Current Model should consequently be regarded as a first step towards a more general two dimensional model of surf zone hydrodynamics.

The utility of Eq. (4-29) lies in its elimination of terms from the depth integrated, time averaged conservation of longshore momentum equation, which in full form is given by

$$\frac{\partial}{\partial x} [A^{xy} + S^{xy} + T^{xy}] + \frac{\partial}{\partial y} [A^{yy} + S^{yy} + T^{yy}] + (\tau_b^y)_s = P_w^y \quad (4-30)$$

upon reference to Eqs. (2-15) and (2-17)-(2-19). The wave setup term vanishes identically upon the assumption of $\eta_x(x)$, while the S^{yy} term, which involves time averaged wave properties that are functions of water depth, likewise has a zero longshore gradient. The Reynolds stress term T^{yy} is given by

$$T^{yy} = \rho (v_f^2)_s h \quad (4-31)$$

$(v_f^2)_s$ may be analyzed in similar fashion to the $(u_f^2)_s$ analysis of Section 3.1.3 upon the assumption of isotropic turbulence, so that T^{yy} may be construed as a function of the wave dissipation D. Since D is homogeneous in the longshore direction, $\frac{\partial T^{yy}}{\partial y} = 0$. Thus, Eq. (4-29) reduces the depth integrated, time averaged conservation of longshore momentum equation to

$$A_s^y + S_w^y + T_f^y + (\tau_b^y)_s = 0 \quad (4-32)$$

where

$$A_s^y = \frac{\partial A^{xy}}{\partial x} + \frac{\partial A^{yy}}{\partial y} \; , \; S_w^y = \frac{dS^{xy}}{dx} \; , \; T_f^y = \frac{dT^{xy}}{dx}$$

Following Eagleson (1966), the depth integrated, time averaged conservation of momentum equation is integrated from 0 to x_B where the limits of integration are independent of y by virtue of Eq. (4-29). In view of Eq. (4-32), the resulting integrated linear longshore stress balance balances the transport of longshore momentum through the breaker line due to time averaged, wave and randomly fluctuating partitions, i.e.,

$$\int_0^{x_B} (\frac{\partial A^{xy}}{\partial x} + S_w^y + T_f^y)dx = A_B^{xy} + S_B^{xy} + T_B^{xy} \tag{4-33}$$

against the bottom shear force and convective acceleration of the fluid in the surf zone

$$\int_0^{x_B} (\frac{\partial A^{yy}}{\partial y} + (\tau_b^y)_s)dx = x_B <\frac{\partial A^{yy}}{\partial y}> + x_B <(\tau_b^y)_s> \tag{4-34}$$

as indicated in Eq. (4-24).

The convection induced transport term A_B^{xy} can be expressed in terms of v_s using conservation of mass considerations. Recalling Eq. (2-20)

$$A_B^{xy} \stackrel{\sim}{=} \rho\{v_s[u_s h + (u_w \eta_w)_s]\}_B \tag{4-35}$$

where $\rho[u_s(v_w\eta_w)_s]_B$ is ignored in accordance with the estimate of Eq. (4-26). Introducing mass conservation via Eq. (4-28)

$$A_B^{xy} = -\rho (v_s x)_B \left\langle h \frac{\partial v_s}{\partial y} \right\rangle \tag{4-36}$$

A_B^{xy} is negative because the shoreward current at the breaker line car-
ries positive longshore momentum into the fluid slice under considera-
tion.

4.2.3 Reyman's (1976) similarity assumption

The longshore current must be further constrained in order for
the integrated linear longshore stress balance to yield a tractable
governing equation. Eagleson (1966), who derives Eq. (4-24) in the
absence of Reynolds stresses, proceeds to an analytical solution by
placing strong assumptions on the velocity field, one of which is the
constancy of the longshore current across the surf zone. The Linear
Longshore Current Model adopts Reyman's (1976) similarity assumption
instead by requiring

$$v_s = v^* v_c \lambda_1 n_B \tag{4-37}$$

The longshore current profile is assumed to be similar to the Modified
Longuet-Higgins Model profile of Eq. (3-76) with scaling reduced by
the convective current reduction factor λ_1, and the energy transport
function n_B. λ_1 is less than unity since part of the integrated driv-
ing stress is spent on the convective acceleration of the longshore
current in the y direction; λ_1 is a function of y which approaches
one with increasing longshore distance as fully developed conditions
are realized. As discussed in Section 4.1.4, the inclusion of n_B re-
flects the decreased integrated driving stress due to the finite wave
height effect.

104

In view of Eqs. (4-36) and (4-37), the integrated convective stress term A_B^{xy} becomes

$$A_B^{xy} = -\rho (v_c x_B n_B)^2 \tan\Delta (v_B^* \langle x^* v^* \rangle) \lambda_1 \frac{d\lambda_1}{dy} \tag{4-38}$$

where the characteristic shorenormal length and velocity scales of Section 3.3.1 are employed. The remaining integrated convective stress term is evaluated in a similar fashion; recalling Eq. (2-20),

$$x_B \langle \frac{\partial A^{yy}}{\partial y} \rangle = 2\rho (v_c x_B n_B)^2 \tan\Delta (\langle x^* v^{*2} \rangle) \lambda_1 \frac{d\lambda_1}{dy} \tag{4-39}$$

where $2\rho v_s (v_w \eta_w)_s$ is ignored in accordance with the estimate of Eq. (4-26). $x_B \langle \frac{\partial A^{yy}}{\partial y} \rangle$ is positive since it represents a net efflux of positive longshore momentum from the fluid slice.

It is convenient to express the remaining terms of Eq. (4-24) in terms of their fully developed counterpart

$$S_B^{xy} + [T_B^{xy} + x_B \langle (\tau_b^y)_s \rangle]_{y=\infty} = 0 \tag{4-40}$$

where S_B^{xy} is given by its finite wave height value for near normal incidence, i.e., n_B from Figure 4-2 is used in Eq. (3-37). The small current and near normal incidence assumptions insure that T_B^{xy} and $x_B \langle (\tau_b^y)_s \rangle$ are linear in v_s so that the downstream variation of these terms if given by

$$T_B^{xy} + x_B \langle (\tau_b^y)_s \rangle = \lambda_1 [T_B^{xy} + x_B \langle (\tau_b^y)_s \rangle]_{y=\infty} \tag{4-41}$$

in view of the similarity assumption of Eq. (4-37). Combining Eqs. (4-40) and (4-41) then,

105

$$T_B^{xy} + x_B <(\tau_b^y)_s> = -\lambda_1 S_B^{xy} \tag{4-42}$$

so that the integrated local driving, Reynolds and bottom shear stresses in Eq. (4-24) may be expressed as

$$S_B^{xy} + T_B^{xy} + x_B <(\tau_b^y)_s> = S_B^{xy}(1-\lambda_1) \tag{4-43}$$

4.2.4 Convective current reduction factor

Combining Eqs. (4-38), (4-39) and (4-43) and changing signs, the integrated linear longshore stress balance may be expressed in terms of the convective current reduction factor

$$\lambda_1 \frac{d\lambda_1}{dy^*} -1 + \lambda_1 = 0 \tag{4-44}$$

with the dimensionless longshore distance y^* defined by

$$y^* = y/y_c \tag{4-45}$$

where the characteristic longshore distance y_c is given by

$$y_c = (\frac{2\kappa^2 n_B}{\sin\theta_B}) c_5 x_B \tag{4-46}$$

with $\cos\theta_B \sim 1$ in Eq. (4-46). P_{sz} is implicit in the constant c_5

$$c_5 = 2<x^* v^{*2}> -v_B^* <x^* v^*> \tag{4-47}$$

and κ is given by Eq. (3-65). S_B^{xy} is given by Eq. (3-37).

The governing equation (4-44), which must obey a kinematic boundary condition at the jetty

$$\lambda_1 = 0 \qquad (y^* = 0) \tag{4-48}$$

106

may be solved by separation of variables with the solution, e.g., Gradshteyn and Ryzhik (1965), given by

$$\ln(1-\lambda_1) + \lambda_1 = -y^*$$

(4-49)

Model use is facilitated with Figures 4-5 and 4-6 which show $c_5(P_{sz})$ and $\lambda_1(y^*)$, respectively. Recalling Eqs. (3-76) and (4-47) and carrying out the integration, the former figure graphs the relationship

$$c_5 = 2c_1^2\{(\frac{1-c_2}{c_2-c_3})^2 \frac{1}{2c_3+2} + (\frac{1-c_2}{c_2-c_3}) \frac{2}{c_3+3} + .25\}$$

$$- \frac{c_1^2(1-c_3)}{c_2-c_3} \{(\frac{1-c_2}{c_2-c_3}) \frac{1}{c_3+2} + .33\} \qquad (P_{sz} \neq 0.4) \qquad (4-50)$$

$$c_5 = 0.068 \qquad\qquad (P_{sz} = 0.4)$$

Figure 4-6 suggests that there is a strong longshore gradient of the longshore current near the shorenormal jetty which induces a relatively strong shoreward current by virtue of the conservation of mass equation. The stronger shoreward current should accordingly be checked for its influence on the shorenormal momentum equation. Solving Eq. (4-28) for the time averaged shorenormal current at the breaker line,

$$(u_s)_B = -[\frac{(u_w \eta_w)_s}{h}]_B - \frac{1}{\tan\Delta} <\frac{\partial}{\partial y} (v_s h)>$$

(4-51)

Recalling Eqs. (3-2), (3-4), (4-37) and (4-44)- (4-46)

$$(u_s)_B = \frac{\alpha_B^2}{8} (gh_B)^{1/2} - \frac{\alpha_B f_{sz}}{5\pi c_5 \tan\Delta} (gh_B)^{1/2} <x^* v^*>(\frac{1}{\lambda_1} - 1) \quad (4-52)$$

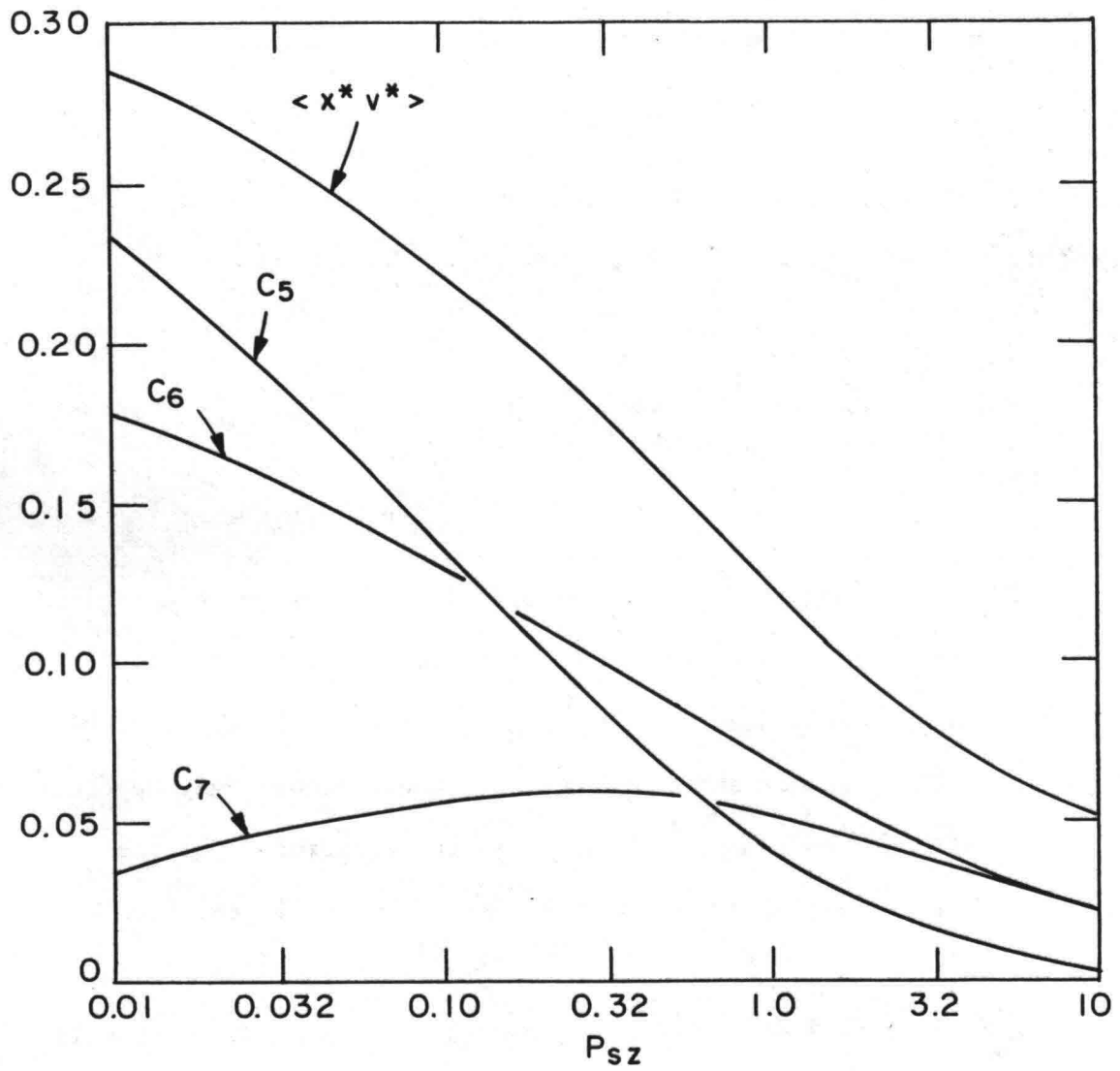where the last term is simplified using Eq. (3-65).

107

Figure 4-5: Linear Longshore Current Model and Linear Longshore Seidment Transport Model Constants
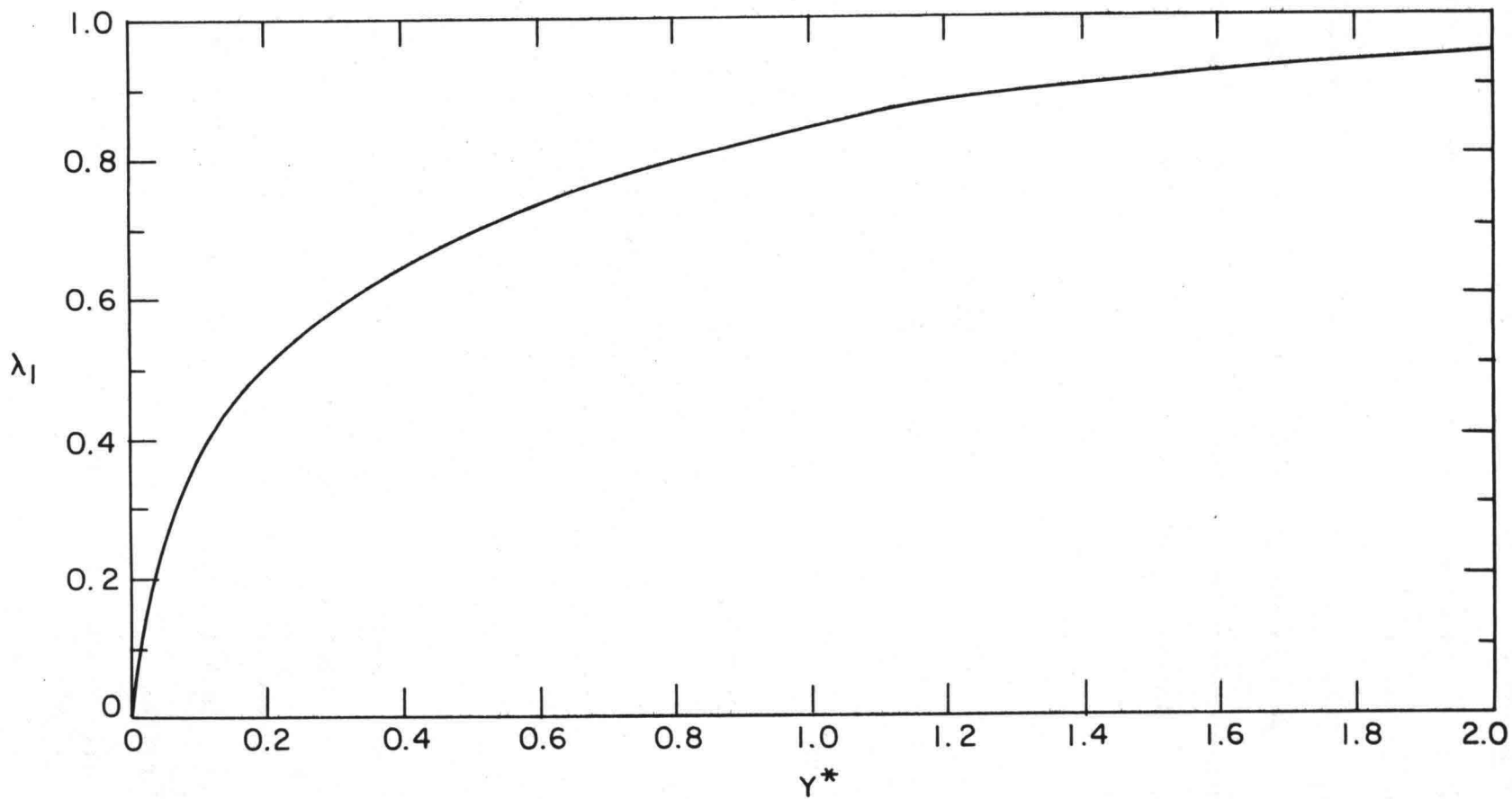
Figure 4-6:   Convective Current Reduction Factor

The first term on the RHS of Eq. (4-52) is the mass transport term discussed in Section 3.1.1 for waves of near normal incidence; this seaward current is counteracted in Eq. (4-52) by the shoreward flow induced by the evolving longshore current. Since the modified bottom slope rests on the neglect of the mass transport induced current, a plausible limit on the applicability of the Linear Longshore Current Model is given implicitly by

$$|u_s|_B < \frac{\alpha_B^2}{8} (gh_B)^{1/2} \tag{4-53}$$

In view of Eq. (4-52), this may be expressed as

$$\lambda > [\frac{5\pi\alpha_B \tan\Delta c_5}{4f_{sz} <v^* x^*>} + 1]^{-1} \tag{4-54}$$

where $<x^* v^*>$ is given by

$$<x^* v^*> = c_1 [\frac{1-c_2}{(c_2-c_3)(c_3+2)} + 0.33] \qquad (P_{sz} \neq 0.4)$$

$$<x^* v^*> = 0.17 \qquad (P_{sz} = 0.4)$$

as sketched on Figure 4-5. Taking the flat, rough beach of Table 3-1 as a worst case and anticipating $\Gamma \stackrel{\sim}{=} 0.01$ in Eq. (3-70), Eq. (4-54) yields a lower λ limit of 0.4 in view of Figure 4-5. Consulting Figure 4-6 this limit corresponds to $y^* > 0.12$ so that the Linear Longshore Current Model describes an appreciable portion of the evolving longshore profile.

The small current requirement of the Linear Longshore Current

110

Model can be quantified by noting that $v_c n_B$ is the reduced character-

istic velocity for uniform conditions so that recalling Eq. (3-64),

κn_B provides a measure of the strength of the longshore current rela-

tive to the wave velocity for waves of finite height. Noting that the

Reynolds stress will reduce the longshore current peak magnitude by

smoothing out the profile, an arbitrary limit on the propriety of the

small current assumption may be stated as

$$\kappa n_B \leq 1 \tag{4-55}$$

4.3 Linear Longshore Sediment Transport Model

The Linear Longshore Sediment Transport Model predicts the time

averaged longshore mass flux of sediment per unit free surface area

induced by water waves of near normal incidence breaking over an in-

finite plane beach comprised of uniform cohesionless spheres in the

presence of a shorenormal jetty. The model follows Reyman's (1976)

application of the nonbreaking wave sediment transport relationship

of Madsen and Grant (1976a) to the surf zone. This sediment transport

formula relates longshore sediment transport and the longshore bottom

shear stress with the latter quantity described by the Linear Longshore

Current Model under the assumption that the bottom shear is unaffected

by the presence of a movable bed. The time averaged longshore sediment

transport q_s^y is given by Eqs. (4-59) and (4-69) as a function of the

longshore sediment transport coefficient; the integrated time averaged

longshore sediment transport, which is the integral of q_s^y from x=0 to

x=∞, is given by Eq. (4-75).

4.3.1 Nonbreaking wave sediment transport

The Linear Longshore Sediment Transport Model rests heavily upon the work of Madsen and Grant (1976a), who demonstrate the applicability of steady flow sediment transport relationships to describe instantaneous sediment transport in a nonbreaking wave field, i.e., outside the surf zone. Madsen and Grant (1976a) suggest that the dimensionless instantaneous sediment transport $\vec{q}^{*}$ due to oscillatory waves flowing over a bed of uniform cohesionless spheres with or without bed forms is given by

$$\vec{q}^{*} = 40|\vec{\psi}|^{2}\vec{\psi} \qquad (|\vec{\psi}| > \psi_{c})$$

$$\vec{q}^{*} = 0 \qquad (|\vec{\psi}| < \psi_{c}) \qquad (4\text{-}56)$$

where $\vec{\psi}$ is the Shields parameter

$$\vec{\psi} = \frac{\vec{\tau}_{b}}{\rho g d_{s}(s-1)} \qquad (4\text{-}57)$$

and the bottom shear stress is determined with Jonsson's wave friction factor in the drag law expression

$$\vec{\tau}_{b} = \frac{1}{2} \rho f_{w} |\vec{u}_{w}|_{b} (\vec{u}_{w})_{b} \qquad (4\text{-}58)$$

As suggested by Eq. (4-56), Madsen and Grant (1976a) show that transport occurs when the norm of the Shields' parameter exceeds a critical value ψ_{c}. The sediment transport $\vec{q}$, which is the mass flux of sediment per unit width perpendicular to the flow, is nondimensionalized by the product of the sediment density, ρ_{s}, fall velocity, w_{F}, and grain size d_{s},

112

$$\vec{q}^{\,*} = \vec{q}/\rho_s w_F d_s \qquad\qquad\qquad\qquad (4\text{-}59)$$

Madsen and Grant (1976b) relate the dimensionless fall velocity w^* to a dimensionless parameter S^*, where

$$w^* = w_F/[gd_s(s-1)]^{1/2}$$

$$\qquad\qquad\qquad\qquad\qquad\qquad\qquad (4\text{-}60)$$

$$S^* = \frac{d_s}{4\nu}[gd_s(s-1)]^{1/2}$$

and ν is the kinematic viscosity of the fluid. Their relationship is approximated in the present investigation by the function

$$w^* = 0.22\ S^* \qquad\qquad (1 < S^*)$$

$$w^* = 0.22\ \exp[-0.054\ \ell n^2 S^* + 0.68\ \ell n\ S^*] \qquad (1 < S^* < 150)$$

$$w^* = 1.80 \qquad\qquad (S^* > 150) \qquad\qquad (4\text{-}61)$$

Madsen and Grant (1976a) note that Eq. (4-56) ignores the effects of finite wave height, wave induced mass transport and bottom slope on the sediment transport rate.

4.3.2 Time averaged longshore sediment transport in the surf zone

The Linear Longshore Sediment Transport Model adopts the nonbreaking wave transport model of Madsen and Grant (1976a) by assuming

$$(q^*)^y = \zeta\,|\vec{\Psi}|^2 \Psi^y \qquad\qquad\qquad\qquad (4\text{-}62)$$

where the longshore sediment transport coefficient ζ must accommodate the effects of wave breaking and a relatively small current. In view of the approximate nature of Eq. (4-62), sediment transport is assumed

113

to occur at all times and locations in the surf zone, or, effectively

$$\Psi_c = 0 \tag{4-63}$$

The shorenormal sediment transport is discussed at the end of this section. Eqs. (4-62) and (4-63) are similar to the longshore component of the model put forth by Reyman (1976) who retains $\zeta = 40$ and uses elliptic integrals to allow for a finite current under uniform longshore conditions with near normal incidence in the time averaging process. The Linear Longshore Sediment Transport Model, which is based on the Linear Longshore Current Model, retains the small current assumption and relaxes the requirement of longshore uniformity instead on the premise that finite longshore currents are usually generated by waves with finite angles of incidence.

Recalling Eq. (4-58), with the friction factor given by the time independent f_{sz} of Section 3.1.2, the Shields parameter may be expressed in terms of the near bottom wave and current velocities using Eq. (4-57),

$$\vec{\Psi} = [\frac{f_{sz}}{2gd_s(s-1)}] \; |\vec{u}_s + \vec{u}_w|_b \; (\vec{u}_s + \vec{u}_w)_b \tag{4-64}$$

so that the dimensionless longshore sediment transport is given by

$$(q^*)^y = \zeta \, [\frac{f_{sz}}{2gd_s(s-1)}]^3 \; |\vec{u}_s + \vec{u}_w|_b^5 \; (v_s + v_w) \tag{4-65}$$

Following the analysis of Section 3.1.2, the small current and near normal incidence assumptions yield

$$|\vec{u}_s + \vec{u}_w|_b^5 \cong (|\vec{u}_w|_b')^5 (\cos^2\phi - 2 \frac{u_s}{|\vec{u}_w|_b'} \cos\theta\cos\phi)^{5/2} \tag{4-66}$$

114

and a Taylor expansion results in

$$|\vec{u}_s + \vec{u}_w|_b^5 \stackrel{\sim}{=} (|\vec{u}_w|'_b)^5 (|\cos\phi|^5 - 5 \frac{u_s}{|\vec{u}_w|'_b} \cos\theta\cos\phi|\cos\phi|^3) \qquad (4\text{-}67)$$

Multiplying by $(v_s + v_w)$ and time averaging to leading order,

$$[(v_s + v_w)|\vec{u}_s + \vec{u}_w|_b^5]_s \stackrel{\sim}{=} (|\vec{u}_w|'_b)^5 |\cos\phi|_s^5 v_s \qquad (4\text{-}68)$$

Combining Eqs. (4-65) and (4-68), noting that $|u_w|'_b$ and v_s are given by Eqs. (3-2) and (4-37), respectively, the dimensionless time averaged longshore sediment transport is given by

$$(q^*)_s^y = \frac{\zeta\kappa\lambda_1 n_B}{60\pi} [\frac{f_{sz}\alpha_B^2 h_B}{2d_s(s-1)}]^3 \quad x^{*5/2}v^* \qquad (x^* \leq 1) \qquad (4\text{-}69)$$

$$(q^*)_s^y = \frac{\zeta\kappa\lambda_1 n_B}{60\pi} [\frac{f_{sz}\alpha_B^2 h_B}{2d_s(s-1)}]^3 \quad x^{*-15/4}v^* \qquad (x^* > 1)$$

with v_c expressed in terms of κ as suggested by Eq. (3-66) and

$$|\cos\phi|_s^5 = 16/15\pi \qquad (4\text{-}70)$$

Eq. (4-69) is derived using linear wave height variation within the breaker line and Green's Law beyond, i.e., Eqs. (2-35) and (3-53).

The time averaged shorenormal sediment transport is neglected in the present investigation,

$$(q^*)_s^x = 0 \qquad (4\text{-}71)$$

so that the developing longshore current erodes the bottom to accommo-date the downstream increase of time averaged longshore sediment trans-

115

port implied by Eq. (4-69). The rate of shore line erosion should de-
crease with increasing downstream distance as fully developed condi-
tions are achieved. As time passes, the erosion accordingly intro-
duces a longshore nonuniformity to the beach topography as has been
noticed experimentally by other investigators, e.g., Savage (1959).
The nonuniformity is in violation of the idealized environment of
Table 1-1, so that the Linear Longshore Current Model and the Linear
Longshore Sediment Transport Model describe only the initial response
of a plane movable bed to wave attack in the developing region down-
stream of a shorenormal jetty.

Eq. (4-69) improperly describes the time averaged longshore sedi-
ment transport in the immediate vicinity of the jetty where wave diffrac-
tion and a strong shoreward current invalidate the Linear Longshre
Current Model, so that the Linear Longshore Sediment Transport Model is
also constrained by Eq. (4-54). The presence of the shoreward current,
which is deduced in Section 4.2.4, may also be inferred by the observed
accumulation of sediment in the downstream region immediately adjacent
to the shorenormal jetty, e.g., Savage (1959).

In defense of the postulated shorenormal transport, it should be
noted that Eq. (4-71) is satisfied identically in the fully developed
flow region far downstream of the jetty if the beach profile is in
equilibirum with the incident waves, as is the case with the laboratory
data of Section 1.4.

4.3.3 Integrated time averaged longshore sediment transport

The total time averaged longshore sediment transport is obtained on a dimensionless basis by integrating Eq. (4-69) from $x^* = 0$ to ∞,

$$\int_{0}^{\infty} (q^*)^y_s \, dx^* = \frac{\zeta \kappa \lambda_1 n_B}{60\pi} \left[\frac{f_{sz_B} \alpha_B^2 h_B}{2d_s(s-1)}\right]^3 (c_6 + c_7) \tag{4-72}$$

where

$$c_6 = <v^* x^{*5/2}> \tag{4-73}$$

$$c_7 = \int_{1}^{\infty} v^* x^{*-15/4} \, dx^*$$

The dimensionless longshore current profile of Eq. (3-76) is now invoked to compute the constants, i.e.,

$$c_6 = c_1 \left\{\frac{1-c_2}{(c_2-c_3)(c_3+3.5)} + 0.22\right\} \qquad (P_{sz} \neq 0.4)$$

$$c_6 = 0.09 \qquad (P_{sz} = 0.4) \tag{4-74}$$

$$c_7 = \left(\frac{1-c_3}{c_2-c_3}\right)\left(\frac{c_1}{2.75-c_2}\right) \qquad (P_\ell \neq 0.4)$$

$$c_7 = 0.06 \qquad (P_\ell = 0.4)$$

The constants are also sketched on Figure 4-5. As suggested by the relative size of c_6 and c_7, the importance of time averaged longshore sediment transport occurring inside of the breaker line is inversely proportional to the mixing parameter. Recalling Table 3-1 and Eq. (3-70) and anticipating $\Gamma \cong 0.01$, P_{sz} varies between 0.01 and 1 so that the amount of time averaged longshore sediment transport occurring with-

117

in the breaker line is between 55% and 85% of the total transport.

Recalling Eqs. (3-57) and (4-59), the integrated time averaged longshore sediment transport is given by

$$\int_0^\infty (q)_s^y dx = \rho_s \; x_B w_f d_s \int_0^\infty (q^*)_s^y dx^*$$ (4-75)

where the RHS integral is given by Eq. (4-72).

4.4 Nonlinear Longshore Current Model

The data base of Section 1 suggests that the typical flow field consists of a relatively strong current response to breaking waves of finite incidence in violation of the linearizing assumptions of a small current and near normal wave incidence. The use of the Linear Long-shore Current Model in this case underestimates the correlation of $|\vec{u}_s + \vec{u}_w|_b$ and $(v_s + v_w)$ in the longshore bottom shear stress compon-ent since terms neglected in the time averaging process of Section 3.1.2 are of significant magnitude. The low estimate in turn artificially increases the size of f_{sz} since the longshore bottom shear stress com-ponent must resist the driving stress with an effectively slower veloc-ity.

The Nonlinear Longshore Current Model uses numerical integration to account for the presence of a finite current and oblique wave in-cidence in the longshore bottom shear stress component of the inte-grated nonlinear longshore stress balance

$$S_B^{xy} + T_B^{xy} + \frac{1}{2} \rho f_{sz} <[|\vec{u}_s + \vec{u}_w|_b (v_s + v_w)]_s> x_B = 0$$ (4-76)

118

As suggested by Eq. (4-76) the Nonlinear Longshore Current Model considers uniform longshore conditions. As with the Linear Longshore Current Model, Reyman's (1976) similarity assumption is adopted in the Nonlinear Longshore Current Model so that the effects of a finite current and oblique wave incidence on the bottom shear stress are modeled by the nonlinear current reduction factor which reduces the scale of the longshore current profile. Eq. (4-76) is recast as a numerical iteration in the nonlinear current reduction factor; Eq. (4-93) is a curve fitted approximation of the resulting solution.

The oblique wave incidence also reduces the integrated driving stress; the factor $\cos\theta_B$ is consequently included in the reduction of the longshore current profile.

4.4.1 Numerical longshore bottom shear stress estimates

Recalling Eq. (2-23), the time averaged longshore bottom shear stress component is given by

$$(\tau_b^y)_s = \frac{1}{2} \rho f_{sz} [(v_s + v_w)_b |\vec{u}_s + \vec{u}_w|_b]_s \qquad (4\text{-}77)$$

With the neglect of shorenormal current and the assumption of linear long waves inside the breaker line, simplifications which are motivated by discussions in Sections 3.1.1 and 3.4.4, respectively, the norm of the near bottom velocity is

$$|\vec{u}_s + \vec{u}_w|_b \overset{\sim}{=} (v_s^2 + 2v_s|\vec{u}_w|_b' \sin\theta\cos\phi + (|\vec{u}_w|_b')^2\cos^2\phi)^{1/2} \qquad (4\text{-}78)$$

Defining the local current strength δ in accordance with

119

$$\delta = v_s / |\vec{u}_w|_b' \qquad (4\text{-}79)$$

the time averaged longshore bottom shear stress may be expressed as

$$(\tau_b^y)_s = \frac{1}{2} \rho f_{sz} (|\vec{u}_w|_b')^2 (\tau_b^y)_s^* \qquad (4\text{-}80)$$

where

$$(\tau_b^y)_s^* = \frac{1}{2\pi} \int_0^{2\pi} (\delta + \sin\theta\cos\phi)(\delta^2 + 2\delta\sin\theta\cos\phi + \cos^2\phi)^{1/2} d\phi$$

$$\qquad (4\text{-}81)$$

For small currents and near normal incidence, $\delta \ll 1$ and $\sin\theta \backsim 0$ and Eq. (4-81) yields $(\tau_b^y)_s^* \overset{\backsim}{=} \frac{2\delta}{\pi}$ and the linear result of the Modified Longuet-Higgins Model is obtained. For finite currents of near normal incidence, the $\sin\theta$ terms drop out of Eq. (4-81) and the elliptic integrals of Reyman (1976) and Jonsson et al. (1974) remain. Liu and Dalrymple (1978), who derive a longshore current model for relatively strong currents in the absence of Reynolds stresses, Taylor expand the square root term in the integrand of Eq. (4-81) to second order for $\delta > 1.25$ to obtain

$$(\tau_b^y)_s^* = \delta^2 + \frac{1 + \sin^2\theta}{4} \qquad (4\text{-}82)$$

Liu and Dalrymple (1978) derive a second model for a relatively weak longshore current and oblique wave incidence, again in the absence of Reynolds stresses; the time averaged longshore bottom shear stress term is approximated by a Taylor expansion for $\delta \ll 1$ similar to that of the Modified Longuet-Higgins Model, but with the addition of a $\sin^2\theta$ term. The authors do not interpolate between their shear stress estimates.

Anticipating an approximate longshore current model valid for any current strength and incident wave angle, the Nonlinear Longshore Current Model evaluates Eq. (4-77) with the following expression

$$
(\tau_b^y)_s^* = \begin{cases} (\tau_b^y)_{s5}^* & (\delta \geq .50) \\ (\tau_b^y)_m^* & (.50 > \delta > .125) \\ 2\delta/\pi & (.125 \geq \delta) \end{cases}
\qquad (4\text{-}83)
$$

where $(\tau_b^y)_{s5}^*$ is a numerical integration using five point Gauss quadrature, Bathe and Wilson (1976), i.e.,

$$
(\tau_b^y)_{s5}^* = .118 \left[(\tau_b^y)^*(\phi = 2.99) + (\tau_b^y)^*(\phi = .147) \right]
$$

$$
+ .239 \left[(\tau_b^y)^*(\phi = 2.42) + (\tau_b^y)^*(\phi = .725) \right]
\qquad (4\text{-}84)
$$

$$
+ .284 (\tau_b^y)^*(\phi = 1.57)
$$

and $(\tau_b^y)^*$ is the integrand of Eq. (4-81). This numerical estimate lies within 1% of Liu and Dalrymple's (1978) approximation, Eq. (4-82), for $\delta \geq 1.0$ and $\theta \leq 40^o$. Gauss quadrature works well for polynomials and poorly for sinusoids so that an interpolation is used for small δ

$$
(\tau_b^y)_m^* = 0.0796 + (\delta - .125)(2.67\tau_{50} - .212)
\qquad (4\text{-}85)
$$

where τ_{50} is the quadrature estimate at $\delta = .50$.

The surf zone integrated, time averaged nonlinear longshore bottom shear stress component may accordingly be written as

121

$$x_B \langle (\tau_b^y)_s \rangle = \frac{1}{2} \rho f_{sz} (|\vec{u}_w|_b')_B^2 \, x_B \int_0^1 x^* (\tau_b^y)_s^* dx^* \tag{4-86}$$

since $|\vec{u}_w|_b'$ is given by the linear long wave theory of Eq. (3-2) and f_{sz} is independent of x. The spatial integral is approximated using four point Gauss quadrature, i.e.,

$$\int_0^1 x^* (\tau_b^y)_s^* dx^* = .174 [x^*(\tau_b^y)_s^*(x^* = .193) + x^*(\tau_b^y)_s^*(x^* = .069)]$$

$$\tag{4-87}$$

$$+ .326 [x^*(\tau_b^y)_s^*(x^* = .670) + x^*(\tau_b^y)_s^*(x^* = .330)]$$

where $(\tau_b^y)_s^*$ is obtained from Eq. (4-83). It should be noted that current refraction is excluded from consideration.

The quadrature order of this and the prior estimate is obtained by studying estimate convergence as the order increases; the spatial estimate is a better behaved function and may be approximated with a lower degree polynomial.

4.4.2 Integrated nonlinear longshore stress balance

Following the Linear Longshore Current Model, the governing momentum equation is simplified with Reyman's (1976) similarity assumption which becomes

$$v_s = v^* v_c \lambda_2 n_B \cos\theta_B \tag{4-88}$$

in the Nonlinear Longshore Current Model where the λ_2 factor accounts for the finite current and oblique wave incidence on the time averaged longshore bottom shear stress, while n_B and $\cos\theta_B$ reflect a reduced integrated driving stress, as in Section 4.1.4.

Substitution of Eq. (4-88) into Eq. (4-76) yields a governing
equation for λ_2. Recalling Eq. (4-86)

$$1 + \frac{T_B^{xy}}{S_B^{xy}} + \frac{\rho f_{sz}(|\vec{u}_w|_b')_B^2 x_B \int_o^1 x^* (\tau_b^y)_s^* dx^*}{2S_B^{xy}} = 0 \qquad (4\text{-}89)$$

where the integrated nonlinear longshore stress balance is nondimens-
ionalized with the finite wave height radiation stress term S_B^{xy}. Using
Eqs. (3-37) and (3-2) to evaluate S_B^{xy} and $(|\vec{u}_w|_b')_B$, and noting that

$$T_B^{xy} = - \frac{\rho \Gamma \alpha_B \tan\Delta}{2} x_B^2 (gh_B)^{1/2} (\frac{dv_s}{dx})_B \qquad (4\text{-}90)$$

upon integration of Eq. (3-56) from 0 to x_B, the assumed similarity
reduces Eq. (4-89) to

$$1.0 + \frac{5P_{sz}\lambda_2}{2} (\frac{dv^*}{dx^*})_B - \frac{5\pi}{4\kappa} (\frac{\int_o^1 x^* (\tau_b^y)_s^* dx^*}{n_B \cos\theta_B}) = 0 \qquad (4\text{-}91)$$

where κ is given by Eq. (3-65). Since the integrand is a function of
δ, which may be expressed as

$$\delta = \frac{\kappa \lambda_2 n_B \cos\theta_B}{x^{*1/2}} v^* \qquad (4\text{-}92)$$

λ_2 appears implicitly in the third term of Eq. (4-91) so that an iter-
ative solution is required, with λ_2 emerging as a function of n_B, θ_B,
P_{sz} and κ.

4.4.3 Nonlinear current reduction factor

The iterative solution to the dimensionless integrated nonlinear longshore stress balance of Eq. (4-91) may be reasonably represented by the following curve fit approximation of the nonlinear current reduction factor

$$\lambda_2 = c_8 \ln \frac{\kappa}{2} + \lambda_c \qquad (\kappa \geq 1.0)$$

$$\lambda_2 = 1.00 + \kappa(\lambda_c - 0.69c_8 - 1.00) \qquad (\kappa < 1.0)$$

(4-93)

where

$$c_8 = (1 - 0.084P_{sz})(\frac{0.0085}{n_B} - 0.18)$$

and λ_c, which is simply $\lambda_2(\theta_B = 20°, \kappa = 2.0)$, approximated by

$$\lambda_c = c_9 n_B + c_{10}$$

with

$$c_9 = 0.0035\ln^2(1000P_{sz}) - 0.30$$

and

$$c_{10} = 0.0015\ln^2(1000P_{sz}) + 0.86$$

The λ_2 iteration of Eq. (4-91) converges to within 30% and 15% accuracy when Eq. (4-93) is used for $\kappa \leq 16.0$ and $\kappa \leq 4.0$, respectively, with $\theta_B \leq 40°$, $0.16 \leq n_B \leq 0.96$, and $0.01 \leq P_{sz} \leq 10$ for both cases. This accuracy is judged to be acceptable in view of the approximate nature of the assumptions underlying the integrated nonlinear longshore surf zone stress balance and the utility of an analytical expression for λ_2. λ_c is sketched on Figure 4-7 to aid in model usage.
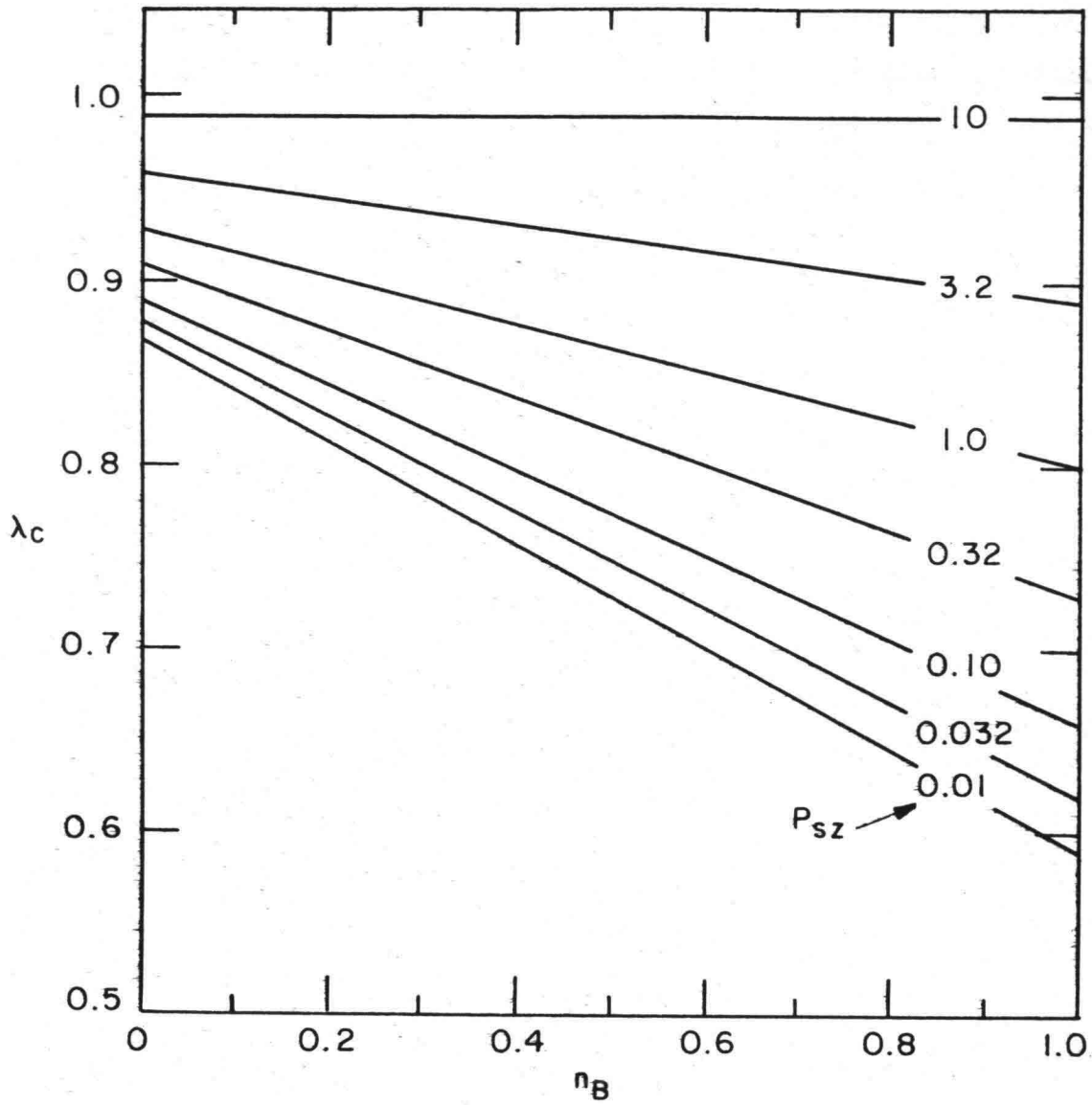
124

Figure 4-7: Characteristic Current Reduction Factor

With n_B, θ_B and $\tan\Delta$ known from the breaking wave iteration of Section 4.1.3, κ, P_{sz} and λ_2 may be computed when the two parameters f_{sz} and Γ are specified; P_{sz} in turn determines v^* by virtue of Eq. (3-76) and Figure 3-1, and λ_2 scales the longshore current profile in accordance with Eq. (4-88). The process is illustrated in Appendix I.

5 MODEL CALIBRATION AND TESTING

5.1 Model Calibration

The model parameters f_{sz}, Γ and ζ are presently unspecified and consequently may be calibrated with the most appropriate data of Section 1.

Transect 6 of the GE data base calibrates f_{sz} and Γ which determine the scale and form of the longshore current profile, respectively. These data are selected since the fixed bed experiments most nearly represent the idealized environment and neglected stresses and accelerations of Tables 1-1 and 1-2; Galvin and Eagleson (1965) are the only investigators to measure longshore current profiles across a transect and the relatively strong longshore current at transect 6 is observed to be reasonably uniform in the longshore direction. Shay and Johnson's (1951) longshore sediment transport data calibrates ζ; the laboratory movable bed data is judged to be more applicable than the field data since the wave conditions are better defined in the laboratory, and the small current assumption of the Linear Longshore Sediment Transport Model is better satisfied with the Shay and Johnson (1951) data than with the data of Saville (1949, 1950).

5.1.1 Surf zone friction factor

The surf zone friction factor calibration consists of a good fit analysis of each of the 28 runs comprising the GE transect 6 data. The analysis searches through all reasonable combinations of f_{sz} and Γ to find the pair of values yielding the smallest error for a given run;

127

the resulting 28 f_{sz} values are examined in order to establish a phys-
ically plausible predictor of the surf zone friction factor. The quan-
tity that is minimized in the calibrating runs in Q_{cal}, defined by

$$Q_{cal} = \Sigma \; \frac{v_s(\text{measured}) - v_s(\text{predicted})}{v_s{'}(\text{predicted})} \tag{5-1}$$

where the summation is over all stations in a run; calculations indicate
that Q_{cal} has a single minimum within the range of interest of the two
parameters for both analyses. The search procedure consists of the
Golden Section Method, e.g., Carnahan and Wilkes (1968), which reduces
the search interval to a prescribed width, and a Lagrangian locator,
which computes the point of zero slope of a parabola through the points
of the reduced search interval.

Figure 5-1 shows the results of the good fit analysis of f_{sz} values
plotted as a function of $\kappa n_B \cos\theta_B \lambda_2$. Recalling Eqs. (3-64) and (4-88),
the independent variable is the ratio of the reduced characteristic
velocity to the maximum near bottom wave velocity at the breaker line
and as such provides a measure of the relative strength of the long-
shore current. The distribution of the good fit f_{sz} values on this graph
suggests that f_{sz} decreases as the relative longshore current magnitude
increases in agreement with the behavior postulated by Jonsson et al.
(1974). The use of the 28 run average Jonsson (1966a) wave friction
factor $\bar{f}_w$ and 28 run average Darcy-Weisbach type current friction factor
$\bar{f}_s$ as a vertical intercept and a horizontal asymptote becomes physically
plausible when the average values of these parameters for the 28 runs

128

evaluated midway through the surf zone are plotted on Figure 5-1; unfortunately the predictor would be iterative since κ appears implicitly in λ_2 as indicated by Eq. (4-93). The simpler approach of using κ as the ordinate is adopted as sketched in Figure 5-2.

The predictor is a branch of a hyperbola with specified rotation, intercept and asymptote, so that only the constant governing horizontal translation is free to vary, i.e.,

$$f_{sz} = \frac{f_w + c_{11}\kappa f_s}{1 + c_{11}\kappa} \tag{5-2}$$

A good fit analysis of c_{11} yields

$$c_{11} = 0.148 \tag{5-3}$$

Eq. (5-2) closely approximates an expression put forth by Jonsson (1966b) for waves and currents outside the surf zone. Since, as suggested by Eq. (3-65), f_{sz} appears in κ, Eq. (5-2) may be rearranged to yield

$$f_{sz} = [-c_{12} + (c_{12}^2 - 4c_{13})^{1/2}]/2 \tag{5-4}$$

where

$$c_{12} = .58\ \tan\Delta\sin\theta_B - f_w$$

and

$$c_{13} = -.58(\tan\Delta\sin\theta_B)f_s$$

In the computation of f_s and f_w the flow is assumed to be turbulent, with smooth and rough regimes determined in accordance with Jonsson's (1966a) "SR" line, which is represented by
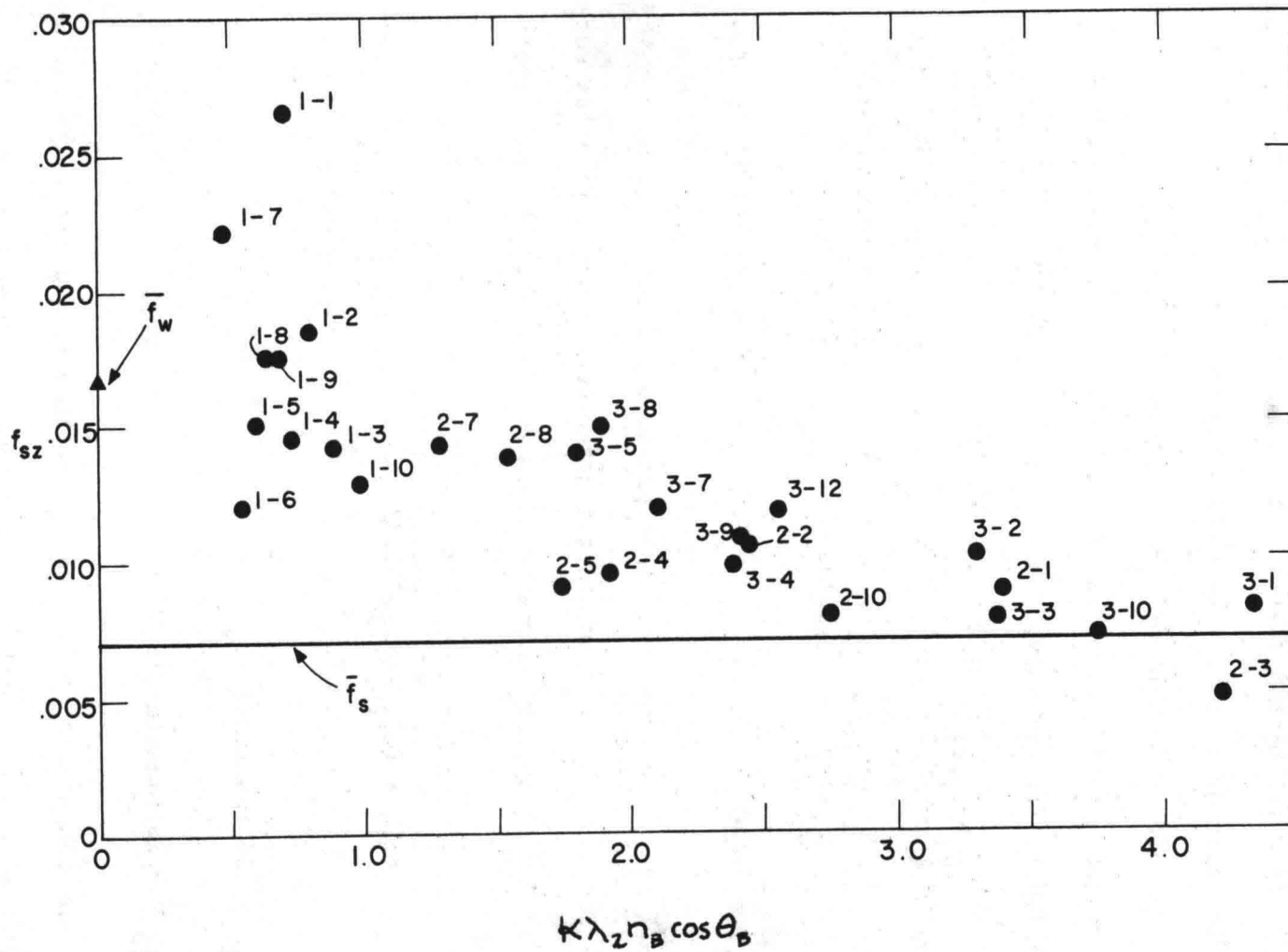
129

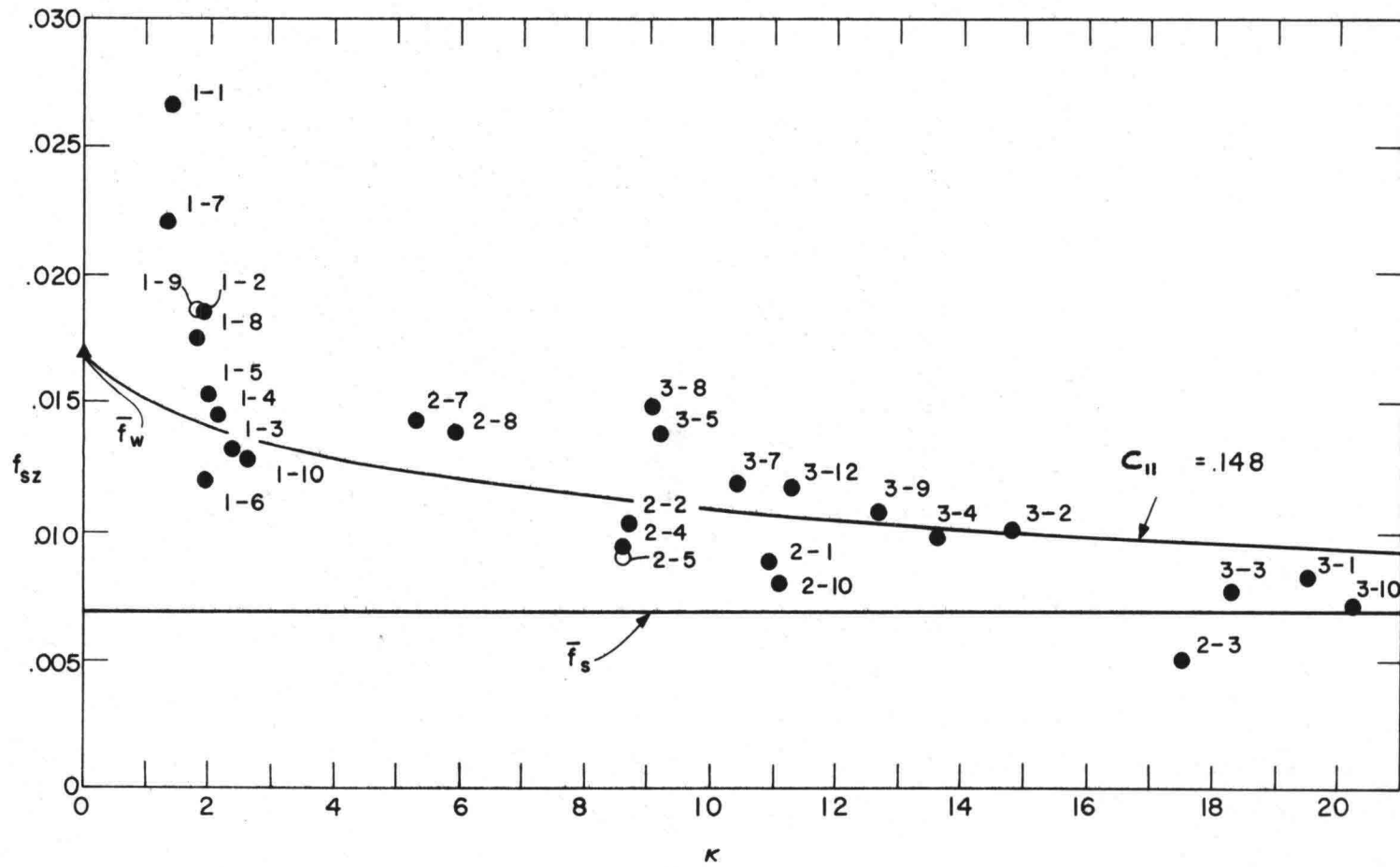Figure 5-1: Good Fit f_{sz} Values vs $\kappa\lambda_2 n_B \cos\theta_B$

Figure 5-2: Good Fit f_{sz} Values vs κ

131

$$\ln \frac{<A_b>}{k_s} \geq .86 \ln R_w - 2.74 \qquad \text{(smooth turbulent)}$$

$$(5\text{-}5)$$

$$\ln \frac{<A_b>}{k_s} < .86 \ln R_w - 2.74 \qquad \text{(rough turbulent)}$$

where $<A_b>$ is the near bottom horizontal excursion amplitude, evaluated mid-way through the surf zone. f_w and f_s for both regimes are sketched in Figure 5-3 as functions of appropriate Reynolds numbers and relative roughnesses and computed in accordance with

Smooth Turbulent Regime

$$f_w = \exp(.0184 \ln^2 R_w - .66 \ln R_w + .462)$$

$$f_s = .0559 \, R_s^{-.25} \qquad (R_s \leq 25,000) \qquad (5\text{-}6)$$

$$f_s = .027 \, R_s^{-.179} \qquad (R_s > 25,000)$$

and

Rough Turbulent Regime

$$f_w = \exp(.0371 \ln^2 \frac{<A_b>}{k_s} - .791 \ln \frac{<A_b>}{k_s} - .97)$$

$$(5\text{-}7)$$

$$f_s = (1.74 \ln \frac{<h>}{k_s} + 4.32)^{-2}$$

where the relative roughness ratios are given by

$$\frac{<h>}{k_s} = \frac{h_B}{2k_s}$$

$$(5\text{-}8)$$

$$\frac{<A_b>}{k_s} = .113 \, \alpha_B \gamma_B \, (\frac{h_B}{2k_s})$$

132
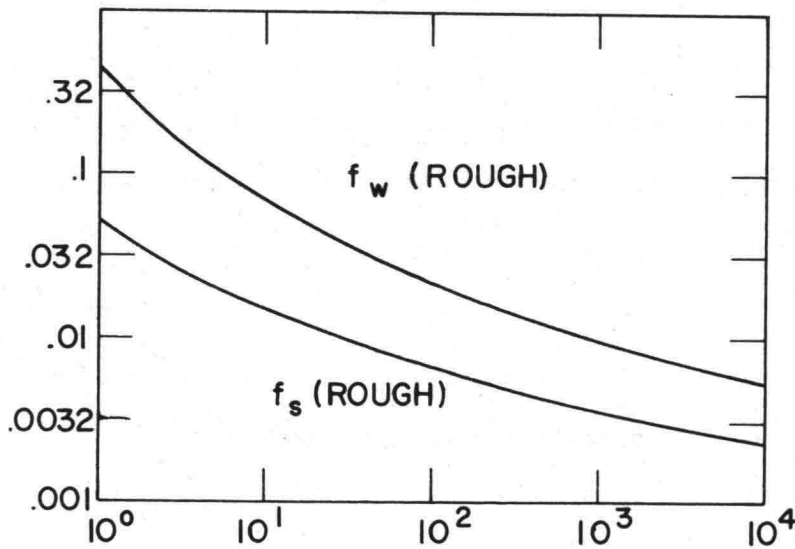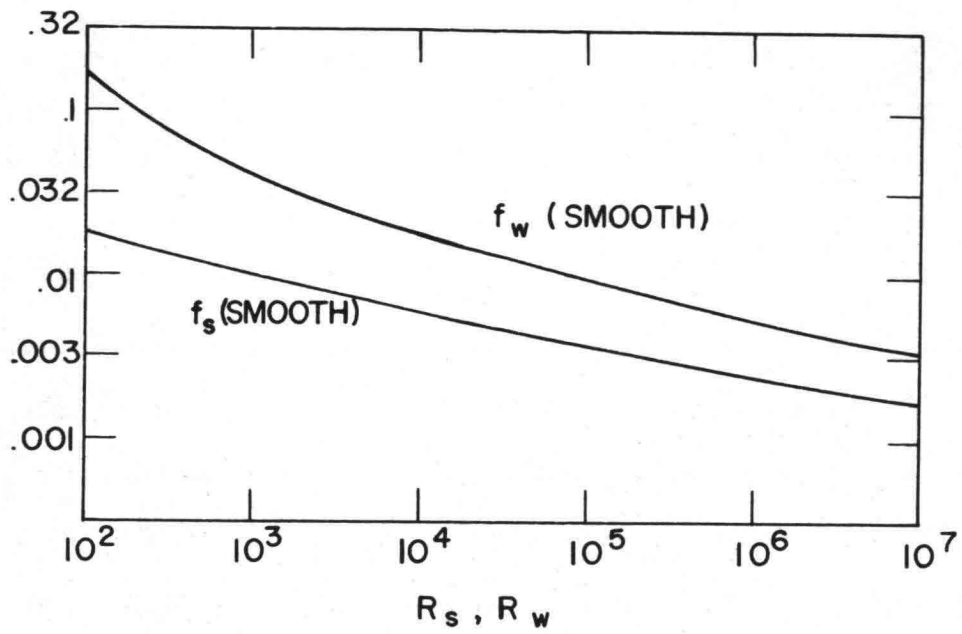
Figure 5-3: Wave and Current Friction Factors

133

while the Reynolds numbers are

$$R_w = \frac{\alpha_B^2 g h_B}{8 \omega \nu}$$

$$R_s = .177 \frac{\alpha_B h_B (g h_B)^{1/2}}{\nu}$$

(5-9)

The longshore current Reynolds number is for simplicity based on the wave velocity since v_s is not known in advance and is of comparable magnitude to $|u_w|_b'$; however, iteration is of course possible, although tedious. The wave friction factor expressions of Eqs. (5-6) and (5-7) are three point polynomials through the Jonsson (1966a) diagram, while the current friction factor expressions are from Chow (1959) and Henderson (1966).

A sample determination of f_{sz} is contained in the numerical example in Appendix I.

5.1.2 Lateral mixing coefficient and Battjes' correlation constant

The surf zone friction factor predictor of Eqs. (5-4) through (5-9) eliminates one free parameter from the Nonlinear Longshore Current Model so that a second good fit analysis searches through Γ values to minimize Q_{cal}, with the results indicated in Table 5-1. A single value is judged to be appropriate, and a good fit analysis on all runs yields

$$\Gamma = .013$$

(5-10)

As indicated by Eqs. (3-29) and (3-55), Γ may be regarded as a function of Battjes' correlation constant M, $\tan\beta$ and α_B. Consequently,

134

Table 5-1

Good Fit Γ Values with f_{sz} Predictor

Γ									
0									
.005	2-4	2-5	3-4*						
.010	1-6	2-2	2-3	2-7	2-8	2-10	3-3	3-9	3-10
.015	1-4	1-5	1-8	1-9	2-1	3-1	3-12		
.020	1-2	1-3	1-10	3-2	3-7	3-8			
.025									
.030									
.035	1-7								
.040									
.045									
.050									
.055	1-1	3-5							
.060									

*I-J of GE run

noting that $\tan\beta = 0.109$ and α_B does not vary appreciably from a value of 1.1 for the GE-6 data base, the good fit analysis may be taken as a search for M and Eq. (5-10) used to generate a calibrated estimate of

$$M = 0.31 \tag{5-11}$$

Battjes' correlation constant is assumed valid for beaches of other slopes, thus introducing a slope dependency into Γ by virtue of Eq. (3-55)

$$\Gamma = 0.42(\tan^4\Delta/\alpha_B)^{1/3} \tag{5-12}$$

135

The primary motive for this assumption is the fact that a constant M yields slightly more accurate test results; it should be noted, however, as discussed in Section 3.2.2, that there are valid physical reasons for this interpretation of the longshore Reynolds stress as well.

5.1.3 Longshore sediment transport coefficient

The longshore sediment transport coefficient is the remaining unspecified model parameter once f_{sz} and Γ are assumed valid for surf zones over movable beds. It is a simple matter to convert total time averaged longshore sediment transport measurements into estimates of ζ using Eqs. (4-72) and (4-75) and the Shay and Johnson (1951) laboratory data of Table 1-10. This exercise yields ζ values of 790, 960 and 240. Taking the arithmetic mean of these estimates, the calibrated longshore sediment transport coefficient is given by

$$\zeta = 660 \tag{5-13}$$

The calibrated ζ value is an order of magnitude larger than the nonbreaking wave value of $\zeta = 40$ put forth by Madsen and Grant (1976a), a difference which may reflect the higher transport capability of breaking wave induced turbulence in the surf zone.

5.2 Model Testing

The calibrated models of the present investigation are tested with appropriate data of Section 1 as cited in Table 5-2.

This data is checked in Table 5-3 against the requirement of transitional spilling-plunging breakers as quantified in Eq. (2-24). As

136

Table 5-2

Model Test Data

NONLINEAR LONGSHORE CURRENT MODEL

Galvin and Eagleson (1965) - Transects 5, 6[*]

Putnam, Munk and Traylor (1949)

Brebner and Kamphuis (1963)

LINEAR LONGSHORE CURRENT MODEL

Galvin and Eagleson (1965) - I = 1, J = 4-8

Saville (1949, 1950)

Komar (1969)

LINEAR LONGSHORE SEDIMENT TRANSPORT MODEL

Shay and Johnson (1951)[*]

Saville (1949, 1950)

Komar (1969)

[*]Calibrating data

---

indicated in the table the majority of the data falls within the suggested constraints; the PMT data is the only set with an appreciable number of plunging breakers, while strongly spilling breakers are excluded from all the data.

The data testing the linear models of the present investigation are also checked in Table 5-3 against the small current requirement of the Linear Longshore Current Model, which is discussed in Section 4.2.4 and quantified in Eq. (4-55). The majority of the data falls around the suggested upper κn_B limit of 1.0, thus underscoring the need for a more safely linear data base or nonlinear models describing longshore sediment transport and an evolving longshore current. In the absence

Table 5-3

Data Applicability

BREAKER TYPE

ξ_B	0.0	0.2	0.4	0.6	0.8	1.0	1.2	1.4
GE	0*	0	28	61	11	0	0	
PMT	3	31	16	19	9	9	13	
BK	7	43	38	12	0	0	0	
SJ	0	0	33	67	0	0	0	
SV	0	29	42	29	0	0	0	
KO	0	33	67	0	0	0	0	

RELATIVE CURRENT STRENGTH

κn_B	0.0	0.2	0.4	0.6	0.8	1.0	1.2
GE $-I-1$, $J=4-8$	0	0	20	0		80	0
SJ	0	0	0	0		67	33
SV	0	0	0	0		43	57
KO	0	33	33	33		0	0

*Percentage of experiments in category

of either alternative, the data testing the linear models is assumed to represent linear conditions; it is anticipated that the resulting linear longshore current predictions will overestimate the measured values due to nonlinear effects.

5.2.1 Linear Longshore Current Model testing

Linear Longshore Current Model accuracy is assessed by using each data set to generate a sample of size n_Q of the variable Q_v, defined by

$$Q_v = \frac{v_s(\text{measured}) - v_s(\text{predicted})}{v_s(\text{predicted})} \qquad (5\text{-}14)$$

Two sample statistics are computed: the sample mean $\overline{Q}_v$ and the sample standard deviation S_Q. $\overline{Q}_v$ is computed in accordance with Eq. (4-14); recalling Eq. (5-14), a positive $\overline{Q}_v$ implies that the prediction underestimates the observed current. S_Q is given by, e.g., Benjamin and Cornell (1970),

$$S_Q = \left[\frac{n_Q}{n_Q - 1} \left(\sum_{i=1}^{n_Q} \frac{Q_{vi}^2}{n_Q} - \overline{Q}_v^2\right)\right]^{1/2} \qquad (5\text{-}15)$$

If Q_v is assumed to be normally distributed, about two-thirds of the sample points fall within $100 S_Q$ percent of $\overline{Q}_v$.

Caution must accompany the selection of n_Q and the interpretation of the sample statistics: systematic errors within a given sample n_Q will not appear in the sample statistics and the use of predicted velocity as a normalizing variable makes serious overpredictions appear to be more accurate than serious underpredictions. To illustrate the first point, consider the PMT data base analyzed in the following section; the systematic error in slope and lack of systematic error in k_s may only be deduced when the entire data base is broken down into smaller samples. To illustrate the second point consider the two sample points $v_{s1}(\text{predicted}) = 0.5 v_{s1}(\text{measured})$ and $v_{s2}(\text{predicted}) = 1.5 v_{s2}(\text{measured})$: the underprediction has $Q_{v1} = +1.0$, while the overprediction, which is off by the same absolute amount, has $Q_{v2} = -0.67$. In defense of Eq. (5-14) it should be noted that this normalization permits direct comparison between estimates of currents of varying strength.

139

With these warnings, then, Linear Longshore Current Model testing may proceed.

The predicted downstream development of the longshore current is tested against the appropriate fixed bed measurements of Galvin and Eagleson (1965) with the results indicated in Table 5-4. As anticipated, the Linear Longshore Current Model predictions overestimate the measurements somewhat due presumably to the finite size of the current. The uniformity of the error with downstream distance which, as discussed in Section 1.3.1 increases with increasing K, suggests that the Linear Longshore Current Model provides a reasonable estimate of the form of the longshore dependency. The S_Q values show that roughly two-thirds of the data lie within 40% of their predictions.

The movable bed longshore current data provide the second test of the Linear Longshore Current Model as summarized in Table 5-5. The Linear Longshore Current Model overestimates the SV and KO data by 33% and 5%, respectively; an error which may be attributed to the nonlinearity displayed in Table 5-3 and to the presence of a movable bed. The

Table 5-4

Linear Longshore Current Model

Tests in y   GE I = 1,   J = 4-8

K	2	3	4	5	6
n_Q	18	23	23	23	23
$\overline{Q}_v$	-0.29	-0.19	-0.15	-0.17	-0.19
S_Q	0.26	0.38	0.38	0.36	0.32

Table 5-5

Linear Longshore Current Model

Movable Bed Tests

Study	n_Q	$\overline{Q}_v$	S_Q
SV Laboratory	7	−0.33	0.09
KO Field	3	−0.05	0.42

latter suggestion is purely speculative since the effect of suspended
sediment on the much simpler uniform steady flow field velocity pro-
file is still undetermined, e.g., Raudkivi (1976). In any event, the
Linear Longshore Current Model does provide at least an order of mag-
nitude estimate of a relatively small longshore current over a movable
bed under laboratory and field conditions.

5.2.2 Nonlinear Longshore Current Model testing

The Nonlinear Longshore Current Model is tested for systematic
errors in bottom slope, roughness and shorenormal distance using the
random variable Q_v of Eq. (5-14). All the data listed in Table 5-2
are run to investigate $\tan\beta$ errors, while the PMT $0.10 \leq \tan\beta \leq 0.15$
data are examined for roughness errors and the GE transect 6 data is
used to identify systematic errors in the form of the velocity profile.

Table 5-6 lists the sample statistics for the entire data base
used to test the Nonlinear Longshore Current Model. The overall
accuracy is judged to be of good quality, particularly for bottom
slopes near the calibrating value $\tan\beta \overset{\sim}{=} 0.10$.

Table 5-6

Nonlinear Longshore Current Model

Tests in $\tan\beta$ and k_s

Study	$\tan\beta$	k_s (cm)	n_Q	$\overline{Q}_v$	s_Q
BK	0.050	0.03	47	0.11	0.24
PMT	0.066	0.10	7	0.02	0.22
BK	0.100	0.03	94	−0.14	0.11
PMT	0.10–0.15	0.03	9	−0.14	0.07
PMT	0.10–0.15	0.10	3	−0.13	0.18
PMT	0.10–0.15	0.63	9	−0.13	0.28
GE-5	0.109	0.03	130	−0.07	0.31
GE-6[*]	0.109	0.03	136	−0.02	0.29
PMT	0.24	0.10	4	−0.34	0.20

[*]Calibrating data

$\overline{Q}_v$ for the GE data uses $<v_s>$ as the normalizing velocity. The Nonlinear Longshore Current Model predicts its calibrating transect, GE-6, reasonably well as one would expect while the greater overprediction of transect 5 suggests that the current may still be accelerating in this region. The relative size of the sample standard deviations reflects the fact that both form and scale of the longshore current profile are tested by the GE data.

The tests conducted with the PMT data base indicate a systematic Nonlinear Longshore Current Model error in $\tan\beta$, in that the model

underpredicts longshore currents over flat slopes and overpredicts longshore currents over steeper beaches. One possible untested explanation for the underprediction lies in the fact that, as discovered in the laboratory data of Horikawa and Kuo (1966) for example, $H/h < \alpha_B$ inside the surf zone for spilling breakers which will occur on flatter beaches. Accordingly the Nonlinear Longshore Current Model overestimates the contribution of the wave motion to the bottom shear force so that the longshore current will be underpredicted. For the steeper slopes, there lies the possibility that the actual longshore current is not fully developed, so that part of the driving stress is accelerating the current. As indicated by Eq. (4-46), y_c increases with increasing κ, hence $\tan\beta$, so that currents flowing over the steeper slopes require more distance to develop. In any event, the discussion of Section 6 notes that the formulation of λ_2 loses physical validity as the bottom slope becomes steep.

As discussed in Section 1.3.3, the k_s value assigned to the beach of the BK data ignores the presence of artificial roughness so that the predicted velocity, which flows over a smoother beach than is actually present, is likely to be too high. It is not surprising then, that $\overline{Q}_V$ is negative for the $\tan\beta = 0.10$ runs, a higher roughness would bring $\overline{Q}_V$ up to zero. The BK data show the same systematic error in $\tan\beta$ as is observed in the PMT data.

The salient feature of the PMT tests shown in Table 5-6 is the equivalence of $\overline{Q}_V$ for the three different surfaces of the $0.10 < \tan\beta < 0.15$ runs which suggest that the f_{sz} predictor is properly responsive

143

to different relative roughnesses. Indeed, the reasonable accuracy of nearly all the tests indicates that the scale of the longshore current, which is sensitive to f_{sz}, is properly determined, and it should be noted that in applications where spatial average is required, the proper scale is sufficient.

The 6 samples presented in Table 5-7 correspond to measurements made at 6 stations across GE transect 6 with a higher X value indicating a larger distance from shore. Station 4 is in the general vicinity of the breaker line. The $\overline{Q}_v$ values show that the Nonlinear Longshore Current Model significantly overpredicts the observed velocity seaward of the breaker line, and immediately casts doubt on the validity of the horizontal eddy viscosity estimate beyond the breaker line; the present estimate allows for too much Reynolds stress through the breaker line. Future estimates would do well to retain more of the driving stress within the breaker line; in this regard v_s would be forced to increase in order to resist the added stress.

Table 5-7

Longshore Current Model

Tests in x GE-6

X	1	2	3	4	5	6
n_Q	28	28	28	28	16	8
$\overline{Q}_v$	+.08	+.13	0	−.11	−.25	−.32

5.2.3 Linear Longshore Sediment Transport Model testing

Linear Longshore Sediment Transport Model testing proceeds with samples of the random variable Q_q defined by

$$Q_q = \frac{\int_0^\infty q_s^y dx(\text{measured}) - \int_0^\infty q_s^y dx(\text{predicted})}{\int_0^\infty q_s^y dx(\text{predicted})} \quad (5-16)$$

Sample means and standard deviations for the three data sets cited in Table 5-2 are presented in Table 5-8. The Linear Longshore Sediment Transport Model matches its calibrating data as is to be expected, while slightly overpredicting the Saville (1949, 1950) laboratory data and substantially overestimating the Komar (1969) field data. In this regard, the sample mean error for the Komar (1969) data implies that the predicted transport is about 5 times greater than the measured transport.

The strong overestimation of the field data suggests that the Linear Longshore Sediment Transport Model be viewed with caution and that more modeling and experimental work is needed on the problem.

Table 5-8

Linear Longshore Sediment Transport Model Tests

Study	n_Q	$\overline{Q}_q$	S_Q
SJ*	3	0.00	0.70
SV	7	-0.20	0.54
KO	3	-0.78	0.18

*Calibrating data

145

6 CONCLUSIONS

The present investigation models the steady longshore current and time averaged longshore sediment transport induced by two dimensional, monochromatic, gravity waves breaking on a plane, impermeable, gently sloping beach in the absence of winds and tides. Three new calibrated momentum based models are tested: the Linear Lonshore Current Model, the Linear Longshore Sediment Transport Model and the Nonlinear Longshore Current Model.

The Linear Longshore Current Model, represented by Eqs. (3-76), (4-37) and (4-49) describes the growth of a relatively small longshore current downstream of a shorenormal jetty for waves of near normal incidence. The Linear Longshore Current Model provides a reasonable estimate of the measured form of the longshore dependency although the predicted longshore current scale exceeds the measurements by about 20%, presumably due to the finite size of the current. The latter finding underscores the need for a nonlinear nonuniform longshore current model. Movable bed tests suggest that the Linear Longshore Current Model, whose parameters f_{sz} and Γ are calibrated with fixed bed data, yields at least an order of magnitude estimate of the longshore current flowing over a movable bed in laboratory and field conditions.

The Linear Longshore Current Model, with its small current and near normal wave incidence assumptions, forms the basis for the Linear Longshore Sediment Transport Model which is represented by Eqs. (4-71), (4-72) and (4-75). The Linear Longshore Sediment Transport Model predicts the initial nonuniform longshore response of a plane, movable bed

146

downstream of a shorenormal jetty and is valid at all times for uniform longshore conditions provided the beach is at equilibrium with the waves. The model slightly overpredicts the laboratory data and overpredicts the field data by a factor of 5. In view of this model inaccuracy, along with the restrictive nature of the model assumptions and the uncertainties of the data base, the time averaged longshore sediment transport process should be considered an unsolved problem. The Linear Longshore Sediment Transport Model should therefore be regarded as a simple first step towards a physically plausible model describing time averaged longshore sediment transport.

The Nonlinear Longshore Current Model, represented by Eqs. (3-76), (4-88) and (4-93), relaxes the small current and near normal incidence assumptions and predicts fully developed longshore currents over fixed beds with considerable success; the general model accuracy is of the order 15%. There are systematic model errors in shorenormal distance and in bottom slope, but not in relative roughness; the latter finding suggests that the Nonlinear Longshore Current Model properly determines the time averaged longshore bottom shear stress over a fixed bed with the physically plausible surf zone friction factor calibration of Eq. (5-4). Since the surf zone friction factor is correctly estimated, the scale of the longshore current is correctly estimated as well and the Nonlinear Longshore Current Model may accordingly be used with some confidence to compute the surf zone averaged longshore current flowing over a fixed bed.

A logical next step in the modeling of longshore transport proces-

ses is to investigate the systematic Nonlinear Longshore Current Model errors in shorenormal distance and bottom slope. In this regard, the Nonlinear Longshore Current Model tends to overpredict measured values beyond the breaker line, so that the longshore Reynolds stress is over-estimated in this region and a different formulation of the horizontal eddy viscosity may be in order. As for the $\tan\beta$ error, it should be noted that the integrated nonlinear stress balance of the Nonlinear Longshore Current Model, as well as the linear counterpart governing the Linear Longshore Current Model, does not consider the balance of longshore Reynolds and bottom shear stresses beyond the breaker line in determining the appropriate current reduction factor, and this latter balance deals with a larger amount of stress for steeper slopes. Indeed the surf zone of very steep beaches may be better treated, in view of the discussion of Section 2.4, as a constant stress boundary so that all attention must be given to the region seaward of the breaker line.

Once the systematic errors for the fixed bed Nonlinear Longshore Current Model are explained or eliminated, the model should be extended to cover the longshore evolution of a finite current downstream of a shorenormal jetty; the resulting extension should approach the Linear Longshore Current Model for progressively smaller currents. Upon completion of this modeling effort, the extended longshore current model should be tested against all available movable bed laboratory and field data to verify the ability of the model, which rests on a fixed bed calibrated surf zone friction factor and a plane bottom assumption, to

describe longshore currents over a movable bed. Once the longshore current model matches the movable bed data, the longshore sediment transport problem may be readdressed; hopefully, better sediment transport data in laboratory and field will be available for model calibration and testing at this time.

REFERENCES

Bathe, K. and Wilson, E.L. (1976), Numerical Methods in Finite Element
Analysis, Prentice-Hall, Englewood Cliffs, N.J., 528pp.

Battjes, J.A. (1974), "Computation of Set-Up,Longshore Currents, Run-Up
and Overtopping Due to Wind Generated Waves," Doctoral Thesis,
Department of Civil Engineering, Delft University of Technology,
244pp.

Battjes, J.A. (1975), "Modeling of Turbulence in the Surf Zone,"
Symposium on Modeling Techniques, ASCE Vol. 2, pp. 1050-1061.

Benjamin, J.R. and Cornell, A. (1970), Probability Statistics, and
Decision for Civil Engineers, McGraw-Hill, New York, N.Y., 684pp.

Bowen, A.J. (1969), "The Generation of Longshore Currents on a Plane
Beach," Journal of Marine Research, Vol. 27, No. 2, pp. 206-215.

Bowen, A.J., Inman, D.L. and Simmons, V.P. (1968), "Wave 'Set-Down'
and Set-Up," Journal of Geophysical Research, Vol. 73, No. 8,
pp. 2569-2577.

Brebner, A. and Kamphuis, J.W. (1963), "Model Tests on the Relationship
Between Deep-Water Wave Characteristics and Longshore Currents,"
Civil Engineering Report No. 31, Queen's University at Kingston,
Ontario, 28pp.

Carnahan, B. and Wilkes, J.O. (1968), "Introduction to Algorithms and
Numerical Methods, Preliminary Edition, University of Michigan,
Ann Arbor, Michigan, 191pp.

Chow, V.T. (1959), Open Channel Hydraulics, McGraw-Hill, New York, N.Y.,
680pp.

Collins, J.I. (1970), "Probabilities of Breaking Wave Characteristics," Proc. 12th Conf. Coastal Engineering, ASCE, Vol. 1, pp. 399-414.

Divoky, D., LeMehaute, B. and Lin, A. (1970), "Breaking Waves on Gentle Slopes," Journal of Geophysical Research, Vol. 75, No. 9, pp. 1681-1692.

Eagleson, P.S. (1965), "Theoretical Study of Longshore Currents on a Plane Beach," Report No. 82, Hydrodynamics Laboratory, Department of Civil Engineering, Massachusetts Institute of Technology, 48pp.

Eagleson, P.S. (1966), "Growth of Longshore Currents Downstream of a Surf-Zone Barrier," Proc. 10th Conf. Coastal Engineering, ASCE, Vol. 1, pp. 487-507.

Fairchild, J.C. (1970), "Laboratory Tests of Longshore Transport," Proc. 12th Conf. Coastal Engineering, ASCE, Vol. 2, pp. 867-889.

Galvin, C.G. (1968), "Breaker Type Classification on Three Laboratory Beaches," Journal of Geophysical Research, Vol. 73, No. 12, pp. 3651-3659.

Galvin, C.G. and Eagleson, P.S. (1965), "Experimental Study of Longshore Currents on a Plane Beach," Technical Memorandum No. 10, U.S. Army Coastal Engineering Research Center, 80pp.

Goda, Y. (1970), "A Synthesis of Breaker Indices," Transactions of JSCE, Vol. 2, Part 2, pp. 227-230.

Gradshteyn, I.S. and Ryzhik, I.M. (1965), Table of Integrals, Series, and Products, Academic Press, New York, N.Y., 1086pp.

Greer, M.N. and Madsen, O.S. (1978), "Longshore Sediment Transport Data: A Review," Proc. 16th Conf. Coastal Engineering, ASCE, (in press).

151

Henderson, F.M. (1966), <u>Open Channel Flow</u>, MacMillan, New York, N.Y., 522pp.

Hildebrand, F.B. (1962), <u>Advanced Calculus for Applications</u>, Prentice-Hall, Englewood Cliffs, N.J., 646pp.

Horikawa, K. and Kuo, C.T. (1966), "A Study on Wave Transformation Inside Surf Zone," <u>Proc. 10th Conf. Coastal Engineering</u>, ASCE, Vol. 1, pp. 217-233.

Hunt, I.A. (1959), "Design of Seawalls and Breakwaters," <u>Journal of the Waterways and Harbor Division</u>, ASCE, Vol. 85, No. WW3, pp. 123-152.

Ingle, J.O. (1966), <u>The Movement of Beach Sand</u>, Elsevier Publ., Amsterdam, Netherlands.

Iwagaki, Y. (1968), "Hyperbolic Waves and Their Shoaling, " <u>Proc. 11th Conf. Coastal Engineering</u>, ASCE, pp. 124-144.

Iwagaki, Y., Sakai, T., Tuskioka, K. and Sawai, N. (1974), "Relation-ship between Vertical Distribution of Water Particle Velocity and Type of Breakers on Beaches," <u>Coastal Engineering in Japan</u>, Vol. 17, pp. 51-58.

James, I.D. (1974a), "Nonlinear Waves in the Nearshore Region: Shoaling and Set-up," <u>Estuarine and Coastal Marine Science</u>, Vol. 2, pp. 207-234.

James, I.D. (1974b), "A Nonlinear Theory of Longshore Currents," <u>Estuarine and Coastal Marine Science</u>, Vol. 2, pp. 235-249.

Jonsson, I.G. (1966a), "Wave Boundary Layers and Friction Factors," <u>Proc. 10th Conf. Coastal Engineering</u>, ASCE, Vol. 1, pp. 127-148.

Jonsson, I.G. (1966b), "The Friction Factor for a Current Superimposed
by Waves," Basic Research Progress Report No. 11, Technical Uni-
versity of Denmark, pp. 2-12.

Jonsson, I.G., Skovgaard, O. and Jacobsen, T.S. (1974), "Computation
of Longshore Currents," Proc. 14th Conf. Coastal Engineering, ASCE,
Vol. 2, pp. 699-714.

Komar, P. (1969), "The Longshore Transport of Sand on Beaches," Doctoral
Thesis, Department of Oceanography, University of California,
San Diego, 143pp.

Krumbein, W.C. (1944), "Shore Currents and Sand Movement on a Model
Beach," Technical Memorandum No. 7, U.S. Army Beach Erosion Board,
44pp.

Liu, P.L.F. and Mei, C.C. (1976), "Water Motion on a Beach in the
Presence of a Breakwater," Journal of Geophysical Research, Vol. 81,
No. 18, pp. 3079-3094.

Liu, P.L.F. and Dalrymple, R.A. (1978), "Bottom Frictional Stresses and
Longshore Currents due to Waves with Large Angles of Incidence,"
Journal of Marine Research, Vol. 36, No. 2, pp. 357-375.

Longuet-Higgins, M.S. (1970), "Longshore Currents Generated by Obliquely
Incident Sea Waves," Journal of Geophysical Research, Vol. 75,
No. 33, pp. 6778-6801.

Longuet-Higgins, M.S. (1972), "Recent Progress in the Study of Longshore
Currents," Waves on Beaches and Resulting Sediment Transport,
Meyer, R.E., editor, Academic Press, New York, N.Y., 462pp.

Longuet-Higgins, M.S. and Stewart, R.W. (1960), "Changes in the Form of Short Gravity Waves on Long Waves and Tidal Streams," <u>Journal of Fluid Mechanics</u>, Vol. 8, pp. 565-583.

Longuet-Higgins, M.S. and Stewart, R.W. (1962), "Radiation Stress and Mass Transport in Gravity Waves," <u>Journal of Fluid Mechanics</u>, Vol. 13, pp. 481-504.

Madsen, O.S. (1976), "Wave Climate of the Continental Margin," <u>Marine Sediment Transport and Environment</u>, Stanley, D.J. and Swift, J.P., editors, Wiley-Interscience, New York, N.Y., 602pp.

Madsen, O.S. and Grant, W.D. (1976a), "Quantitative Description of Sediment Transport by Waves," <u>Proc. 15th Conf. Coastal Engineering</u>, ASCE, Vol. 2, pp. 1093-1112.

Madsen, O.S. and Grant, W.D. (1976b), "Sediment Transport in the Coastal Environment," <u>Report No. 209</u>, Ralph M. Parsons Laboratory for Water Resources and Hydrodynamics, Department of Civil Engineering, Massachusetts Institute of Technology, 105pp.

Meadows, G.A. (1976), "Time Dependent Fluctuations in Longshore Currents," <u>Proc. 15th Conf. Coastal Engineering</u>, ASCE, Vol. 1, pp. 660-680.

Miche, R. (1944), "Forme Limite de la Houle lors de son Deferlement," <u>Annales de Ponts et Chausees</u>, Vol. 114, pp. 131-164.

Monzoni, A.A. and Whitham, G.B. (1977), "On the Excitation of Edge Waves on Beaches," <u>Journal of Fluid Mechanics</u>, Vol. 79, pp. 273-287.

Phillips, O.M. (1977), <u>The Dynamics of the Upper Ocean</u>, Cambridge University Press, New York, N.Y., 336pp.

Putnam, J.A., Munk, W.H. and Traylor, M.A. (1949), "The Prediction of Longshore Currents," *Transactions, American Geophysical Union*, Vol. 30, No. 3, pp. 337-345.

Raudkivi, A.J. (1976), *Loose Boundary Hydraulics*, Pergamon Press, New York, N.Y., 397pp.

Reyman, A.S. (1976), "An Analytical Model for Longshore Sediment Transport," Masters Thesis, Department of Civil Engineering, Massachusetts Institute of Technology, 257pp.

Sauvage de Saint Marc, M.G. and Vincent, M.G. (1954), "Transport Littoral Formation de Fleches et de Tombolos," *Proc. 5th Conf. Coastal Engineering*, ASCE, pp. 296-328.

Savage, R.P. (1959), "Laboratory Study of the Effect of Groins on the Rate of Littoral Transport: Equipment Development and Initial Tests," *Technical Memorandum No. 114*, U.S. Army Beach Erosion Board, 56pp.

Savage, R.P. (1962), "Laboratory Determination of Littoral Transport Rates," *Journal of the Waterways and Harbors Division*, ASCE, Vol. 88, No. WW2.

Saville, T. (1949), "Preliminary Report on Model Studies of Sand Transport along an Infinitely Long, Straight Beach," *Report No. HE-116-305*, Fluid Mechanics Laboratory, Department of Engineering, University of California, 23pp.

Saville, T. (1950), "Model Study of Sand Transport along an Infinitely Long, Straight Beach," *Transactions, American Geophysical Union*, Vol. 31, No. 4, pp. 555-565.

Shay, E.A. and Johnson, J.W. (1951), "Model Studies on the Movement of Sand Transported by Wave Action along a Straight Beach," Series 14, Issue 7, Institute of Engineering Research, Department of Engineering, University of California, 58pp.

Svendsen, I.A. (1974), "Cnoidal Waves over a Gently Sloping Bottom," Series Paper No. 6, Institute of Hydrodynamics and Hydraulic Engineering, Technical University of Denmark, 181pp.

Svendsen, I.A. and Buhr Hansen, J. (1977), "The Wave Height Variation for Regular Waves in Schoaling Water," Coastal Engineering, Vol. 1, pp. 261-284.

Thornton, E.B. (1970), "Variation of Longshore Current Across the Surf Zone," Proc. 12th Conf. Coastal Engineering, ASCE, Vol. 1, pp. 291-308.

White, F.M. (1974), Viscous Fluid Flow, McGraw-Hill, New York, N.Y., 725pp.

APPENDIX I NUMERICAL EXAMPLES

I.1 Linear Longshore Current Model

The Linear Longshore Current Model computes $v_s(x,y)$ for given wave $(H, h, \theta)_G$, T and beach $\tan\beta$, k_s conditions in four steps: (1) determination of breaker line conditions $(H, h, \theta, n)_B$ by iteration, (2) estimation of f_{sz}, (3) computation of v_c and y_c and (4) determination of v_s. The process is best described by an example; accordingly the longshore current for a station (I=1, J=5, K=4, X=3) of the GE data is calculated below.

<u>Given</u>: H_G = 0.105 ft, h_G = 1.15 ft, θ_G = 10°, T = 1.5 sec,

k_s = 0.001 ft, $\tan\beta$ = 0.109 y_m = 11 ft x_m = 0.38 ft

<u>Required</u>: Compute v_s

<u>Solution</u>:

(1) <u>Determination of breaker line conditions</u>

The breaking wave predictor requires $(\sin\theta/c^*)_G$ and c_4 as input. Recalling Eqs. (2-27) and (2-28), γ_G = 7.9 and α_G = .091 so that c_G^* = .11 and n_G = .82 from Figures 4-1 and 4-2, respectively, and, in view of Eq. (4-15), c_4 = 36 while $\sin\theta_G/c^*_G$ = 1.6. The breaking wave iteration of Table 4-2 may now begin.

An initial estimate of γ_B = 15 yields α_B = 1.1 from Figure 4-3 since $\tan\beta$ = 0.109; Figure 4-1 gives c_B^* = 0.087, while Snell's Law shown in Figure 4-4 provides the breaker angle estimate θ_B = 8° using the offshore $(\sin\theta/c^*)_G$ as input. The energy transport function estimate from Figure 4-2 is n_B = 0.50, hence, in view of Eq. (4-17), the second estimate of γ_B obtained from radiation stress constancy is γ_B = 23.

157

A recommended revision of the initial estimate is as follows

$$\gamma_B(\text{revised}) = \frac{\gamma_B(\text{initial}) + 4\gamma_B(\text{second estimate})}{5} \qquad \text{(I-1)}$$

so that a new value $\gamma_B = 22$ should be used in the iteration. The re-vised γ_B value yields breaking conditions $\alpha_B = 1.14$, $n_B = .35$, $\theta_B = 6^o$ and a second γ_B estimate of 20 which is judged to be suffici-ently close to the revised γ_B value. Recalling Eq. (2-27) $h_B = 0.15$ ft.

(2) Determination of f_{sz}

The first order of business is to determine the flow regime by using Eq. (5-5) which requires the wave Reynolds number and relative roughness. Recalling Eqs. (5-8) and (5-9) $\frac{<A_b>}{k_s} = 212$ and $R_w = 16000$, where $\nu = 1.2 \times 10^{-5}$ ft^2/sec. Thus, using Eq. (5-5), the flow in the GE experiment is taken as rough turbulent, so that f_w and f_s are func-tions of relative roughness $\frac{<A_b>}{k_s}$ and $\frac{<h>}{k_s}$ respectively, with $\frac{<h>}{k_s} = 75$ in view of Eq. (5-8).

From Eq. (5-7), $f_w = 0.016$ and $f_s = 0.007$ so that f_{sz} may be computed from Eq. (5-4) with $\tan\Delta$ and $\sin\theta_B$ known. The former is given by Eq. (3-29) in terms of α_B and $\tan\beta$; for this problem, $\tan\Delta = 0.073$. The constants c_{12} and c_{13} are equal to -0.0116 and -3.1×10^{-5} respectively, so that $f_{sz} = 0.014$.

(3) Determination of v_c and y_c

κ may be evaluated once f_{sz} is known and Eq. (3-65) yields $\kappa = 2.1$. The propriety of the small current assumption should be checked at this point; $\kappa n_B = 0.75$ so that the GE run is properly

158

linear by virtue of Eq. (4-55). It is a simple matter to compute v_c from Eq. (3-66); $\underline{v_c = 2.63 \text{ fps}}$.

y_c evaluation requires c_5 which is presented as a function of P_{sz} in Figure 4-5. Recalling Eq. (3-70) $P_{sz} = .21$ where $\Gamma = .013$ by virtue of Eq. (3-55) with the calibrated value of $M = .31$ from Section 5.1.2. In view of Figure 4-5, $c_5 = .11$ so that $\underline{y_c = 6.8 \text{ ft}}$ from Eq. (4-46), where the breaker distance $x_B = 2.1$ ft, using the modified bottom slope of Eq. 3-30.

(4) <u>Determination of v_s</u>

The dimensionless longshore distance is obtained by dividing y_m by y_c, with the result $y^* = 1.6$. Accordingly $\lambda_1 = .92$ from Figure 4-6 and the station is far enough downstream to justify use of the Linear Longshore Current Model since the value satisfies the constraint of Eq. (4-54), $\lambda_1 > .07$.

With P_{sz} and the various scaling factors determined, the dimensionless velocity profile appears as a member of the family of curves on Figure 3-1 so that, with the scale given by Eq. (4-37), the longshore current at any shorenormal location is known for the given y_m. In particular, noting that x_m for this problem refers to the still water shore line, $x^* = (x_m + x_s)/x_B$, where $x_s = .67$ ft from Eq. (3-34). Thus, $x^* = .5$ so that $v^* = .43$ from Figure 3-1 and, finally, $\underline{v_s = 0.36 \text{ fps}}$ recalling Eq. (4-37). The prediction compares favorably with the measured value of 0.38 fps.

159

I.2 Linear Longshore Sediment Transport Model

Most of the computation associated with the Linear Longshore Sediment Transport Model is identical to that of the Linear Long-shore Current Model described above; only the additional work is illustrated here. The numbers correspond to the $I = 1$ run of the SJ data and are reported as if the breaker conditions were known.

Given: h_B = 4.6 cm θ_B = 5.7 degrees T = 1.08 sec

$\tan\beta$ = .116 ρ_s = 2.69 gm/cm^3 d_s = 0.3 mm

ν = 1.2 x 10^{-2} cm^2/sec s = 2.69 λ_1 = 1.0

Required: Compute $\int_0^\infty q_s^y\, dx$

Solution: The relative wave length parameter at breaking may be computed from Eq. (2-27) with the result γ_B = 16 and the empirical breaking criterion on Figure 4-3 consulted to obtain α_B = 1.09. The relative wave length and relative wave height then determine the breaking wave energy transport function from Figure 4-2, hence n_B = 0.48. Following the method of the prior example, it is straight-forward to compute $\tan\Delta$ = 0.08, x_B = 58 cm, κ = 2.0, f_{sz} = .016 and P_{sz} = .22.

Recalling Eq. (4-72), the dimensionless integrated time averaged longshore sediment transport is given by $\int_0^\infty (q^*)_s^y dx^*$ = .0035ζ(c_6 + c_7). In view of the calibration of Section 5.1.3, ζ = 660 while (c_6 + c_7) = .18 from Figure 4-5, so that $\int_0^\infty (q^*)_s^y dx^*$ = .42.

The dimensionless parameter S^* = 4.3 from Eq. (4-60) so that the dimensionless and dimensional fall velocities are w^* = .53 and w_F = 3.7 cm/s as obtained from Eqs. (4-61) and (4-60) respectively.

160

Thus, in view of Eq. (4-75) the integrated time averaged longshore sediment transport is estimated as $\int_{0}^{\infty} q_s^y dx = 7.2 \text{ gm/sec}$. Recalling Table 1-10, the corresponding measured transport is 8.2 gm/sec.

I.3 Nonlinear Longshore Current Model

The Nonlinear Longshore Current Model computes v_s using the four steps described in the Linear Longshore Current Model example; the calculation of the first three steps is similar in both models so that only the final step of v_s determination in the Nonlinear Longshore Current Model is discussed. v_s for station 3, transect 6 of the Galvin and Eagleson (1965) run I = 3, J = 9 is computed below.

Given: $\theta_G = 51^{\circ}$, T = 1.25 sec, $H_G = 4.0$ cm $h_G = 35$ cm

$\tan\beta = .109$, $k_s = 0.3$ mm, $x_m = 40$ cm

Required: Compute v_s

Solution: Using the method of Section I.1, the computed values follow: $n_B = 0.43$, $\theta_B = 28^{\circ}$, $\alpha_B = 1.12$, $h_B = 5.1$ cm, $\tan\Delta = .074$, $f_{sz} = .010$, $\kappa = 12.6$, $P_{sz} = .28$. Noting that $x_s = 22$ cm and $x_B = 69$ cm by virtue of Eqs. (3-34) and (3-30) respectively, the dimensionless distance to the measuring station is $x^* = 0.90$, so that with $P_{sz} = .28$, $v^* = 0.35$. The nonlinear current reduction factor is computed next using Eq. (4-93). With P_{sz} and n_B known, $\lambda_c = 0.82$ from Figure 4-7 while $c_8 = -0.16$ so that $\lambda_2 = 0.53$. In view of Eq. (3-66) $v_c = 500$ cm/sec, thus recalling Eq. (4-88), $v_s = 35$ cm/sec. The measured value is 28 cm/sec.

161

APPENDIX II   COMPUTER SUBROUTINES

Table II-1 lists input and output variables for subroutines used
to computerize the breaking wave iteration and the calibrated surf
zone friction factor of the present investigation. Table II-1 cites
called subroutines as well, and is followed by a FORTRAN IV listing
of the subroutines.

Table II-1

Subroutine Input, Output and Calls

SUBROUTINE	INPUT	OUTPUT	CALLS	COMMENT
ALPH	$\gamma_B, \tan\beta$	α_B	DISTRA	Modified Madsen empirical breaking criterion
BWI	$(\gamma, \alpha, \theta)_G$, $\tan\beta$	$(\gamma, \alpha, \theta, n)_B$	ALPH DISTRA SIN2	Breaking wave iteration
CELT	α	c_T^*	CNOIDL STOKES	Dimensionless transitional phase speed
CNOIDL	γ, α	n, c^*	None	Cnoidal dispersion and energy transport function
DISTRA	γ, α	n, c^*	CELT CNOIDL STOKES	Stokes-transitional-Cnoidal dispersion and energy transport function
FSURF	R_w, R_s, $\dfrac{\langle h \rangle}{k_s}$, $\dfrac{\langle A_b \rangle}{k_s}$, $\tan\Delta$, θ_B	f_{sz}, f_s, f_w	FWC	Surf zone friction factor

Table II-1 (Continued)

SUBROUTINE	INPUT	OUTPUT	CALLS	COMMENT
FWC	$R_w, R_s, \dfrac{<h>}{k_s}, \dfrac{<A_b>}{k_s}$	f_s, f_w	PWR	Wave and current friction factors
PWR	x, y	x^y	None	Power function
SIN2	θ(deg)	$\sin 2\theta$	None	Trigonometric function
STOKES	γ	kh, c^*, n	None	Linear dispersion and energy transport function

```
      FUNCTION ALPH(GAMMB,TANB)
C  ALPH IS THE EMPIRICAL BREAKING CRITERION
      IF(GAMMB.LE.3.5)GO TO 10
      IF(TANB.GE.0.10)GO TO 11
      A=TANB
      GO TO 12
11    A=0.10
12    ALP=C.72*(1.0+6.4*A)
      DO 14 I=1,10
      CALL DISTRA(GAMMB,ALP,
     1  EN,CEL)
      B=CEL*GAMMB*GAMMB
      C=(0.80+5.0*A)*6.283/B
      ASTO=0.14*TANH(C)*B
      TAL=ABS(ASTO-ALP)/ALP
      IF(TAL.LE.0.001)GO TO 15
14    ALP=ASTO
      ALP=100.0
      GO TO 15
10    ALP=0.0223*GAMMB*GAMMB
15    ALPH=ALP
      RETURN
      END




      SUBROUTINE BWI(GAMMG,ALPHG,TANB,THG,
     1  GAMMB,ALPHB,THB,ENB)
C  BWI IS THE BREAKING WAVE ITERATION
      CALL DISTRA(GAMMG,ALPHG,
     1  ENG,CELG)
      B=SIN(THG*0.01745)/CELG
      A=ALPHG*ALPHG*ENG*SIN2(THG)
      C4=GAMMG/PWR(A,0.25)
      GAMMB=15.0
      DO 10 I=1,10
      ALPHB=ALPH(GAMMB,TANB)
      CALL DISTRA(GAMMB,ALPHB,
     1  ENB,CELB)
      THB=57.3*ARSIN(CELB*B)
      A=ENB*SIN2(THB)
      STOR=SQRT(ALPHB)*C4*PWR(A,0.25)
      TAL=ABS((STOR-GAMMB)/GAMMB)
      IF(TAL.LE.0.001)GO TO 15
10    GAMMB=(GAMMB+4.0*STOR)/5.0
      GAMMB=100.0
15    RETURN
      END
```

```
      FUNCTION CELT(ALPHA)
C  CELT COMPUTES TRANSITIONAL DISPERSION
      GAMMT=7.0+1.6/ALPHA
      DO 10 I=1,10
      CALL STOKES(GAMMT,
     1 HK,CELS,ENS)
      CALL CNOIDL(GAMMT,ALPHA,
     1 CELC,ENC)
      TAL=ABS(ENC-ENS)/ENS
      IF(TAL.LE.0.001) GO TO 11
   10 GAMMT=GAMMT*ENC/ENS
      CELT=100.0
      GO TO 12
   11 CELT=CELC
   12 RETURN
      END




      SUBROUTINE CNOIDL(GAMMA,ALPHA,
     1 CELC,ENC)
C  CNOIDL ESTIMATES CELERITY AND ENERGY TRANSPORT FUNCTION
C  USING CNOIDAL THEORY
      US=GAMMA*GAMMA*ALPHA
      IF(US.LE.50.0) GO TO 10
C  FIND URSELL NUMBER BY ITERATION ON A
      A=0.50
      DO 11 I=1,10
      U=US*(1.0+ALPHA*A)
      C=ALOG(U)
      D=C*C*C
      E=C*C
      AST=0.00718493*D-0.175838*E+1.50637*C-3.60339
      UST=US*(1.0+ALPHA*AST)
      TAL=ABS((UST-U)/UST)
      IF(TAL.LE.0.001) GO TO 12
   11 A=AST
      ENC=100.0
      CELC=100.0
      GO TO 13
C  COMPUTE DISPERSION AND ENERGY TRANSPORT FUNCTIONS BY CURVE FITTING
   12 CELC=SQRT(1.0+ALPHA*A)/GAMMA
      ENC=8.0*(0.00088233*D-0.0144948*E+0.053364*C+0.075144)
      GO TO 13
C  SMALL URSELL APPROXIMATION
   10 ENC=1.0-0.0016*US
      CELC=1.0/GAMMA
   13 RETURN
      END
```

```fortran
      SUBROUTINE DISTRA(GAMMA,ALPHA,
     1  EN,CEL)
C  DISTRA COMPUTES CELERITY AND ENERGY TRANSPORT
C  USING STOKES-TRANSITIONAL-CNOIDAL THEORY
      CALL STOKES(GAMMA,
     1  HK,CELS,ENS)
      CALL CNOIDL(GAMMA,ALPHA,
     1  CELC,ENC)
      IF(ENS.GT.ENC) GO TO 10
      EN=ENS
      IF(GAMMA.LE.4.0.OR.ALPHA.LT.0.2)GO TO 11
      A=CELT(ALPHA)
      IF(A.GT.CELS)GO TO 13
11    CEL=CELS
      GO TO 12
13    CEL=A
      GO TO 12
10    EN=ENC
      CEL=CELC
12    RETURN
      END




      SUBROUTINE FSURF(BS,BW,RS,RW,TAND,THB,
     1  FSZ,FW,FS)
C  FSURF ESTIMATES SURF ZONE FRICTION FACTOR
      CALL FWC(BS,BW,RS,RW,
     1  FW,FS)
      C12=0.58*TAND*SIN(THB*0.01745)-FW
      C13=-1.0*0.58*TAND*SIN(THB*0.01745)*FS
      A=SQRT(C12*C12-4.0*C13)
      FSZ=(-1.0*C12+A)/2.0
      RETURN
      END
```

```
      SUBROUTINE FWC (BS,BW,RS,RW,
     1 FW,FS)
C  FWC COMPUTES JONSSON FW AND DARCY-WEISBACH FS FOR TURBULENT FLOW
      XW=ALOG (RW)
      YW=ALOG (BW)
      XC=ALOG (RS)
      YC=ALOG (BS)
C  DETERMINE FLOW REGIME
      C=0.863*XW-2.74
      IF (YW.GE.C)GO TO 10
C  ROUGH TURBULENT
      A=1.74*YC+4.32
      FS=1.0/ (A*A)
      A=0.0371*YW*YW
      B=0.791*YW
      FW=EXP (A-B-0.97)
      GO TO 11
C  SMOOTH TURBULENT
   10 A=0.0184*XW*XW
      B=0.66*XW
      FW=EXP (A-B+0.462)
      IF (RS.GE.25000.0)GO TO 24
      FS=0.0559/PWR(RS,0.25)
      GO TO 11
   24 FS=0.027/PWR(RS,0.179)
   11 CONTINUE
      RETURN
      END




      FUNCTION PWR (X,Y)
C  PWR RAISES X TO THE Y POWER
      PWR=EXP (Y*ALOG (X))
      RETURN
      END
```

```fortran
      FUNCTION SIN2(TH)
C  SIN2 COMPUTES SINE OF 2*TH
      STH=SIN(TH*0.017453)
      CTH=COS(TH*0.017453)
      SIN2=2.0*STH*CTH
      RETURN
      END




      SUBROUTINE STOKES(GAMMA,
     1  HK,CELS,ENS)
C  STOKES ESTIMATES DISPERSION AND ENERGY TRANSPORT FUNCTION
C  USING LINEAR THEORY
      A=GAMMA*GAMMA
      IF(GAMMA.GT.3.54)GO TO 10
C  DEEP WATER
      HK=39.48/A
      CELS=0.159
      ENS=0.50
      GO TO 14
 10   IF(GAMMA.GT.5.91)GO TO 11
C  FIRST POWER REGION
      HK=0.251+36.4/A
      GO TO 13
 11   IF(GAMMA.GT.20.5)GO TO 12
C  SECOND POWER REGION
      HK=5.84/GAMMA+10.6/A
      GO TO 13
C  SHALLOW WATER
 12   HK=6.283/GAMMA
 13   D=TANH(HK)
      A=SQRT(D/HK)
      CELS=A/GAMMA
      B=0.5/(A*A)
      ENS=0.50+B*(1.0-D*D)
 14   RETURN
      END
```